PCCP
Physical Chemistry Chemical Physics

Accepted Manuscript

This article can be cited before page numbers have been issued, to do this please use: N. Biliškov, *Phys. Chem. Chem. Phys.*, 2022, DOI: 10.1039/D2CP01458K.

ROYAL SOCIETY OF CHEMISTRY

rsc.li/pccp

View Article Online
DOI: 10.1039/D2CP01458K

Infrared Spectroscopic Monitoring of Solid-State Processes

Nikola Biliškov[a,b*]

[a] *Rudjer Bošković Institute, Bijenička c. 54, 10000 Zagreb, Croatia*

[b] *Department of Chemistry, McGill University, 801 Sherbrooke St. West, Montreal, QC H3A 0B8, Canada*

ORCID: 0000-0002-6981-944X

E-mail: nikola.biliskov@irb.hr

Abstract

Infrared spectroscopy, practically ubiquitous in contemporary chemical laboratory, is frequently underutilised exclusively for a basic characterisation of products. However, its unique richness in molecular-level information on matter, together with its simplicity and flexibility in applications, as well as its ability to be combined with a variety of techniques, make it one of the common for deep understanding of microscopic background of chemical and physical phenomena, especially those of relevance for applications of materials. This tutorial review turns the spotlight of material science toward IR spectroscopic investigations by providing a critical insight to state of the art of this technique, and it covers both fundamental aspects and illustrative examples of its utilisation, as well as current challenges and perspectives focused to physical and chemical transformations in solid state.

View Article Online
DOI: 10.1039/D2CP01458K

Introduction

Human curiosity directed toward understanding of the macroscopic manifestations of microscopic structure of the matter is embedded at the very core of chemistry. From this point of view, structure and transformations of molecules fundamentally determine the function of materials surrounding us. This is generally true for liquids, gases, crystals, glasses, nanostructures, composites, from the simplest industrial feedstocks to the most complex supramolecules or proteins. In order to satisfy our research passion to gain as detailed an insight as possible into the very fundamental core of these phenomena, numerous analytical techniques are available, from those found in everyday laboratory work to the most sophisticated experimental facilities.

Infrared (IR) spectroscopy is today one of the ubiquitous methods, widespread in chemical laboratories. In most cases, it is routinely used for characterisation of products. However, its full applicability goes far beyond these routine analyzes. It is this disproportion between the usability of the method and its underutilisation that has led the author to present the possibilities offered by this powerful, yet highly accessible method. Therefore, this review will be focused to mid-infrared spectroscopic monitoring of chemical and physical processes occuring in solid-state systems, relevant to understanding of materials. Although the various applications of IR spectroscopy to monitor the solid-state processes are covered by numerous reviews,[1–10] the author's intention is to bring to focus some specific applications and perspectives, that have so far remained somewhat out of focus. Numerous recent excellent reviews of IR the specific applications of IR spectroscopy are available, for example on applications of IR spectroscopy in monitoring of liquid[2,11–13] or gaseous systems,[14–16] as well as interfaces.[2,9,17–23]

View Article Online
DOI: 10.1039/D2CP01458K

Infrared Spectroscopy

A Historical Overview

History of IR spectroscopy is painted with numerous admirable manifestations of scientific passion and ingenuity. The initial period was marked by key discoveries that paved the way for the emergence and development of IR spectroscopy in the full sense of the term (Fig. 1). The understanding of the real meaning of spectra in general is out of the reach of classical physics. However, this did not hinder the researchers in their efforts to obtain the highest quality spectra, which led to exciting development of instrumentation, but also to the opening of window into hitherto inaccessible microscopic phenomena.

The very birth of IR spectroscopy can be attributed to experiments performed by Wilhelm Herschel in 1800, which lead to discovery of infrared radiation.[24] Further development of instrumentation was outlined by Seeback's discovery of thermoelectricity, Becquerel's application of thermoelectric effect for precise temperature measurements and Nobili's invention of thermopiles.[25] These discoveries lead to measurement of the spectrum of the Sun by J. F. W. Herschel in 1840.[26] The third crucial moment in the early history of IR spectroscopy was Langley's application of Svanberg's bolometer,[27] a highly sensitive thermometer, that enabled enormous increase of temperature sensitivity, thus allowing measurement of the temperature with respect of the particular wavelength. This finally gave rise to emergence of the first dispersion instruments in 1881.[28]

In the full sense of the word, the development of the IR spectroscopy began in the early 1900s, when William Weber Coblentz demonstrated that chemical functional groups exhibited specific and characteristic absorption features in the mid-IR region of the spectrum. In this early work, Coblentz collected the IR spectra of 135 compounds with high accuracy.[29] This pioneering work paved the way for beginning of the penetration of IR spectroscopy into experimental chemistry in the first decades of the twentieth century.[30] It was enabled by rapid development of quantum mechanics[31] and Einstein's theory of interaction of light with

View Article Online
DOI: 10.1039/D2CP01458K

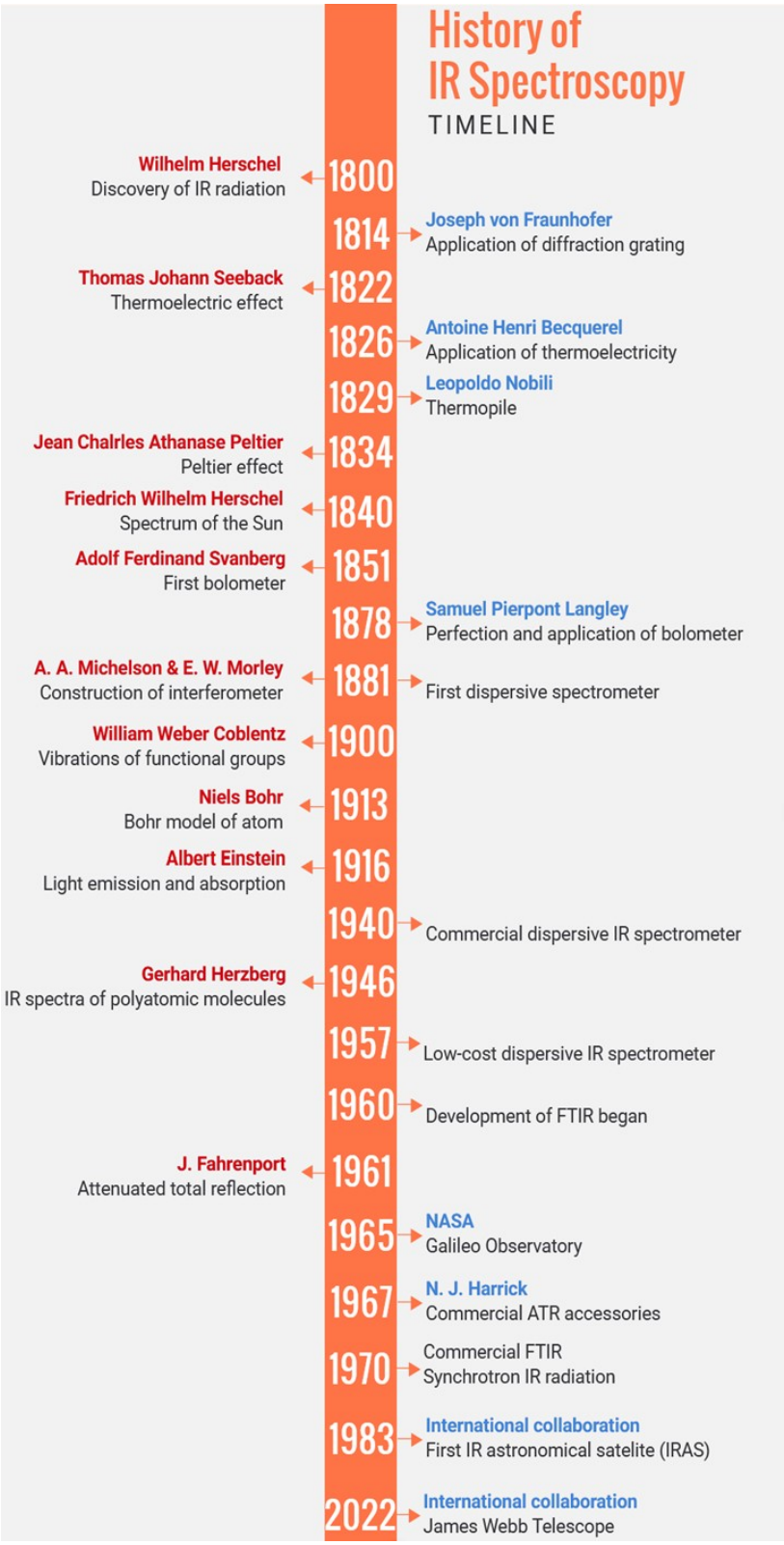

Figure 1: Timeline of IR spectroscopy. Fundamental discoveries are listed on the left side, while breakthrough instrumental developments are shown on the right side.

View Article Online
DOI: 10.1039/D2CP01458K

matter,[32,33] which explained the origin and appearance of atomic and molecular spectra, thus enabling their proper interpretation.

The first generation of commercial spectrometers began to appear in 1940s, and the first low-cost instruments emerged in 1957. These instruments were dispersive IR spectrometers, and they were used exclusively until the emergence of commercial Fourier-transform (FTIR) IR spectrometers. In dispersion spectrometers, the radiation emitted from the source is dispersed by a monochromator (prisms, gratings or their combinations and slits) into its component frequencies, which pass through the sample, and the intensity of transmitted radiation at each frequency is measured. Thus, the acquisition of the typical spectrum requires several minutes. This is acceptable in the case of samples not subject to any external change-inducing perturbation. However, this slowness of the spectral acquisition is often a serious drawback, which prevents quality monitoring of dynamic processes.

Thus, a crucial breakthrough in the history of IR spectroscopy was the replacement of the optical dispersion system with Michelson interferometer, which largely overcame the above mentioned critical drawback of dispersive instruments. In fact, this is an adapted version of the interferometer used by Michelson and Morley in their historical experiment on propagation of light through the hypothetical '*luminiferous aether*'. The original interferometer was described in two papers by Albert Abraham Michelson,[34,35] while Lord Rayleigh practically instantaneously recognised the relation of interferogram with spectrum through the Fourier transformation.[36] However, being far ahead of its time, full utilisation of this concept had to wait for more than 50 years, when computers enabled the required calculations in acceptable time. Although the development of FTIR during 1960s followed three different lines, utilisation of Michelson interferometer enabled rapid scanning. Its combination with He-Ne laser fringe referencing system enabled high resolution, thus giving rise to their commercial breakthrough, starting in 1970, and finally to widespread presence of FTIR spectrometers in chemical laboratories.[37,38]

Modern low-cost benchtop FTIR spectrometers are extremely easy to use and able to

View Article Online
DOI: 10.1039/D2CP01458K

record high-quality, reproducible and accurate spectra in only a few seconds. On the other hand, availability of various commercial accessories, and those developed by researchers themselves, makes IR spectroscopy one of the common, practically unavoidable techniques in contemporary chemistry, physics and materials science. Modern commercial FTIR spectrometers are able to acquire high-resolution (less than $1\,\mathrm{cm}^{-1}$) spectra with Δt up to 4 ns, with a diffraction-limited lateral resolution ($\Delta x \leq 3\,\mu\mathrm{m}$).

FTIR Spectrometers - Basic Principles

In order to use the FTIR spectrometers in their full capacity, it is important to understand their basic functional principles. For a more elaborate description of applications of Fourier transformation in spectroscopies the reader is directed to other sources.[39]

Most generally, any FTIR spectrometer consists of IR source, laser, Michelson interferometer, sample compartment and detector (Fig. 2). As a source of IR radiation, a heated element or glower is used, which is practically considered as black body radiator, emitting a continual IR spectrum. The emitted light is collimated and optical system directs it towards beamsplitter of the Michelson interferometer. The resulting beam then passes through another optical system, that focuses it at the position of the sample. Sample partially absorbs the incident light, and the frequency-dependant intensity of the final beam is measured by detector.

Being the central part of the FTIR spectrometer, principal understanding of Michelson interferometer is crucial for understanding of the function of the whole spectrometer. Michelson interferometer is an optical system consisting of two perpendicular mirrors M_1 and M_2 and semi-transparent beamsplitter B.(Fig. 2) Mirror M_1 is fixed, while M_2 is moving. Collimated IR beam comes from the source to beamsplitter, which is for mid-IR usually KBr or CsI supported thin film of germanium. It transmits and reflects the incoming IR radiation, thus sending it simultaneously to M_1 and M_2. Thus, two separate beams are created from the original incident light.

View Article Online
DOI: 10.1039/D2CP01458K

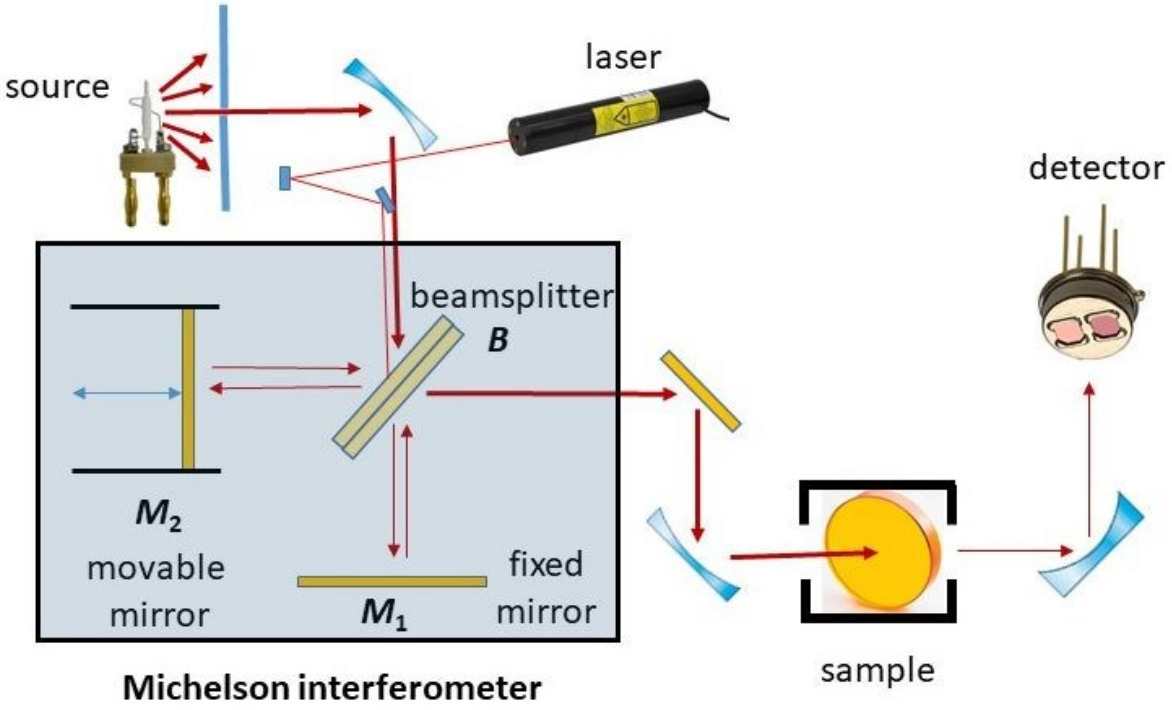

Figure 2: Scheme of the FTIR spectrometer. IR radiation is shown by red arrows.

Now, the light is reflected from both fixed M_1 and movable mirror M_2 back to beamsplitter, where the beams interfere. The beam which reaches sample and detector is a sum of these two beams. It is now obvious that the intensity of the resulting beam (I) is directly correlated to optical path difference δ, which is

$$\delta = 2(|M_2B| - |M_1B|)$$

(factor 2 comes from the fact that the light travels back and forth from the mirrors) and the wavelength of the light λ.

Consider first the simplest case of monochromatic (single-frequency) light. If $\delta = 0$, the two beams are in phase at the beamsplitter, giving a maximal resulting intensity $I(\delta)$. However, if M_2 is displaced by $\lambda/4$, it gives the optical path difference of $\delta = \lambda/2$, and the two beams are 180° out of phase and $I(\delta) = 0$. By further movement of the M_2, $I(\delta)$ reaches maxima when δ is an integral multiple of λ ($\delta = n\lambda$; $n = 0, \pm1,...$) and minima when δ is an

View Article Online
DOI: 10.1039/D2CP01458K

odd multiple of $\lambda/2$ ($\delta = (n + 1/2)\lambda$), giving an interferogram, which follows cosine function (in terms of wavenumbers $\tilde{\nu} = 1/\lambda$):

$$I(\delta) = B(\tilde{\nu}) \cos(2\pi\delta\tilde{\nu}) \tag{1}$$

where $B(\tilde{\nu})$ stands for intensity of the incident light.

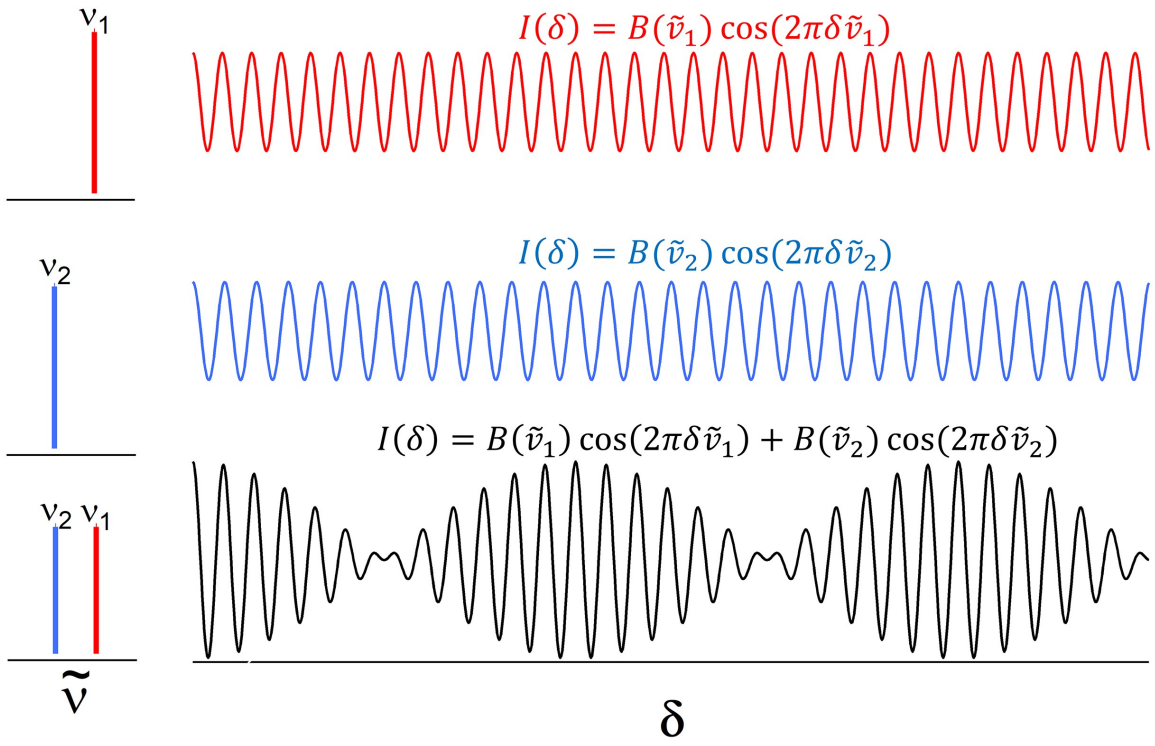

Figure 3: The interferogram of the monochromatic source is a simple cosine function, which periodicity is determined by the frequency of the incident light. In the case of two-frequency (ν_1 and ν_2) source, the resulting interferogram is a linear combination of individual interferograms.

If the light consists of more than one frequency, each frequency can be treated separately, and the resulting interferogram is a sum of individual contributions (Fig. 3), i.e. linear combination of contributions given by eq. (1):

$$I(\tilde{\nu}) = \sum_{\tilde{\nu}_1}^{\tilde{\nu}_n} B(\tilde{\nu}_i) \cos(2\pi\delta\tilde{\nu}_i) \tag{2}$$

View Article Online
DOI: 10.1039/D2CP01458K

The spectrum of the incident IR light, in FTIR spectrometers is a continuum, so the summation (2) should be represented as an integral:

$$I(\tilde{\nu}) = \int_0^\infty B(\tilde{\nu}) \cos(2\pi\delta\tilde{\nu})\, d\tilde{\nu} \tag{3}$$

The interferogram is shown in Fig. 3. For a precise wavelength calibration of the interferogram, a He−Ne laser ($\lambda = 632.8\,\text{nm}$) is used as an external monochromatic source. At $\delta = 0$, interferferograms of all the present frequencies are in phase, which results in a strong maximum (centerburst). Outward of the center in either direction, the multidinous cosine contributions start to reinforce and cancel each other, so the intensity of the interferogram rapidly decreases into a series of oscillations of lower amplitude. If the source radiation contains less spectral information, the oscillations more rapidly decrease. Additionally, the higher resolution of the spectral information is contained farther out of the center in the interferogram. So, the spectral resolution $\Delta\tilde{\nu}$ increases with δ_{max}:

$$\Delta\tilde{\nu} = \frac{1}{\delta_{max}} \tag{4}$$

Strictly speaking, this resolution is in practice compromised by truncation and apodization.

The obtained interferogram represents intensity as a function of time $I(t)$. It is translated into readable spectrum $B(\tilde{\nu})$ (Fig. 4), expressed by its Fourier pair

$$B(\tilde{\nu}) = \int_{-\infty}^\infty I(\delta) \cos(2\pi\delta\tilde{\nu})\, d\delta \tag{5}$$

Modern algorithms do this translation by fast Fourier transformation (FFT).[39]

To obtain a complete spectrum, as presented by eq. 5, integration must be performed from $-\infty$ to $+\infty$, which is practically impossible. Thus, in practice spectra are obtained by truncating the full interferogram, i.e. by limiting it to a finite interval. The original interferogram is convoluted with some function $R(\delta, \delta_{max})$. This process is known as apodization.

View Article Online
DOI: 10.1039/D2CP01458K

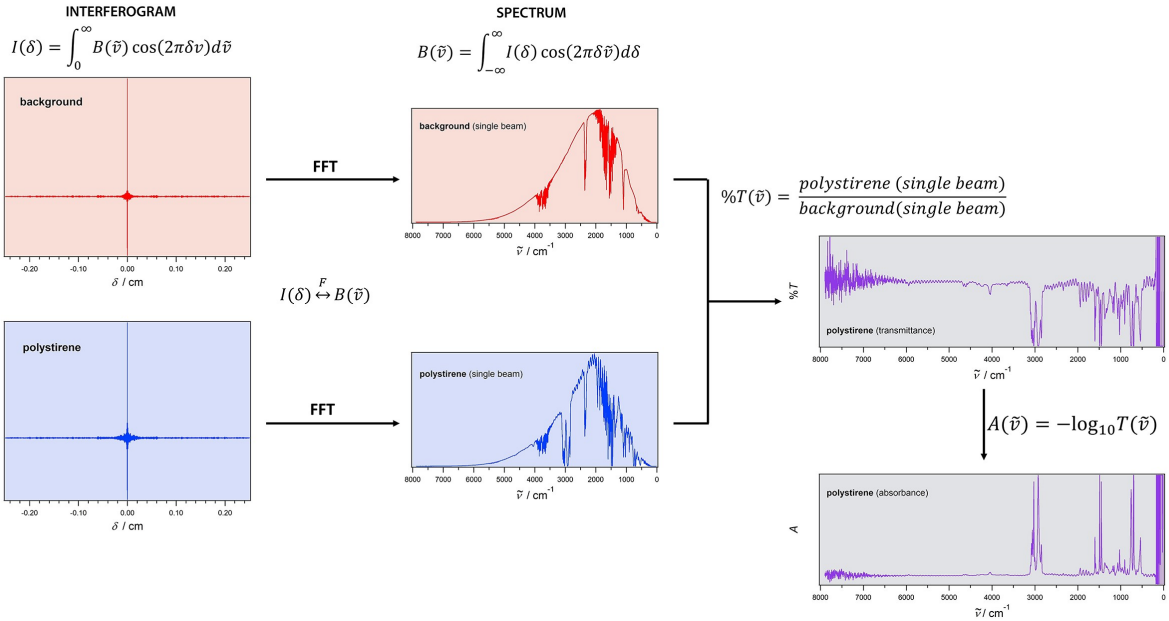

Figure 4: The generation of the IR spectrum by FTIR spectroscopy. Two interferograms of the background and sample, respectively, were collected and transformed by means of FFT to single beam spectra, which are then combined (divided), giving transmission ($\%T$) spectrum. Absorption spectrum, which is linear in Lambert-Beer's law, is then easily obtained. The polystyrene spectrum is used here for illustration.

The simplest apodization function is Boxcar. However, since it significantly distort the band shape, in practice the most commonly used apodization functions are Triangle and Norton–Beer functions, which minimize the influence of apodization process to band shape.[39]

In practice, the most usual setup of the Michelson interferometer for FTIR provides a continuous-scan interferometry, where the mirror M_2 moves continuously at a constant velocity v, and the optical path difference in time t is given by $\delta = 2vt$. Continuous-scan interferometry is preferred for routine static or relatively slow kinetic measurements that require time resolution not faster than 20 ms. For highly dynamic and processes occurring at rates faster than 20 ms time scales, continuous-scan is no longer applicable, because the temporal Fourier frequencies become convolved with the time-dependence of the processes.

This problem is overcame with step-scan interferometry, which provides advantages for spectroscopic measurements of dynamic processes, where the signal is phase- or time-dependent.[40–42] In step-scan setup, the mirror M_2 moves incrementally in steps. In this way,

View Article Online
DOI: 10.1039/D2CP01458K

the interference of the Fourier modulation encountered in continuous-scan FTIR is overcame, which enables measurements as an explicit function of phase, time, or space.[41] Thus, typical applications of step-scan FTIR are phase-resolved spectroscopy for modulation experiments, such as photoacoustic depth profiling[43,44] and polymer rheo-optical characterization[45] and time-resolved spectroscopy[9,46] for fast kinetic processes down to nanosecond time scales.

Today, depending on the time resolution required, a number of additional advanced interferometric techniques are available. They are based on rapid[9] and ultra-rapid scanning,[47] stroboscopic sampling,[48] or asynchronous sampling.[49] These techniques are capable of covering time domains from seconds to picoseconds.[50–52] IR spectroscopic insight to even faster phenomena, which occur at the femtosecond time scale, is enabled by recent development of advanced laser pump-probe methodologies.[53–57] The period of the mid-IR electromagnetic waves covers the $\sim 10 - 300\,\mathrm{fs}$ region, which defines the limit of time resolution that can be achieved by IR spectroscopy.

Since the FTIR spectrometers are single-beam in their performance, recording of background is required before the acquisition of spectrum of a sample (Fig. 4). The background spectrum is practically the black-body spectrum of the IR source, partially influenced by the contents of the medium through which the beam is propagated. This means that the background spectrum, if recorded in ambient conditions (normal atmosphere), will contain bands due to H_2O and CO_2, which are IR active components of the air. Single beam spectrum, as obtained by passing the IR beam through the sample, will be a superposition of spectrum of the sample and spectrum of the atmosphere. Division of two of them will give rise to transmission spectrum:

$$T(\tilde{\nu}) = \frac{B(\tilde{\nu})_{\mathrm{sample}}}{B(\tilde{\nu})_{\mathrm{background}}} \tag{6}$$

Although $T(\tilde{\nu})$ is the most common form in which IR spectra are presented, one should be aware that Lambert-Beer's law is linear in absorbance $A(\tilde{\nu})$, and not in transmittance:

View Article Online
DOI: 10.1039/D2CP01458K

$$A(\tilde{\nu}) = \epsilon(\tilde{\nu})cl \tag{7}$$

where $\epsilon(\tilde{\nu})$ is molar absorption coefficient, c is concentration, and l pathlength of the light through the sample. Thus, in some cases it is more convenient to translate the transmittance to absorbance spectra:

$$A(\tilde{\nu}) = -\log T(\tilde{\nu}) \tag{8}$$

At the end of this introduction to basics of FTIR spectroscopy, it should be underlined that in most cases satisfactorily acceptable approximation, IR spectra, as obtained by a FTIR spectrometer, are practically identical to those obtained by an dispersive IR spectrometer. However, the use of the term "FTIR spectrum" is widespread in the literature, so this requires a short terminological notice. The spectroscopic technique is correctly named FTIR spectroscopy, since in this technique Fourier transform is used to obtain the spectra from interferograms, which are output signals from a FTIR spectrometer (i.e. IR spectrometer with Michelson interferometer). However, the resultant spectra are not FTIR, but IR, since the spectrum is an information on interaction of electromagnetic radiation, in this case IR, with sample. The only difference is in very delicate details of band shape, which are due to apodization process. However, this distortion from a natural band shape is important only in strict analyses. In a vast majority of cases, especially in in-situ process monitoring, a relative change is of central interest, not absolute values of parameters of band shape and intensity.

The Basics of In-situ Spectroscopic Monitoring

In general terms, spectroscopy is any measurement of the absorption or emission of light and other radiation by matter. Thus, to perform a spectroscopic measurement, one needs a source of light, the optical system that enables separation of individual frequencies of light, a sample and a detector, which measures frequency-dependant intensity of resulting light

View Article Online
DOI: 10.1039/D2CP01458K

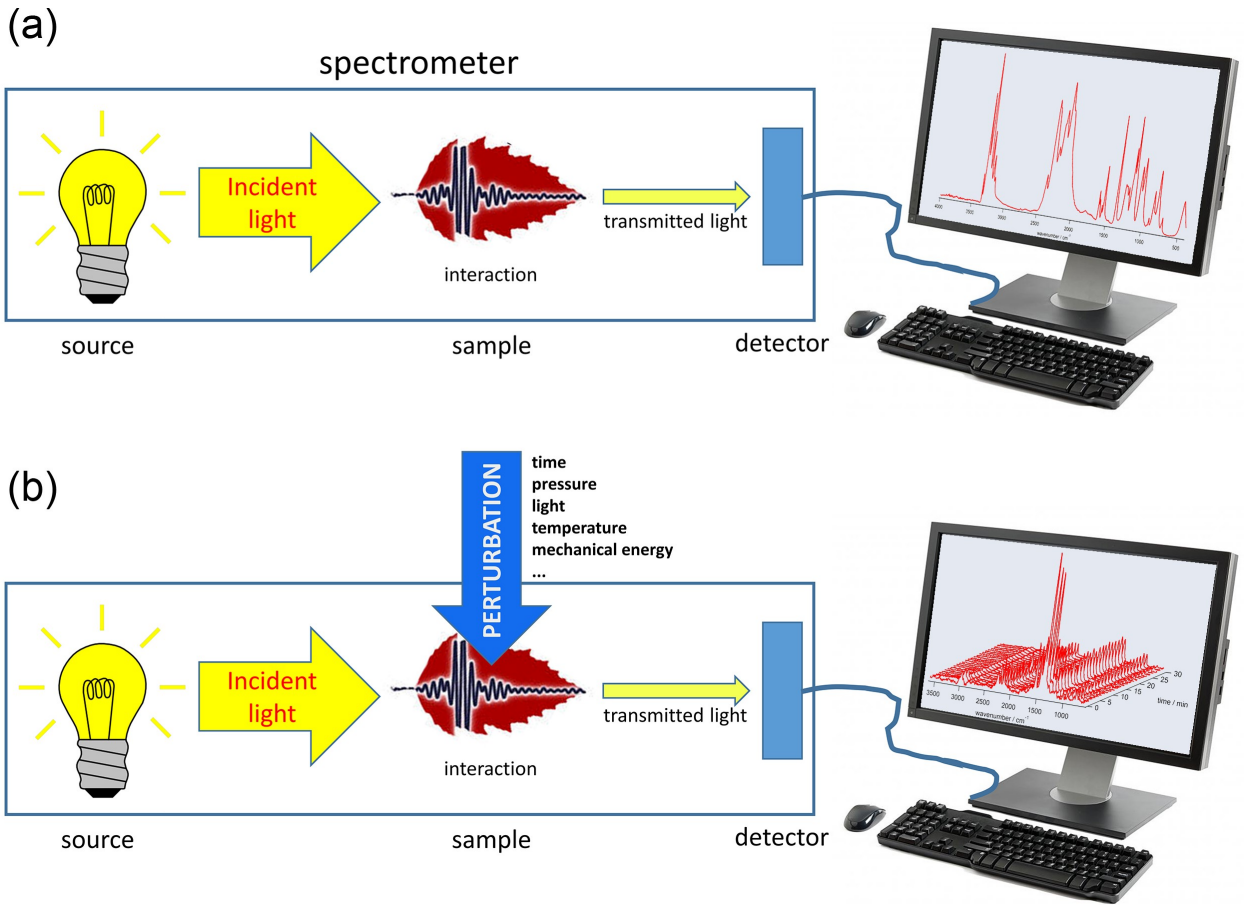

Figure 5: General scheme of (a) spectroscopy and (b) in-situ spectroscopy. In in-situ spectroscopy, the sample is subject of a perturbation, and the resulting spectra reflect changes in the sample as a function of applied perturbation.

View Article Online
DOI: 10.1039/D2CP01458K

(Fig. 5 (a)). In these terms, the spectrum is simply given by:

$$A(\tilde{\nu}) = \frac{I(\tilde{\nu})}{I_0(\tilde{\nu})} \tag{9}$$

where I_0 and I are frequency-dependant intensities of incident and transmitted light, respectively.

Since the frequencies of the radiation in the IR part of the electromagnetic spectrum correspond to frequencies of intra- and intermolecular vibrations, they mutually resonate.[58–65] Thus, IR spectra result from transitions between quantized vibrational energy states. Basically, if the symmetry of a vibration mode makes it IR active, it will be manifested as an IR spectral band.[31,58,64] Molecular vibrations can range from the simple coupled motion of the two atoms of a diatomic molecule to the much more complex motion of each atom in a large polyfunctional molecule, as well as supramolecular aggregates bound by intermolecular forces. Although the information on molecular structure is provided by numerous experimental techniques, the information that can be deduced by IR spectroscopy is complementary to that of other methods, but it provides valuable information on intra- and intermolecular dynamics and interactions, unattainable by other methods. This is especially enabled by high sensitivity of molecular vibrations to present environmental conditions, which is evidently reflected in parameters of IR spectral features of individual functional groups.

In practice, this means that a change in environmental conditions, such as concentration, temperature, pressure, light, application of mechanical force etc. or just a mere passage of time, on the molecular level, will affect the vibrations of particular functional groups (Fig. 5 (b)). In IR spectrum, this change in vibration will be observed in change of some or all parameters of spectral band due to this vibration.

Generally, IR spectral band (Fig. 6) is defined by position $\tilde{\nu}$ at which it reaches maximal absorbance A, its intensity I, i.e. area under the band, and full width at half maximum $FWHM$ (Γ). The band lies at a baseline. In ideal case, the baseline is constant $y = y_0$, and

View Article Online
DOI: 10.1039/D2CP01458K

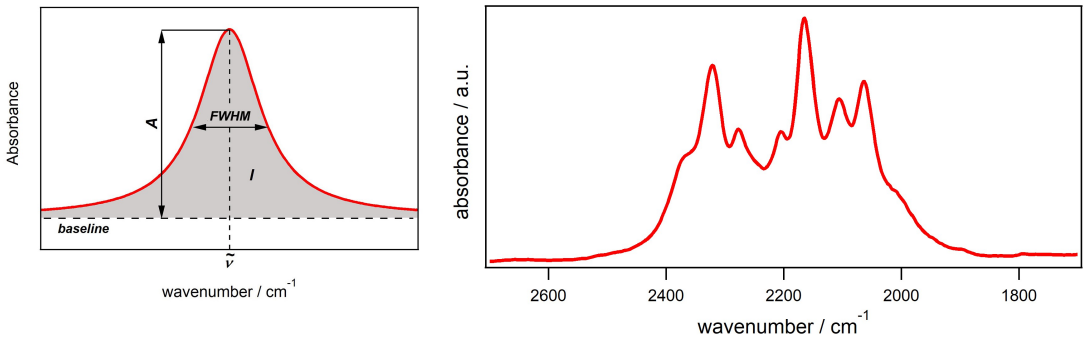

Figure 6: IR spectral band: (a) ideal Lorentzian band with its parameters. The band is lying on a baseline at y_0. Band height A is defined as the difference between maximal absorption at peak position $\tilde{\nu}_{\max}$ and y_0, intensity I is area under the band profile and, while $FWHM$ is full width at half maximum. (b) Real IR spectrum generally consists of envelopes rather than individual bands.

the band shape is described by Lorentzian:

$$y = y_0 + \frac{\frac{1}{2\pi}\Gamma}{(x - \tilde{\nu}_{\max})^2 + (\frac{1}{2}\Gamma)^2} \tag{10}$$

or Gaussian function:

$$y = y_0 + A \exp\left[-\left(\frac{x - \tilde{\nu}_{\max}}{\Gamma}\right)^2\right] \tag{11}$$

It can be also described by some of their combinations, among which the Voigt function has most direct physical meaning.

In reality, IR spectral bands are associated in more or less resolved envelopes on a non-constant and generally nonlinear baseline (Fig. 6 b). This disables a direct extraction of spectral parameters from recorded spectra. In practice, they are derived by fitting the spectral envelope to appropriate model function (Fig. 7).[66] The accurate parameters, as obtained by fitting, are used in further analysis.

As noted earlier, the purpose of in-situ IR spectroscopy is not to give information in absolute values of spectral parameters, but to provide an accurate quantitative information on their trends, relative to some reference, as a response to applied perturbation. Thus, data

View Article Online
DOI: 10.1039/D2CP01458K

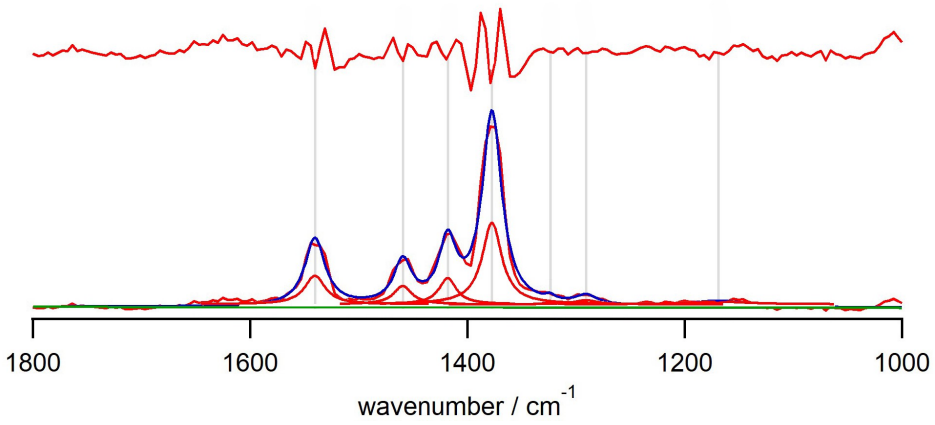

Figure 7: IR spectral envelopes consist of more or less resolved bands, whose parameters are obtained by fitting to Lorentzian or Gaussian functions (red). Sum of thus obtained contributions model the real spectrum (blue). Difference between the real and modelled spectrum is shown as red curve above the spectrum (not in scale).

analysis of in-situ measurements comes down to derivation of accurate kinetic parameters from absorbances or intensities or changes in chemical identity of the system from band position or width. Besides curve fitting, data on perturbation-induced evolution of the chemical system can be obtained by other statistical methods, among them factor analysis is the most widely used.[67,68]

In this field, the term 'operando' is very frequently used to describe the measurement approach. However, a very subtle difference between the terms 'operando' and 'in situ' often leads to a confusion among readers, due to to the frequently incorrectly used terms. For this reason, it is worth to make a brief comment on the differences between operando and in situ techniques at this point. In fact, all operando measurements are in situ, but not all in situ measurements are operando. 'In situ' has always referred to a measurement of the system performed under relevant reaction conditions. On the other hand, 'operando' refers to measurements of the system under realistic reaction conditions, where the reaction products are measured.[69] For example, the measurement of catalyst surface is in situ, but if one do the same, simultaneously monitoring formation of the product, it is operando. There are numerous examples of the misuse of this terminology, and here just a few illustrative examples are brought. Although the term 'operando' mainly refers to what it actually is, i.e.

View Article Online
DOI: 10.1039/D2CP01458K

monitoring of chemical processes with simultaneous measurement of reaction products,[70] it is a very frequent case that studies titled as 'in situ' are focused to monitoring of the evolution of chemical species during the processes,[71] especially products, which is often evident even from the very publication title.[72] For the sake of terminological simplification without losing the essence, exclusively the term 'in situ' will be used further in the text.

A variety of commercially available spectroscopic accessories is useful for in-situ measurements. However, specific systems itself often require adjustments of the existing or development of completely novel experimental setups. Due to the universally valid law of conservation of energy, interaction of incident light I_0 with a sample results in transmission I_T, absorption I_A, reflection I_R and scattering I_S of light (Fig. 8):

$$I_0 = I_\mathrm{A} + I_\mathrm{T} + I_\mathrm{R} + I_\mathrm{S} \tag{12}$$

Thus, basic experimental geometries, namely transmission, specular reflection, diffuse reflection (Fig. 8) and attenuated total reflection (ATR), are common to all the techniques.

Transmission

In transmission measurements, the incoming light simply passes through the sample, which results in transmitted light, partially absorbed by the sample, so the transmittance T is given by:

$$T(\tilde{\nu}) = \frac{I_\mathrm{T}(\tilde{\nu})}{I_0(\tilde{\nu})} \tag{13}$$

Normal incidence is required to minimize reflection from the surface of the sample. This geometry is in principle applicable to samples in all aggregate states.

Transmission IR spectroscopic measurements of powders are usually made by use of KBr pellets, but also some other alkali halide salts can be used for this purpose.[73] These matrices are used due to their high transparency over a wide IR region (Table 1). In order

View Article Online
DOI: 10.1039/D2CP01458K

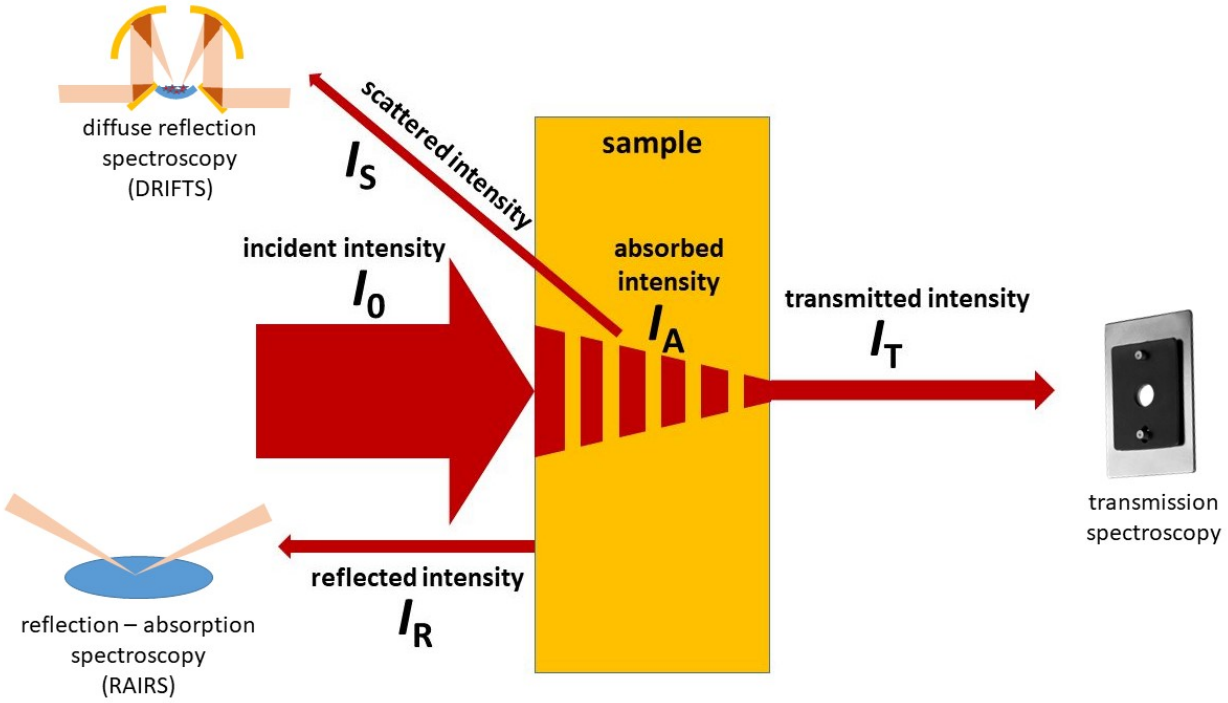

Figure 8: Balance of radiative energy upon interaction with a sample and corresponding spectroscopic techniques.

to maximize reproducibility of the measurements, the mixture should be finely ground and homogenized. At this point one should be aware that ideal homogeneity of the pellet is never achieved, which is especially the case for in-situ measurements, where perturbed sample changes its physical and chemical properties. This causes formation of agglomerates, cracks etc. Additionally, particles bigger than 2 µm of samples which refraction index significantly differs from KBr result in Christiansen effect. In this case, the absorption coefficient κ of the complex refraction index $\hat{n}$:

$$\hat{n}(\tilde{\nu}) = n(\tilde{\nu})[1 - i\kappa(\tilde{\nu})] \tag{14}$$

becomes smaller than dispersive contribution n due to its increase, which is then manifested in artifacts in the form of spikes that accompany spectral bands.[74] One should also be aware that alkali halides are not necessarily chemically inert with respect to the sample.[75,76]

As an alternative to pellets, mulls, usually in liquid paraffin (Nujol), Fluorolube (a chlo-

View Article Online
DOI: 10.1039/D2CP01458K

rofluorocarbon polymer) or hexachlorobutadiene can be used. However, all of these matrices have some bands in the mid-IR region, so this technique is reserved for samples that interact with alkali halides.[77,78]

Soft or plastic samples are more suitable for preparation of films. However, by passing the light through the films, which thickness is comparable to wavelength of IR radiation, interference fringes of significant intensity are produced.

External Reflection

In reflection measurements, the incoming light is reflected and partially absorbed from the optically flat surface of the sample. Similar to transmittance (13), reflectivity R is expressed as:

$$R(\tilde{\nu}) = |r^2(\tilde{\nu})| = \frac{I_{\mathrm{R}}(\tilde{\nu})}{I_0(\tilde{\nu})} \tag{15}$$

where r is amplitude coefficient. Transmittance is related to reflectivity by:

$$T(\tilde{\nu}) = 1 - R(\tilde{\nu})$$

which leads to:

$$I_{\mathrm{T}}(\tilde{\nu}) = (1 - R(\tilde{\nu}))I_0(\tilde{\nu}) \tag{16}$$

Since the measured reflectivity depends on polarisation, the amplitude coefficient for parallel and perpendicular polarisation, respectively, are given by:

$$r_{\parallel}(\tilde{\nu}) = \frac{n_2(\tilde{\nu})\cos\alpha - n_1(\tilde{\nu})\cos\beta}{n_1(\tilde{\nu})\cos\alpha + n_2(\tilde{\nu})\cos\beta} \tag{17}$$

$$r_{\perp}(\tilde{\nu}) = \frac{n_1(\tilde{\nu})\cos\alpha - n_2(\tilde{\nu})\cos\beta}{n_1(\tilde{\nu})\cos\alpha + n_2(\tilde{\nu})\cos\beta} \tag{18}$$

For absorbing media, the refractive index takes its complex form (14). Absorption index κ is related to absorption coefficient a and decadic molar absorptivity ϵ in the Lambert-Beer

View Article Online
DOI: 10.1039/D2CP01458K

law (7):

$$\kappa(\tilde{\nu}) = \frac{a(\tilde{\nu})\lambda}{4\pi} = \frac{\epsilon(\tilde{\nu})c\lambda}{4\pi \ln 10} \tag{19}$$

where c is molar concentration of the sample, and λ is wavelength of the light. Due to the complex form of the refraction index for the reflection spectra, they significantly differ from transmission spectra for the same sample. For this reason, Kramers-Kronig transformation is used to translate reflection to transmittance.[79–81]

In reflection absorption IR spectroscopy (common abbreviations are RAIRS or IRRAS), sample is placed on a highly reflective substrate, which can be optically flat or diffusively reflective (Fig. 8). In this geometry, the light passes twice through the sample, so effectively a sort of transmission spectrum is obtained. From a very basic geometric consideration it is obvious that the pathlength through the sample increase with angle of incidence. The extreme case is grazing incidence technique, where the angle of incidence is maximized.

The output spectrum is a superposition of spectrum of the bulk and the sample in interaction with substrate. A great advantage of RAIRS over the other techniques for surface studies lies in the fact that it does not require vacuum environment, making the RAIRS one of common techniques for characterisation of phenomena at the interface.[82–84] The resulting spectrum, however, very much depends on the thickness of the sample. For thick films, i.e. those where pathlength is larger than wavelength ($l > \lambda$), the absorbance of the light by bulk sample dominates, so the measured absorbance values correspond to the pathlength, making Lambert-Beer law valid in this case. Thus, if one is interested in interactions of the sample with substrate, the sample should be as thin as possible. However, for $l \leq \lambda$, the field amplitude of the standing wave that emerges due to reflection regularly varies, and this effect become predominant for very thin films.[83,85–88] Grazing incidence technique is sensitive exclusively to the components of transition dipole moments normal to the reflecting surface. This makes it very important for studies of surface coatings, very thin films and adhesives, as well as studies of near-surface molecular orientation.[89]

It is important to note that the RAIRS spectra of thin films, especially those cast on

View Article Online
DOI: 10.1039/D2CP01458K

partially reflective substrate, contain significantly intense fringes, which arise due to the interference of the IR light reflected from the upper and lower layer of the film. These interference fringes can completely shadow spectral features of interest, making the quantification of chemical of physical changes, derived from the spectra, highly inaccurate or impossible. To eliminate this problem, a variety of approaches were employed. Concretely, the problem was chronologically first attacked by calculation of optical constants of the film[90] by applying classical Roessler's application of Kramers-Kronig transformations to analyze the reflection on thin films.[91–93] These initial attempts were upgraded by determination of the effective film thickness[94] and modification of the optical system.[95,96] Later advance brought the method which in principle combines the two above mentioned approaches. First, the thickness and complex refractive index of the film in regions of little or no IR absorption are determined from interference fringes. This information is then used to calculate the fringe-free optical constant spectra by use of a Kramers-Kronig transformation.[97] This method, with some improvements, is today integrated to IR spectroscopic software and in routine use as a support for RAIRS.

Diffuse Reflection

If the surface of the sample is rough down to the range of the wavelength, the incident light will partially enter the substrate and will be partially scattered. The former part undergoes absorption within particles, diffract at grain boundaries, and re-emerge at the surface and combine with simply reflected part. The measured reflectivity includes all of the mentioned contributions.

The reflectivity of an optically indefinitely thick (I_T) R_∞ sample is:

$$R_\infty(\tilde{\nu}) = \frac{R_\infty(\tilde{\nu})_\mathrm{sample}}{R_\infty(\tilde{\nu})_\mathrm{reference}} \tag{20}$$

By use of the empirical Kubelka-Munk relation, it can be translated into the parameter

View Article Online
DOI: 10.1039/D2CP01458K

$f(R_\infty)$, which is proportional to absorption:

$$f(R_\infty(\tilde{\nu})) = \frac{[1 - R_\infty(\tilde{\nu})]^2}{2R_\infty(\tilde{\nu})} = \frac{k(\tilde{\nu})}{s} \tag{21}$$

where k represents absorption, and s scattering contribution, respectively, and they vary with particle size and packing density. It is assumed that the sample is weakly absorbing, and scattering contribution s is independent on frequency, which is justified by a proper preparation of the sample.

In the mid-IR spectral range, diffuse reflectance is very weak and it became practical only with breakthrough of commercial FTIR spectrometers. It is known under acronym DRIFTS (diffuse reflectance infrared Fourier-transform spectroscopy).[98] Due to the lack of efficient non-absorbing scattering substrates in the mid-IR, relatively large ellipsoidal mirrors are used in order to capture as many scattered photons as possible.[99]

Attenuated Total Reflection (ATR)

In attenuated total reflection, the incoming light passes through the highly refractive crystal, and is totally reflected at the interface between crystal and sample. Sample partially absorbs (attenuates) the light, and the reflected beam is measured. Since this technique isR extremely easy in use and practically does not require any sample preparation, it became one of the most widespread techniques in contemporary IR spectroscopy. The popularity of ATR was also boosted by enormous increase of accessibility of the water-containing systems by introduction of this method.[100]

The core of ATR accessory is a precisely processed highly refractive crystal (Table 1). The optical system, consisting of plane mirrors and lenses, directs the incident light normally to the crystal. The light is then once or more times totally reflected on the interface between optically dense crystal and sample, which is applied to the exposed face of the crystal. In its design, ATR accessories can allow single- or multiple reflections, as well as fixed or variable

View Article Online
DOI: 10.1039/D2CP01458K

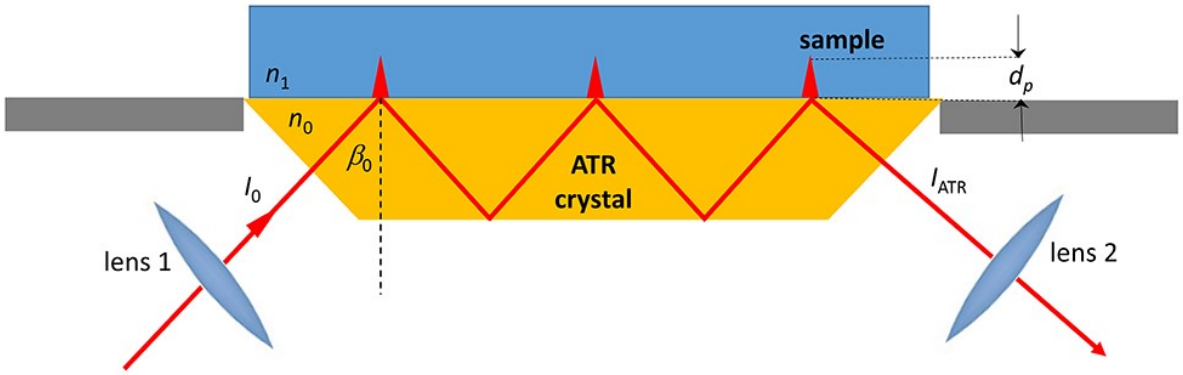

Figure 9: ATR experiment. In this case, the incident light is triple reflected at the angle β_0 on the boundary between optically dense crystal n_0 and sample n_1, where $n_0 > n_1$. Evanescent wave, which penetrates into the sample by d_p, is shown by red triangles.

angle of incidence.[101,102]

According to Snell equation for refraction:

$$n_0 \sin \beta_0 = n_1 \sin \varphi \tag{22}$$

where n_0 and n_1 are refractive indices of the optically denser and rarer medium, respectively, β_0 is the angle of incidence and reflection, while φ is angle between transmitted light and normal of the boundary. Amplitudes of reflected light r are polarisation-dependent and are given by Fresnel equations:

$$r_{\parallel}(\tilde{\nu}) = \frac{\tan\left(\varphi(\tilde{\nu}) - \beta_0\right)}{\tan\left(\varphi(\tilde{\nu}) + \beta_0\right)}$$

$$r_{\perp}(\tilde{\nu}) = -\frac{\sin\left(\varphi(\tilde{\nu}) - \beta_0\right)}{\sin\left(\varphi(\tilde{\nu}) + \beta_0\right)}$$

Evidently, there is some critical angle of incidence β_c (Brewster angle), for which extinction of the transmitted light is given by:

$$R_{\mathrm{T}} = 0 \quad \forall \quad \beta_0 \geq \beta_c$$

In this case, the light will be entirely reflected, i.e. angle φ becomes imaginary, and this is

View Article Online
DOI: 10.1039/D2CP01458K

total reflection. From the condition

$$\sin^2 \beta_0 > n_{10}^2$$

of eq. (22), where $n_{10} = n_1/n_0$, imaginary φ is given by:

$$\cos \varphi = \sqrt{1 - \sin^2 \varphi} = i \frac{\sqrt{\sin^2 \beta_0 - n_{10}^2}}{n_{10}}$$

and now Fresnell equations take the following form:

$$\begin{aligned} r_{\parallel} &= \frac{n_{10}^2 \cos \beta_0 - i\sqrt{\sin^2 \beta_0 - n_{10}^2}}{n_{10}^2 \cos \beta_0 + i\sqrt{\sin^2 \beta_0 - n_{10}^2}} \\ r_{\perp} &= \frac{\cos \beta_0 - i\sqrt{\sin^2 \beta_0 - n_{10}^2}}{\cos \beta_0 + i\sqrt{\sin^2 \beta_0 - n_{10}^2}} \end{aligned} \tag{23}$$

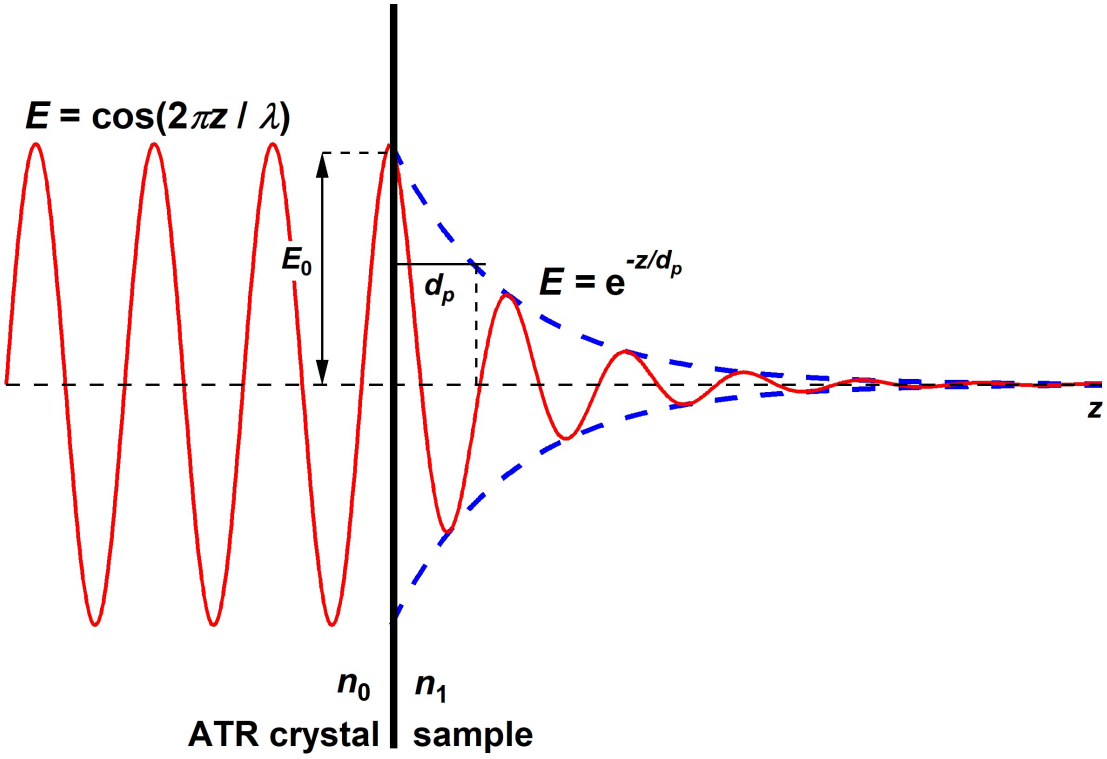

Figure 10: Behaviour of the E component of the incident light at the boundary between ATR crystal and sample.

However, in his pioneering paper, which introduced ATR, Fahrenport has shown that the

View Article Online
DOI: 10.1039/D2CP01458K

radiation incident from the optically dense dielectric crystal on its boundary with optically rare sample at an angle $\beta_0 \geq \beta_c$ will be totally reflected, but only in those frequency regions where the sample does not absorb (where $\kappa = 0$). In regions where $\kappa \neq 0$, reflection will not be total anymore and, accordingly, a spectrum is obtained, which strongly resembles a transmission spectrum. Reflectivity is again given by eq. (23), but refraction index of the sample becomes complex (eq. (14)). The absorbing sample thus causes a perturbation or frequency-dependent attenuation of the totally reflected light. The incident light penetrates the sample, while the frequency is preserved, but the amplitude of electric field E exponentially decreases with distance from the boundary between the ATR crystal and sample:

$$E(\tilde{\nu}) = E_0 e^{-\frac{z}{d_p(\tilde{\nu})}} \tag{24}$$

where z is distance from the boundary, while d_p is penetration depth, i.e. distance from the boundary at which $E = E_0 e^{-1}$ and it is given by:

$$d_p(\tilde{\nu}) = \frac{\lambda_0}{2\pi\sqrt{\sin^2\beta_0 - \left(\frac{n_1(\tilde{\nu})}{n_0(\tilde{\nu})}\right)^2}} \tag{25}$$

where λ_0 is wavelength of the light in optically denser medium.

The penetrating field E is built on the sinusoid wave on the boundary. It is important to note in eq. (25) that light of bigger λ will penetrate deeper inside the sample, and generally the d_p is not directly transferable to l for transmission geometry. Thus, ATR spectra are not simply related to transmittance, and for this translation Kramers-Kronig transformation is required, which resolve real from imaginary part of the complex refraction index, and absorbance is then obtained from κ.[80,100] Further, attenuation by the sample, which is in higher or lower extent present in the whole spectral region causes that $R(\tilde{\nu}) < 1$, and it is given by:

$$R = (1 - a)^{N_R}$$

View Article Online
DOI: 10.1039/D2CP01458K

where a is an absorption parameter and N_{R} effective number of reflections, which is obtained from the N, defined by the geometry of ATR element of thickness D:

$$N = \frac{1}{D} \cot \beta_0 \tag{26}$$

which is corrected by taking into account experimental conditions, such as convergence of the beam, diffraction of parallel polarized component of incident radiation etc.[101] However, for the purposes of in-situ measurements, since only the relative values with respect to reference spectrum are of importance, these considerations are in the majority of cases not required.

By its performative easiness and flexibility with respect to the nature of sample, ATR is now, together with transmission, the most commonly used technique for acquisition of IR spectra. Since its applicability encompasses coatings, films, polymers, adhesives etc., it practically pushed out mull technique. The sample has only to be brought into optical contact with ATR crystal, which is in practice done by use of press. Incident light undergoes single or multiple internal reflections. The bevel edges of the crystal can be flat (for fixed β_0) or rounded (which allows variable β_0). Multireflection crystals could be of trapezoidal, parallelepiped or rod shape. Single-reflection ATR crystals are trigonal prisms in shape. Most commonly used materials are ZnSe, or Ge for multiple-reflection ATR, while for single-reflection, diamond is the most commonly used (Table 1).

Physical Processes

By definition, physical processes does not influence chemical identity of the sample. However, they influence the arrangement of the molecules and pattern of intermolecular contacts, thus changing their properties at macroscopic scale. Being very sensitive to changes in molecular environment, IR spectroscopic techniques provide important information on the molecular background of these macroscopic changes.

View Article Online
DOI: 10.1039/D2CP01458K

Mechanics

Needless to say, mechanical properties are crucial for end-use of numerous materials. Mechanical properties refer to both elastic and plastic deformations as well as fracture which occur under the action of applied load on the molecular crystals. Thus, understanding of microscopic manifestations of macroscopic forces, applied to materials from outside, are of considerable interest. Being sensitive to orientation of dipole moments, as well as molecular environment, IR spectroscopy provides a unique means of understanding of both static and dynamic molecular structure of materials. Studies of molecular background of elastic deformation or pressurization, i.e. changes in molecular orientation initiated by applied force from outside, are by far the most common in this field.

Elasticity, i.e. ability of material to return to its original shape after being stretched or compressed, is an important property of polymers. When relaxed, polymeric molecules are disordered. When stretched, they fold in parallel threads. To investigate elasticity of polymeric materials, Siesler introduced rheo-optical FTIR,[103–105] which enables recording of IR spectra of elastic materials simultaneous with its stretching and heating or cooling. Theoretical background of the technique is also well established by the same group.[103] The monitoring of response of specific vibrational bands to applied force and temperature recovered the orientation and orientational relaxation in bimodal blends of PMMA, as well as the strain-induced crystallization of the soft segments during cyclic elongation and recovery of polyuretane elastomers.[104] Conjugated polymers have attracted much attention as semiconductive materials for use in flexible devices, but they are generally more rigid than conventional plastics. Nishino et al. applied a combination of X-ray diffraction and polarized IR microspectroscopy to understand the response of crystallites and individual molecules of the amorphous bulk of polythiophene to stretch and addition of disiloxane. In this way, the change in orientation of the crystallites by addition of disiloxane, while the polarization-dependent IR absorption bands are more sensitive to stretch, showing that the amorphous bulk of the polymer is responsive to mechanical strain.[106]

View Article Online
DOI: 10.1039/D2CP01458K

Pressure-induced effects on structure and properties of various materials are of considerable interest in materials science. Thus, high-pressure IR (HP-IR) spectroscopic studies are widespread used to understand systems, such as strongly correlated electron systems (SCES).[107] Additionally, regular molecular solids under high pressure have also attracted a great deal of attention in this respect. The examples of HP-IR spectroscopic measurements include ice,[108] dense nitrogen,[109] hydrogen,[110] and their mixtures.[111] Another field, highly targetted by HP-IR techniques are those falling to domain of Earth and planetary science.[112–114] In this respect, various minerals at high pressures have been studied by IR spectroscopy to understand their properties in the deep interior of the Earth and other planets.[115–117] From the application point of view, HP-IR have important implications in industries such as in pharmaceuticals, photonics, etc.

Accordingly, HP-IR instrumentation developed by different groups have been reported.[118–126] A diamond anvil cell (DAC)[127,128] is most commonly used as a central part. Ruby particles are used for precise measurement of the pressure inside DAC.[129] Due to the quite limited space inside the cell, synchrotron radiation as a brilliant source of IR light is required to obtain accurate spectra.[107] Combination of HP cells with synchrotron sources significantly expanded the scope of these investigations. Such an enormous progress in HP science practically revolutionized ultrafine characterization of condensed matter.[10] This is particularly true for synchrotron-based IR microspectroscopy (SIRMS) with its extended measurement conditions enabled by very high signal-to-noise ratio, spatial resolution and sensitivity. In order to get as much data as possible by using a single DAC in a synchrotron facility, they are often designed to enable measurements in both reflection and transmission mode.[119,123,124] This is usually accomplished by switching the angle of corresponding mirrors inside the sample compartment.[123] However, designs that allow exclusively reflection are also available.[118,121,122]

Generally, the application of force along particular crystal axes causes structural changes, leading to denser crystal packing of the molecules. At high pressures (in the GPa or-

View Article Online
DOI: 10.1039/D2CP01458K

der of magnitude) chemical bonding, molecular configuration and crystal structures are significantly affected. This is especially evident in organic molecular crystals, for example 2,3-dichlorobenzylidine-4-bromoaniline (DBA),[130] 2,6 dichloro-N-benzylidene-4-fluoro-3-nitro aniline (DFA) and 2,5-dichloro-N-benzylidene-4-chloroaniline (DPA).[131] By application of force, most of the prominent bands, including aromatic and aliphatic CH and CCl bands showed significant shifts toward the higher wavenumbers, which is, together with broadening of the bands is attributed to changes in pattern of intermolecular interactions in the crystals. Structural reversibility upon decompression is evident for all these systems, which reflects essentially short-range perturbations. Difference in response to compression and decompression of the two crystals is attributed to difference in their packing configurations. Specifically, results indicate that relative orientation of π stacks plays a pivotal role in overall elasticity of the studied molecular crystals. These evidences lead to precise and detailed models of elasticity of these molecular systems.

Inorganic crystals also respond to applied pressure by structural rearrangements of crystal lattices, which often leads to significant change of their electronic properties. For example, HP-IR spectroscopy in the pressure range from ambient up to 20 GPa was performed to investigate pressure-induced transition from insulator to metal state of YbS at room temperature.[132] The original reflectance spectra were translated to optical conductivity, which directly reflects the electronic character of the sample, i.e. its transition from from an ionic insulator into a metal. In another example, HP-IR was combined with Raman spectroscopy and X-ray diffraction to investigate pressure-induced phase transition in multiferroic $h-Lu_{0.6}Sc_{0.4}FeO_3$. It was observed that symmetry breaking across the transition from polar to antipolar state takes place via changes in the bipyramidal tilting direction and Lu/Sc displacement pattern, which is analogous to the strain-driven distortion in $h-LuFeO_3$ and temperature-induced transitions in the rare-earth manganites.[133]

It is especially interesting to explore the behaviour of systems for solid-state hydrogen storage at high pressures. It has been demonstrated that uptake of H_2 drastically increases

View Article Online
DOI: 10.1039/D2CP01458K

at GPa scale of hydrogen pressure. Especially interesting in this respect are various complexes with H_2 and pressure-induced phase transitions of ammonia borane[134–137] and its derivatives,[138] alanates,[139] metal amides[140] and borohydrides.[137,141,142] The majority of these systems were thoroughly explored by means of HP-Raman spectroscopy, but, for sure, employment of IR spectroscopy would add very interesting information of high importance for their utilisation. In recent publication, Marizy et al. have reported HP-IR study of polymorphism of $LiBH_4$ and $NaBH_4$.[142] The authors pointed out the impossibility of determining the details of the phase transition of $NaBH_4$ from tetragonal $Pnma$ to $\alpha - LiBH_4$-type monoclinic $P2_1/c$ by using Raman spectroscopy,[141] claiming that "it is not possible to confirm the phase transition above 20 GPa from the Raman spectra alone". Thus, they performed HP-IR measurements up to 200 GPa. In this way, the phase diagrams of both $LiBH_4$ and $NaBH_4$ have been experimentally extended to pressure region above 100 GPa. $LiBH_4$, with at least 5 detected polymorphs shows richer polymorphism than $NaBH_4$. Important details of these phase transitions were revealed by IR spectroscopy, which shows that tetragonal phase of $LiBH_4$ undergoes a pressure-induced monoclinic distortion, which is not observed in the case of $NaBH_4$. It is also interesting to note that IR transmission measurements on tetragonal phase of $LiBH_4$ revealed for the first time the presence of a weak absorption near $4550\,cm^{-1}$, which is attributed to stretching vibration of H_2 molecules trapped inside the $LiBH_4$ crystal lattice. Since the calculations of molecular dynamics predicted formation of $NaBH_4 \cdot (H_2)_{0.5}$ complex at pressures above 200 GPa, which would have a characteristic IR active absorption due to H−H stretching at $\sim 4400\,cm^{-1}$. The preliminary experiment were possible for the H_2 pressure up to 88 GPa, and this band was not observed, which is actually in agreement with predictions. This observation raised the question of the possible insertion of H_2 to nanosized alkaline borohydrides, entrapped in metal-organic frameworks.

View Article Online
DOI: 10.1039/D2CP01458K

Nanodimensional Materials

On a nanometer scale, systems generally behave significantly different than when the particle dimensions of the same substance are macroscopic. This is caused by significant disruption of extended networks of intermolecular contacts, which causes certain properties of molecules to come to the fore, while the bulk properties cease to be expressed. In general, nanomaterials are those systems in which at least one of the dimensions is nanometric ($1 - 100\,\text{nm}$), while other dimensions can be incomparably larger, i.e. macroscopic. Thus, two-dimensional (2D) materials are those for which length and width are macroscopic, while their thickness is of nanometer dimensions. So, 2D materials are layered solids, from which individual sheets can be delaminated (exfoliated) from the bulk crystal. One-dimensional (1D) materials are characterised by macroscopic length, while their width and thickness are nanometric. So, they are nanotubes, nanowires and nanorods. Zero-dimensional materials are nanoparticles, for which all dimensions are nanometric.

2D materials are obtained by bottom-up or top-bottom approach. In bottom-up approach, their preparation starts with the atomic or molecular ingredients and assemble them together into the layers, usually grown on a substrate. The common techniques are chemical vapor deposition (CVD),[143] physical vapor deposition (PVD)[144] or various solution-based chemical synthetic methods.[145,146] Both CVD and PVD require high vacuum conditions, which significantly complicate the instrumentation required for accurate monitoring of film growth. However, due to its great flexibility in approaching the sample, IR spectroscopy has found its place in this technologically very important area, which does not include only thin films, but also adsorbates on the substrate's surface.[147,148] RAIRS is IR spectroscopic mode of best choice for these phenomena, especially under ultrahigh vacuum (UHV) conditions,[149,150] but transmission[151,152] and ATR[9,152,153] (Fig. 11) configuration are also employed to solve specific problems. Additionally, a highly sensitive experimental setup for the spectroscopic characterization of submonolayer coverages of hydrocarbon fragments on single crystals under UHV was developed. In this case, the experiments are performed by focusing the IR

View Article Online
DOI: 10.1039/D2CP01458K

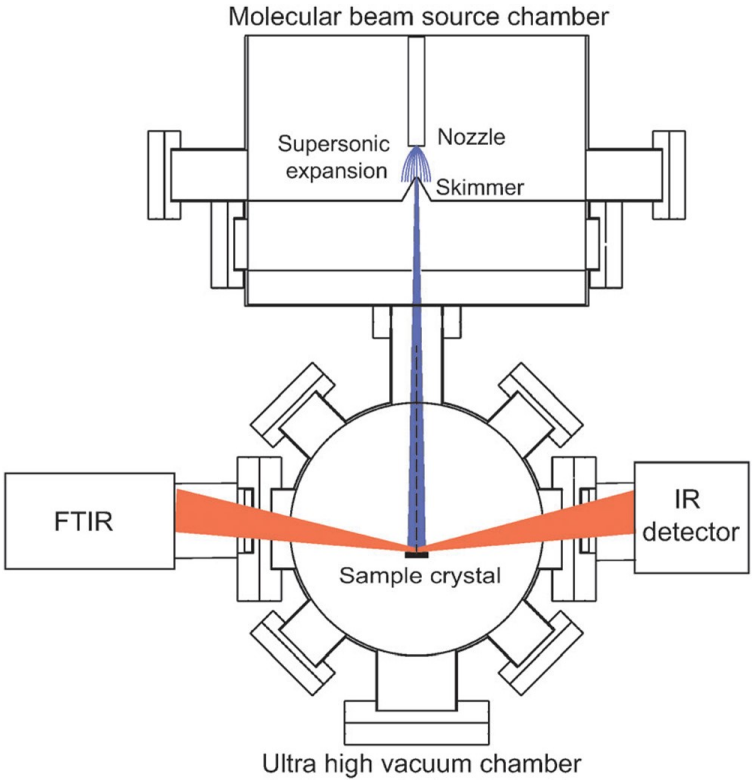

Figure 11: A general scheme of the chamber for ultrahigh vacuum RAIRS experiments. Reprinted with permission from Chadwick and Beck, *Chem. Soc. Rev.* 2016, **45**, 3576-3594

View Article Online
DOI: 10.1039/D2CP01458K

beam from a commercial FTIR through a polarizer and a NaCl window onto the sample at grazing incidence, passing the reflected beam through a second NaCl window, and refocusing it onto a detector.[154]

ATR was also employed to provide an insight into the processing of silicon wafers in order to facilitate the spatially resolved growth of thin solid films on their surfaces. Specifically, Guo and Zaera tested a combination of silylation and UV/ozonolysis as a way to control the concentration of the surface OH groups required for subsequent atomic layer deposition (ALD) of metals or oxides.[153] In this regard, ATR-IR spectroscopy enabled in situ monitoring of the evolution of the surface of the Si(100) wafers after the silylation and O_3/UV-ozonolysis steps. After the treatment of Si surface with hexamethylenedisilazane (HMDS), the growth of the band at $1257\,cm^{-1}$ due to the symmetric deformation of the CH_3 in the newly formed $SiCH_3$ indicates silylation. Additionally, the reaction of the HMDS with the Si surface is indicated by the disappearance of the peaks at 945 and $1184\,cm^{-1}$ due to the symmetric SiNSi stretching and NH deformation modes, respectively, with simultaneous rise of a broad peak at $1120\,cm^{-1}$ associated with the $Si-O-CH_3$ moiety. The monitoring of the further step shows that the spectra for the sample exposed to O_3, but not to UV radiation, is similar to that recorded for the surface before treatment; the feature at $1120\,cm^{-1}$ from the $SiOCH_3$ moiety and the double $1251+1257\,cm^{-1}$ envelope due to the SiO_2 and CH_3 deformation modes, respectively, remain the same. From this observation, it is evident that methyl groups of the adsorbed HMDS survive intact upon exposure to O_3. On the other hand, the spectra from the sample treated with both O_3 and UV only retains the sharp absorption from the SiO_2 substrate at $1251\,cm^{-1}$, while the features at 1257 and $1120\,cm^{-1}$, associated with the surface CH_3 groups are no longer visible, which indicate removal of the organic matter from the surface.

However, in the case of small-sized mono- or few-layered samples, the ratio $\Delta R(\tilde{\nu})/R(\tilde{\nu})$ or $\Delta T(\tilde{\nu})/T(\tilde{\nu})$ are of the 10^{-5} order of magnitude, and the traditional RAIRS and ATR methods cannot obtain a satisfactory signal-to-noise ratio, which makes the resultant spectra

View Article Online
DOI: 10.1039/D2CP01458K

useless for further analysis. In this cases, a step-scan FTIR spectroscopic photoreflectance (PR) or photoluminescence (PL) approach, modulated by a lock-in amplifier, is used (Fig. 12).[155] The setup enables measurements under vacuum, which eliminates the influence of atmospheric CO_2 and water. For modulated PR and PT measurements, a halogen or globar can be used as the source of the probe beam. By using switchable mirrors, different experiment modes and detectors can be selected within the same setup configuration and by sample mounting. The pump laser beam is mechanically chopped. A lock-in amplifier enables a phase sensitive detection, and thus a high optical response was obtained, which significantly increases signal-to-noise ratio, thus making the accurate IR spectroscopy of nanomaterials possible.

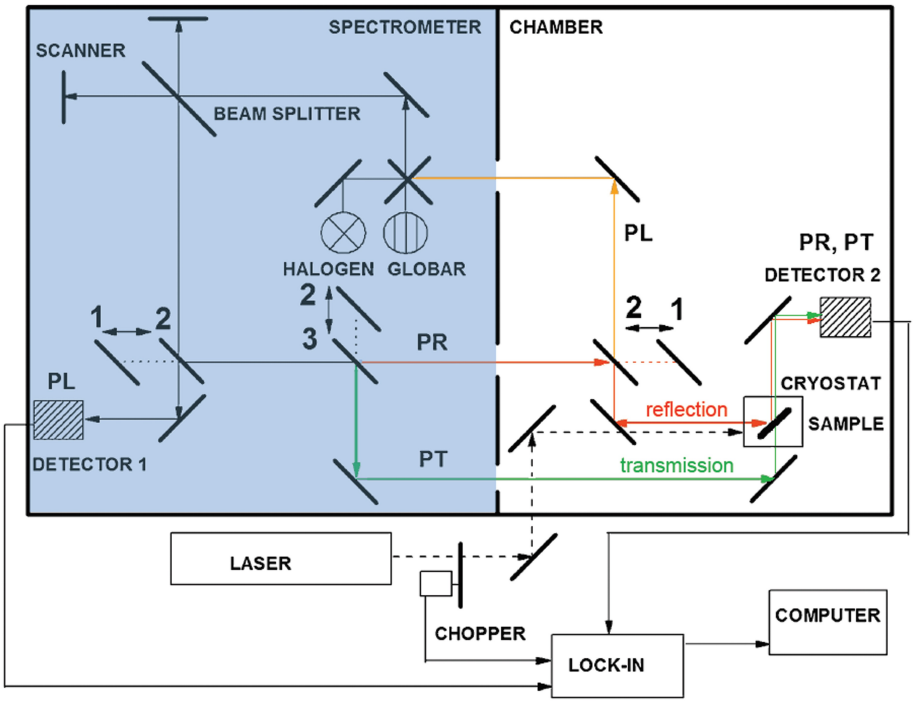

Figure 12: Scheme of the FTIR photoluminescence (PL), photoreflection (PR) and phototransmission (PT) setup. The module is a FTIR spectrometer together with a vacuum chamber. Mirror positions 1, 2, 3, and detector positions 1, 2 show the setup's versatility with possible configurations for PL, PR, and PT measurements. The laser pumping beam is chopped by a mechanical chopper and phase sensitive lock-in amplifier detection is employed. Adapted with permission from Motyka et al. *Appl. Phys. Exp.* Copyright (2009) The Japan Society of Applied Physics.

Due to the fundamental experimental limitations associated with diffraction limit, con-

View Article Online
DOI: 10.1039/D2CP01458K

ventional IR spectroscopy cannot be directly applied to directly characterize individual particles of the nanoscale materials. However, in the past decade, a significant progress in this respect was made by development of FTIR nano-spectroscopy (nano-FTIR), which combines scanning near-field optical microscopy with FTIR spectroscopy. It provides a powerful tool to study polymers, 2D-materials, semiconductor devices, and biomaterials at the nanoscale.[156] The probe of a typical nano-FTIR setup is generally made of metal or metal-coated (e.g. Au, Ag, Pt) dielectric materials. Because of the probe's mirror dipole effect, and lightning-rod effect, the tip-sample region will form a strong electric field enhancement, i.e. a "hotspot". The interaction between the tip, sample and light induces an elastic scattering signal that contains the sample's fingerprint information. Then, this scattered light is collected by an off-axis parabolic mirror and forms an interference spectrum with the reference beam. Finally, the IR spectra of this tip-sample region, including the amplitude and phase spectra, is obtained. Among the other applications, this technique is used for characterization of 2D materials, especially to distinguish monolayer and few-layer 2D materials,[157] which is only indirectly reachable by conventional IR spectroscopy. Nano-FTIR was also employed to study the surface phonon polarons (SPhP) on the surface of hexagonal BN.[158,159] It is found that the SPhP dispersion characteristics of hexagonal BN systematically change with the sample-edge distance, which can be applied in design of sensors and in modulating nano-photons. Additional important application of nano-FTIR is a study of perovskite materials,[160] which are currently among the most popular materials for photovoltaic cells. They became especially attractive since they reach power conversion efficiency over 20 %. However, under the influence of different external factors such as light, temperature, and humidity, they are prone to organic depletion and structural changes, resulting in the degradation of material properties. Szostak et al. employed nano-FTIR to study single nanoparticles in the organic-inorganic hybrid perovskite (OIHP) film, revealing the process of material property depletion,[160] while Wang et al. applied it to detect formation of intersubband polariton states for the first time in a single nanoantenna (Fig. 13).[161]

View Article Online
DOI: 10.1039/D2CP01458K

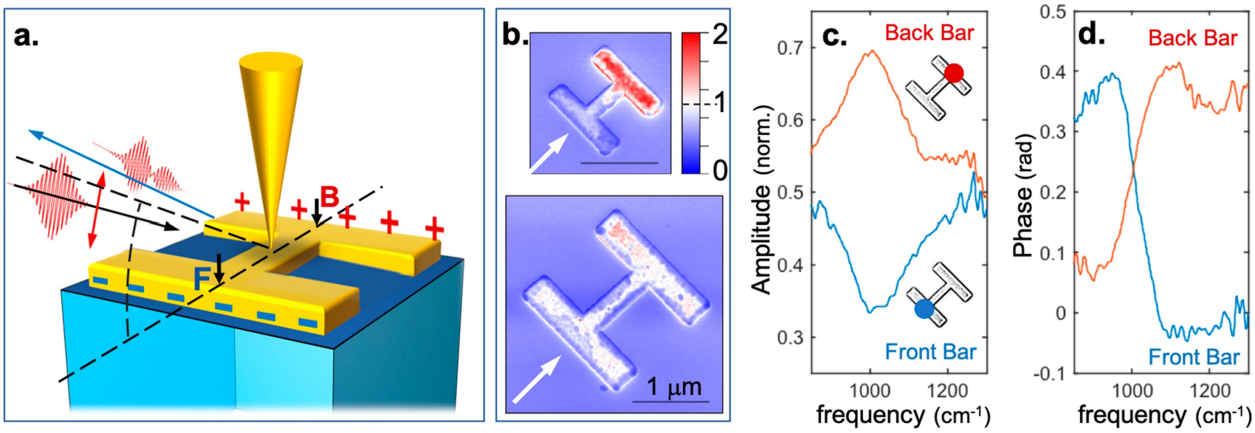

Figure 13: Near-field imaging and nano-FTIR spectroscopy of dogbone nanoantennae. (a) Schematic diagram of the experimental setup with black arrows marking the position of the scattering-type scanning near-field optical microscope probe on the front (F) and back (B) bars. (b) Near-field amplitude images for two nanoantennae illuminated at $1000\,\mathrm{cm}^{-1}$: (top) nanoantenna in resonance with excitation ($\lambda = 950\,\mathrm{nm}$) and (bottom) nanoantenna with the resonance below $1000\,\mathrm{cm}^{-1}$ ($\lambda = 1600\,\mathrm{nm}$). In both images, the scale bars are $1\,\mu\mathrm{m}$, and the scattered field amplitude is normalized to the average amplitude on the gold surface of the nonresonant (bottom) antenna. The white arrows indicate the propagation direction of the excitation beam. Nano-FTIR amplitude (c) and relative phase (d) for the $\lambda = 950\,\mathrm{nm}$ nanoantenna at the front/back (blue/red) bars; positions on the antenna surface where the spectra were taken are marked in insets in part c. Reprinted with permission from Wang et al. *Nano Lett.* **19** (2019) 46204626. Copyright 2019 American Chemical Society.

View Article Online
DOI: 10.1039/D2CP01458K

A continuous and ever growing interest in porous materials leads to development of the rational designs of these materials. Equally important for their utilisation is understanding of mechanisms of their interactions with guest molecules, that govern sorption, confinement and desorption. Being inherently highly sensitive to intermolecular interactions and molecular arrangements and microenvironment, IR spectroscopy provides a unique insight into these processes, especially when combined with other available techniques. Thus, a huge body of literature about applications of IR spectroscopy in investigation of processes relevant for understanding of action of porous materials is available and extensively reviewed.[162–166] Here, only a few representative examples will be presented.

IR spectroscopy is often employed to monitor the occupation of pores of the porous materials, such as metal-organic frameworks (MOF),[167–170] zeolites,[171–174] porous carbons[166,175–177] etc.[178] IR spectroscopy confirmed a successful and controllable preparation of C_{60} encapsulated inside the pores of zeolitic-imidazolate framework 8 (ZIF-8) by solvent-free mechanochemical process.[170] Having large cages and narrow cage-apertures, this MOF cannot accept rigid C_{60} molecules, so the author's approach was to build the cage around the guest molecule. The occupancy of ZIF-8 cavities by C_{60} was quantitatively determined by IR spectroscopy (Fig. 14). Additionally, a combination of measured IR spectra with molecular dynamics simulations show that the fullerene is accommodated in the cage's center and that the cage-to-cage transport is a hardly feasible and energetically unfavored process.[170]

On the other hand, small H_2O molecules, confined in the cavities of MOF, can interact to each other and to migrate between neighbouring voids. However, nanoconfined water shows distinct properties that are markedly different from those of bulk. These unique properties stem not only from the $H_2O\cdots H_2O$ interaction, but also from the interactions between water and the surrounding confining environment. The authors have employed a combination of vibrational spectroscopies (Raman, FTIR, and IR electroabsorption) and a multivariate curve resolution to study the interactions of water within a prototype of pillared layer-type MOFs.[168] Multivariate curve resolution analysis of IR spectra, obtained

View Article Online
DOI: 10.1039/D2CP01458K

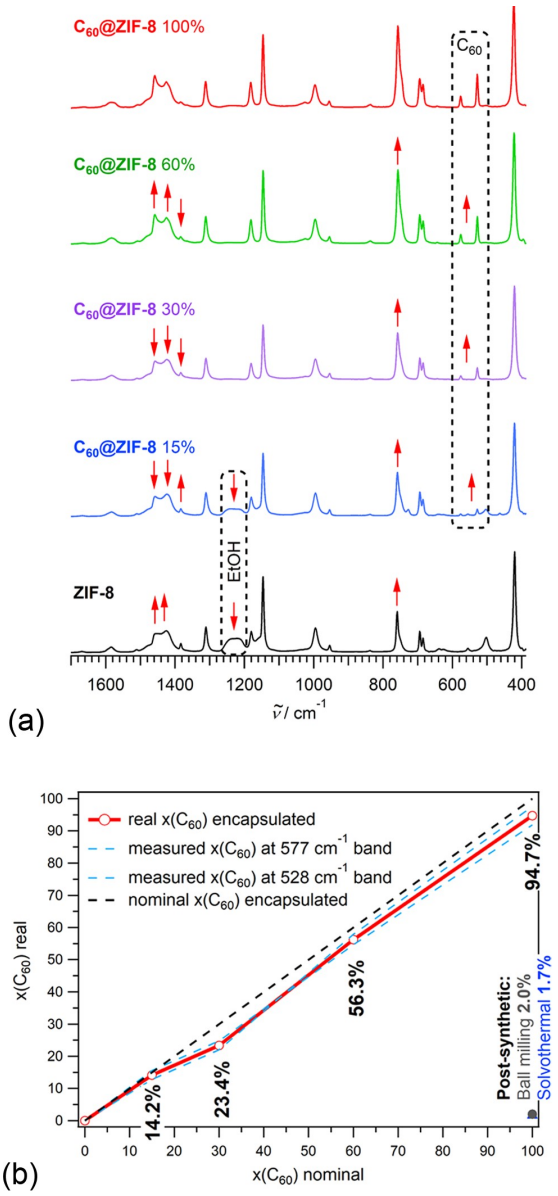

Figure 14: (a) Changes in the experimental IR spectra of ZIF-8 occurring due to encapsulation of C_{60}. Features due to the dynamic relation of C_{60} and EtOH are framed by dashed rectangles. (b) Efficiency of mechanochemical C_{60} encapsulation by ZIF-8. The postsynthetic loading attempts were done in excess of fullerene but resulted in low loading of ZIF-8 (black and blue points in the lower right corner). Reprinted with permission from Martinez et al. *Chem. Mater.* **32** (2020) 10628–10640. Copyright 2020 American Chemical Society.

View Article Online
DOI: 10.1039/D2CP01458K

by monitoring of water desorption from MOF allowed accurate distinction of the MOF's carboxylate vibrational modes of the water-filled and empty nanopores, respectively, and a quantification of these pores. Furthermore, IR electroabsorption measurements showed that the hydrogen-bonding interaction with confined water has little impact on the response to electric fields of the MOF's vibrational modes.

In another example, scattering-type scanning near-field optical microscopy (sSNOM) combined with nano-FTIR spectroscopy was employed to reveal the vibrational characteristics of the systems where large molecules are encapsulated in MOF.[169] Probing individual MOF single crystals, the authors pinpoint the local molecular vibrations, thus shedding a new light on the host-guest interactions at the nanoscale (Fig. 15). Their strategy not only confirms the successful encapsulation of luminescent guest molecules in ZIF-8, but further provides a new methodology for nanoscale-resolved physical and chemical identification of wide-ranging framework materials and design of porous systems for highly sophisticated applications.

Phase Transitions

Although phase transitions are already addressed in previous section, the importance of these processes and understanding of underlying mechanisms require a special consideration. During a phase transition of a given system, certain properties change, often discontinuously, as a result of the change of external conditions, such as temperature, pressure, or others. These macroscopically observed changes are caused by microscopic, molecular-level processes. Thus, the understanding of microscopic background of phase transitions is an important objective, addressed by numerous methods, including, of course, IR spectroscopy in all of its incarnations. All the applications of IR spectroscopy to monitor phase transitions would be itself too wide a topic to be considered here in its entirety, and specific aspects of this enormously broad topic are discussed in other available reviews.[179–183] On the other

View Article Online
DOI: 10.1039/D2CP01458K

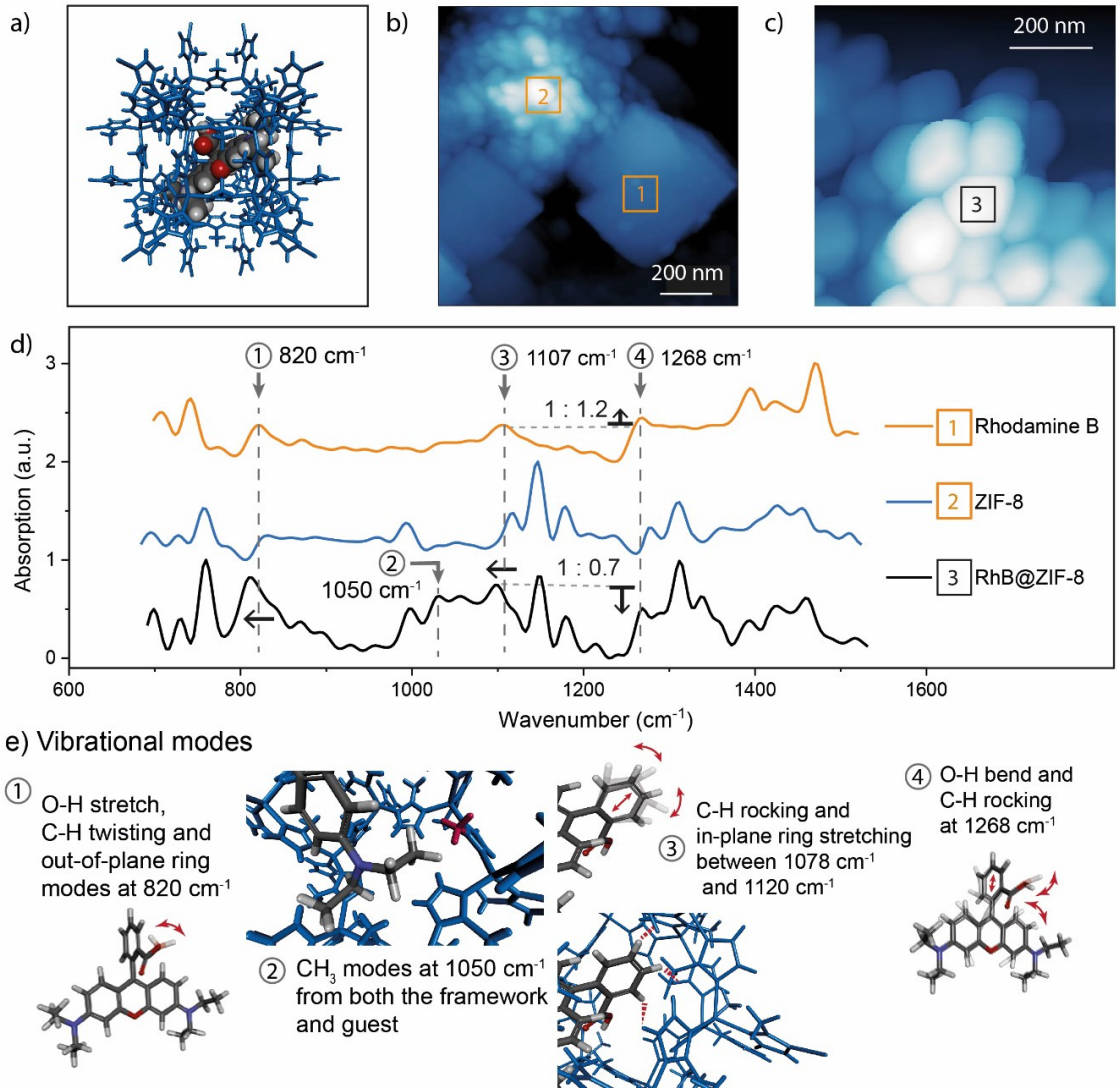

Figure 15: Vibrational analysis of rhodamine B (RhB) and ZIF-8 via nano-FTIR and DFT calculations. (a) Schematic representation of the Rh@ZIF-8 composite, depicting a RhB guest molecule being encapsulated in the pore of the ZIF-8 host framework (in blue). (b) AFM image of the as-synthesised sample containing two distinctive phases: (1) RhB and (2) ZIF-8 showing the positions where IR spectra were recorded. (c) AFM image of a single-phase sample of ZIF-8 nanocrystals adsorbing RhB. (d) nano-FTIR spectra determined at the designated locations on the AFM image. (e) Vibrational modes of the RhB@ZIF-8 composite illustrating the interactions between the ZIF-8 host framework and the RhB guest.Reprinted with permission from Möslein et al. *Nano Lett.* **20** (2020) 7446–7454. Copyright 2020 American Chemical Society.

View Article Online
DOI: 10.1039/D2CP01458K

hand, phase transitions are occasionally discussed thorough this text. Thus, this section will be focused exclusively to a few, readily accessible and easy-to-perform approaches.

It was shown that a simple analysis of variation of IR baseline absorption of spectra obtained in transmission mode with respect of the perturbation applied to the observed sample bear information on perturbation-induced phase transition. It is well known that the baseline of the perturbation-dependant transmission IR spectra varies by application of the perturbation. However, the obtained raw spectra are usually corrected before further analysis, i.e. baseline is usually subtracted from them. The rationale of the developed method lies in the fact that the IR baseline appearance is a direct result of optical properties of the sample and therefore can not be automatically excluded without taking care of the sample nature. The concept was confirmed for variable temperature transmission IR spectroscopy, but it is generally applicable for perturbations other than temperature. In the first study dealing with this problem, phase transition temperatures were determined by 2D correlation analysis,[184] by using the whole IR spectrum, including temperature-induced baseline variations being included.[185] However, a primary cause of noticeable spectral changes remained unclear. This problem was resolved by Zimmermann and Baranović, who performed a simple analysis of temperature-induced variation of baseline, compared this approach with results as obtained by 2D correlation analysis, and shown that IR spectroscopy can be applied for a rapid determination of conditions at which phase transition occurs.[186,187] In practice, baseline absorption was taken from raw (as-recorded) spectra as absorbance at an arbitrary chosen wavenumber, assumed to be free of sample absorption, most often in the $2800 - 1800\,\mathrm{cm}^{-1}$ region. Then, a simple plot of baseline absorbance vs. temperature (or more generally perturbation) indicates temperatures at which phase transitions occur (Fig. 16). In the paper, which introduces the method, the concept was applied to several systems, namely phenanthrene, trans-4-haptylcyclohexanecarboxylic acid, benzo[a]pyrene and a series of phenylacetylenes.[186] Additionally, the simple measurement of baseline absorbance were compared with 2D correlation analysis,[185] which proves the equivalency of the obtained

View Article Online
DOI: 10.1039/D2CP01458K

results.

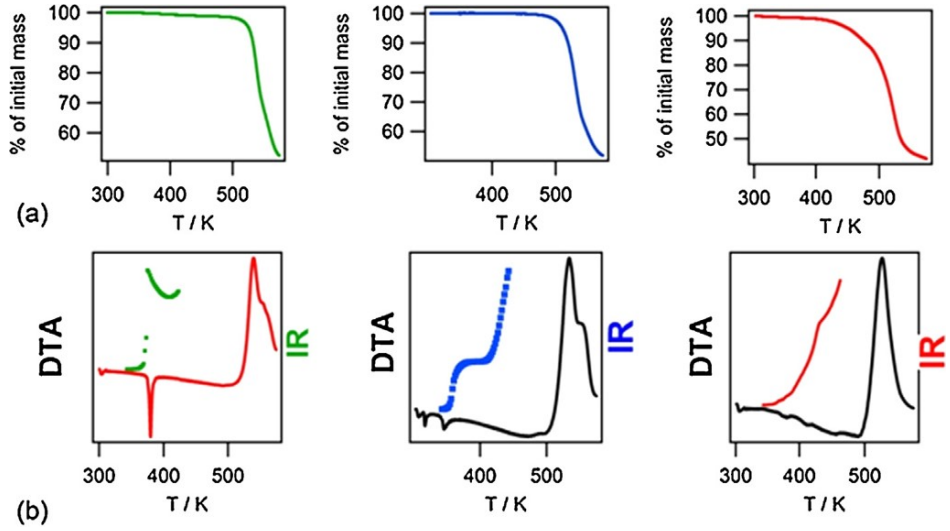

Figure 16: Thermogravimetry, TG (a), and (b) differential thermal analysis, DTA (black lines) with temperature-dependent IR baseline variation (coloured dots) of oligomeric picrates, as measured at 2000 cm^{-1}. Reprinted with permission from Tomašić et al. *Thermochim. Acta* **569** (2013) 25– 35. Copyright 2013 Elsevier.

The methodological easiness and accuracy of the important data provided by a simple measurement of baseline absorbance makes this method highly applicable in determination of conditions that induce phase transitions. For this reason, it is somewhat surprising that this method has not come into a wider use, and the literature in which it has been applied is limited to a very narrow circle of authors.[187–195] Beyond its original use to detect temperature-induced solid-solid phase transitions, the method found its use in monitoring of isothermal crystallization of cocrystalline phase from the melt.[194] Additionally, the temperature-dependant baseline measurements, together with changes in spectral features of a series of picrate surfactants indicate a phase transition, not evident from DSC or DTA measurements, thus indicating an adiabatic phase transition, which causes change in optical, and not thermal properties of the sample. This finding is important in light of the ability of IR spectroscopy to detect phase transitions invisible for thermal methods (Fig. 16).[192]

View Article Online
DOI: 10.1039/D2CP01458K

Gas Sorption and Desorption

In general, the rationale of adopting spectroscopies for investigation of the sorption behavior of materials lies in the wealth of information at molecular level, unavailable when relying on purely gravimetric data. In practice, IR spectroscopy is applicable for monitoring evolution of both gaseous and solid products, including parameters of diffusion, which will be discussed in separate section.

It should be pointed out that qualitative and quantitative changes of both gaseous and solid phase, involved to processes of gas sorption and desorption can be monitored by IR spectroscopy. Experimental setups for IR spectroscopy of solid samples are discussed thorough the text. Although they are in general applicable for monitoring of changes in solid materials by gas sorption or desorption, there are numerous examples of advanced dedicated setups tailored for specific problems.[152]

A variety of cells for IR spectroscopic analysis of gases are commercially available. Effective pathlengths of IR light through the gaseous sample varies from a few centimeters to several meters. the longer pathlengths are usually obtained in compact cells by providing reflective internal surfaces, so that the beam effectively passes many times through the sample before exiting the cell. Very often, FTIR spectrometers are coupled with thermogravimetric balance. Such a setup enables accurate chemical identification of gaseous products of thermal decomposition. Besides these, commonly used equipment, there are numerous examples of more specific setups that meet particular, more complex requirements. For example, online monitoring of gases in industrial processes is an ambitious task due to adverse conditions such as mechanical vibrations and temperature fluctuations. To meet these conditions, Köhler et al. designed a compact gas measurement system, that combines the advantages of conventional FTIR spectrometers with a static single-mirror. The setup works in range from 650 to 1250 cm^{-1} at measurement rates of up to 200 Hz. Additionally, the use of gas cell that allows optical pathlength of up to 120 cm, gases in the low ppm range can be accurately quantified.[196]

View Article Online
DOI: 10.1039/D2CP01458K

The experimental protocol for quantitative IR measurements of gas sorption by solid materials is described in details by Drenchev et al.[16] The procedure and the power of the technique is demonstrated by water-enhanced CO_2 adsorption on a metal-organic framework UiO-66. For this purpose, a custom-made system, consisting of a combination of high- and low-temperature sample cell, was designed. For high-temperature measurements, the KBr pellet with sample is placed in a mobile holder that enables transition of the sample from heating zone (furnace) to IR beam. The cells also provide the possibility of fixing the pellet in an intermediate position, allowing an easy acquisition of the background spectrum while cooling the sample down to room temperature. Low-temperature measurements were enabled by fixing the sample, surrounded by a a Dewar filled with liquid nitrogen, in a position on the path of the IR beam. In order to prevent the condensation of water vapor on the outside walls of the system, a water circulating system is built between Dewar and cell windows (Fig. 17). The adsorption efficiency was measured by monitoring the absorbance of a band due to adsorbed CO_2 vs. the total amount of introduced CO_2. On the other hand, monitoring of the ν(OH) envelope enabled response of the UiO-66 to adsorption of CO_2. Additionally, the results of IR spectroscopy indicated the enhancement of the CO_2 adsorption by water.[16]

Due to the importance of the process, publications focused on IR monitoring of sorption of CO_2.[197–207] or methane[208–211] by solids are numerous. In principle, qualitative or semi-quantitative monitoring of the changes in solid samples due to gas sorption does not require any additional accessories. For example, it is well known that product of decomposition of ammonia borane, as obtained by its heating at 150 °C show an increase of the mass when exposed to air. Biliškov et al. have observed this system by time-dependent IR spectroscopy.[75] They used a simple transmission to monitor the changes due to air exposure of the thermal decomposition products of ammonia borane, obtained by its heating to 125, 150 and 200 °C. While the low-temperature product did not show any changes, the products obtained at 150 and 200 °C show significant changes, reflected in increase of the mass, as well as absorption of both ν(NH) and ν(BH) envelope. However, the authors did not further

View Article Online
DOI: 10.1039/D2CP01458K

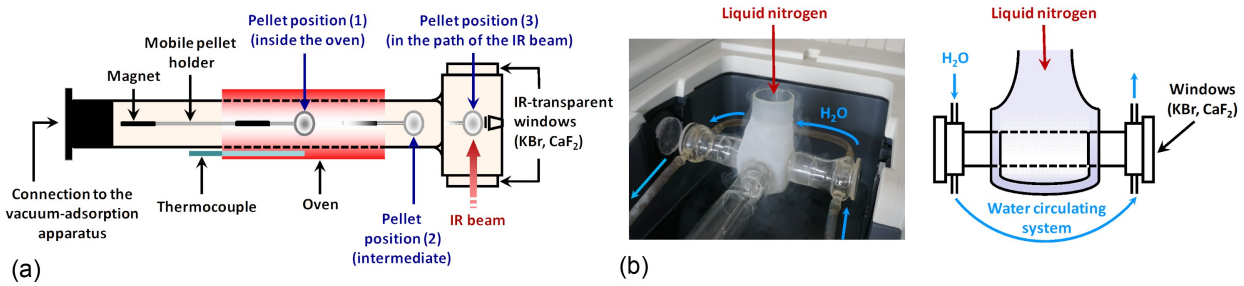

Figure 17: Simple horizontal glass IR cell for adsorption studies. (a) Scheme of the cell. The sample pellet is put into the holder which can be moved along the cell with a ferrite block magnet. Position (1) is in the sample oven and allows thermal treatment. Position (2) is intermediate and allows tempering the sample and registering background immediately before registering the sample spectrum. In position (3), the sample is fixed perpendicularly to the IR beam for taking spectrum. To ensure transmission of the IR beam, the cell is equipped with IR transparent windows. The cell can be connected to a vacuum/adsorption device. (b) When the sample is fixed in a position on the path of the IR beam, it is surrounded by a Dewar which can be filled with liquid nitrogen. Between the Dewar and the cell windows there is a water circulating system aimed at keeping the temperature of the window enough high (to prevent condensation of water vapors). Reprinted with permission from Drenchev et al. JOVE (2020) doi: 10.3791/60285.

investigate the system, leaving the results on a level of interesting observation.

IR spectroscopy is also frequently employed to investigate materials for chemical solid-state hydrogen storage. In this regard, only physisorptive processes will be addressed here. However, only a weak interaction of H_2 with metal organic frameworks and other porous or low-dimensional solids is responsible for its physisorption. Thus, IR spectroscopy is here only of limited use, mainly oriented to second-order effects of hydrogen sorption. Actually, there is only one example where IR spectroscopy was employed for direct measurement of the changes due to the H_2 physisorption, namely monitoring of hydrogen and deuterium sorption by lithium-intercalated fulleride $Li_{12}C_{60}$. In this case, IR spectra indicate that physisorption is only apparent, and chemisorption is actually responsible for successful holding of H_2 in this system. Namely, only a minor part of absorbed hydrogen is present in ionic hydride LiH, while the major part is covalently bound to C_{60}.[212] The other types of materials for solid-state hydrogen storage, where hydrogen is chemically bound through covalent interaction, will be addressed together with other thermal decompositions.

View Article Online
DOI: 10.1039/D2CP01458K

Beyond the common materials, the use of IR spectroscopic monitoring expand to complex materials, such as gas-processing metalloenzymes in action.[213] In a perspective publication, the author introduces ATR-FTIR for the analysis of gas-processing metalloenzymes like cytochrome c oxidase, nitrogenase, and hydrogenase. In this respect, IR spectroscopy provides information about the geometry and redox state of the catalytic cofactors, the protonation state of amino acid residues, the hydrogen-bonding network, and protein structural changes. For this purpose, the gas exchange and deuteration experiments exploring the reactivity of these enzymes with their natural reactants were monitored. This approach allows recording sensitive steady-state difference ATR-IR spectra with time resolution on the level of seconds. The author also noted that IR spectroscopy allows investigation of the protein samples under biologically relevant conditions, that is, at ambient temperature, ambient pressure, and in the presence of liquid water.

Besides gas sortion processes, IR spectroscopy is frequently employed for investigations of sorption of various liquids and solids. Among sorption of liquids, probably the most important process is confinement of water in porous matrices.[214–224] Sorption of solids by encapsulation is also frequently investigated by IR spectroscopy.[170,225–229]

Surface Processes

Surface can be generally defined as a thin layer of a substance at the boundary of contiguous bodies, media, or phases. Surface phenomena arise from the excess free energy of the surface layers and from the special features of the layer's structure and composition. They may be purely physical, or they may be accompanied by chemical transformations. The molecular nature and properties of a surface may be radically altered as a result of the formation of surface monomolecular layers or polymolecular films. These changes usually result from adsorption, surface diffusion, spreading of liquids or from the chemical interaction of components of the contiguous phases. Evidently, any modification of the surface layer causes

View Article Online
DOI: 10.1039/D2CP01458K

a change of molecular interaction between contacting phases. From the chemical point of view, physical or chemical transformation of surface layer strongly affect the nature and rate of various highly important heterogeneous phenomena, like adsorptions, as well as corrosive, electrochemical, catalytic, and membrane processes. For these reasons, the interest in detailed understanding of the microscopic background of surface and interface phenomena is ever rising and various experimental techniques are employed in this field.

Structure and properties of the surface, including the presence of the exposed functional groups responsible for intermolecular contacts with adsorbed species, is crucial for understanding of surface phenomena. For this reason, it is of high importance to characterize the surface at the molecular level. IR spectroscopy was one of the first techniques employed for the characterization of surface phenomena, especially heterogeneous catalysis, and still its popularity does not fade. Actually, among all the available optical spectroscopies applied in this respect, IR spectroscopy is by far the most used. Thus, it sounds paradoxically that IR spectroscopy in general is not surface sensitive, but it may be made so by applying a proper experimental geometry. In particular, due to its high sensitivity to intermolecular interactions, it is able to differentiate between free molecules in gas or liquid phase and adsorbates bound to solid surface. Raman spectroscopy is also frequently utilised to investigate the surfaces,[230] especially in the case of phenomena out of the reach of IR spectroscopy.[231]

Regarding the techniques used for acquisition of spectral information, ATR is frequently thought to be applicable for spectroscopic characterisation of surfaces. However, strictly speaking, this technique does not specifically address the very surface, since the evanescent wave penetrates a few micrometers inside the sample.[100,102] Thus, the ATR spectra consist of unresolved information on surface and near-surface layer of the sample. Although in principle all the external reflection techniques are useful for investigation of surfaces, RAIRS and a variety of its derivatives is privileged. However, regardless this critical review, the variety of surface phenomena allows the use of all available and combined techniques to obtain high-quality spectroscopic information, of course depending on the nature of the sample to be

View Article Online
DOI: 10.1039/D2CP01458K

probed and what the researcher is interested in.

Geometry of the RAIRS experiment is conceptually simple, and it relies on collection of the IR light reflected by a an optically flat, mirror-like surface, thus making RAIRS highly specialized technique. The samples, which are typically monolayers adsorbed on a small area, yield weak IR signals, thus requiring attempts to improve the intensities, for example by using multiple-reflection arrangements. Despite these difficulties, RAIRS is particularly useful for characterization of the systems with low surface area, as well as to investigate adsorption of gas/solid and liquid/solid interfaces,[232,233] by providing accurate information on intermolecular interactions, and additionally the bonding geometry of adsorbates.[234–243] Actually, the pioneering application of RAIRS was to investigate the adsorption of carbon monoxide on metal films.[244,245] Additionally, application of the polarization modulation is frequently used to improve signal-to-noise ratio and to discriminate between adsorbed and free surrounding molecules.[246,247]

Heterogeneous Catalysis on Metal Surfaces

Understanding of the adsorption of small molecules to surfaces of transition metals is an important prerequisite for rational design of new materials with improved catalytic properties. Since the adsorption geometry might critically affect the ability of the surface to activate the selected chemical bonds, it is important to investigate sorption to a particular crystal plane. It is clear that in dealing with such problems, the full power of RAIRS technique comes to the fore. Dependence of intramolecular vibrational frequency of adsorbates on site of their adsorption on the surface of the metal is well documented.[248–251] This reflects weakening or strengthening of a particular bond with respect of the interaction with surface, which is in turn of crucial importance for understanding of catalytic action of the metal. Recent examples of studies focused on this issue include adsorption of acetophenone or carbon monoxide on Pt(111),[238,239] methane on Pt(211) (Fig. 18 a),[252] acetic acid on Ni(110)[240] or titanyl phthalocyanine on Au(111) surface.[243]

View Article Online
DOI: 10.1039/D2CP01458K

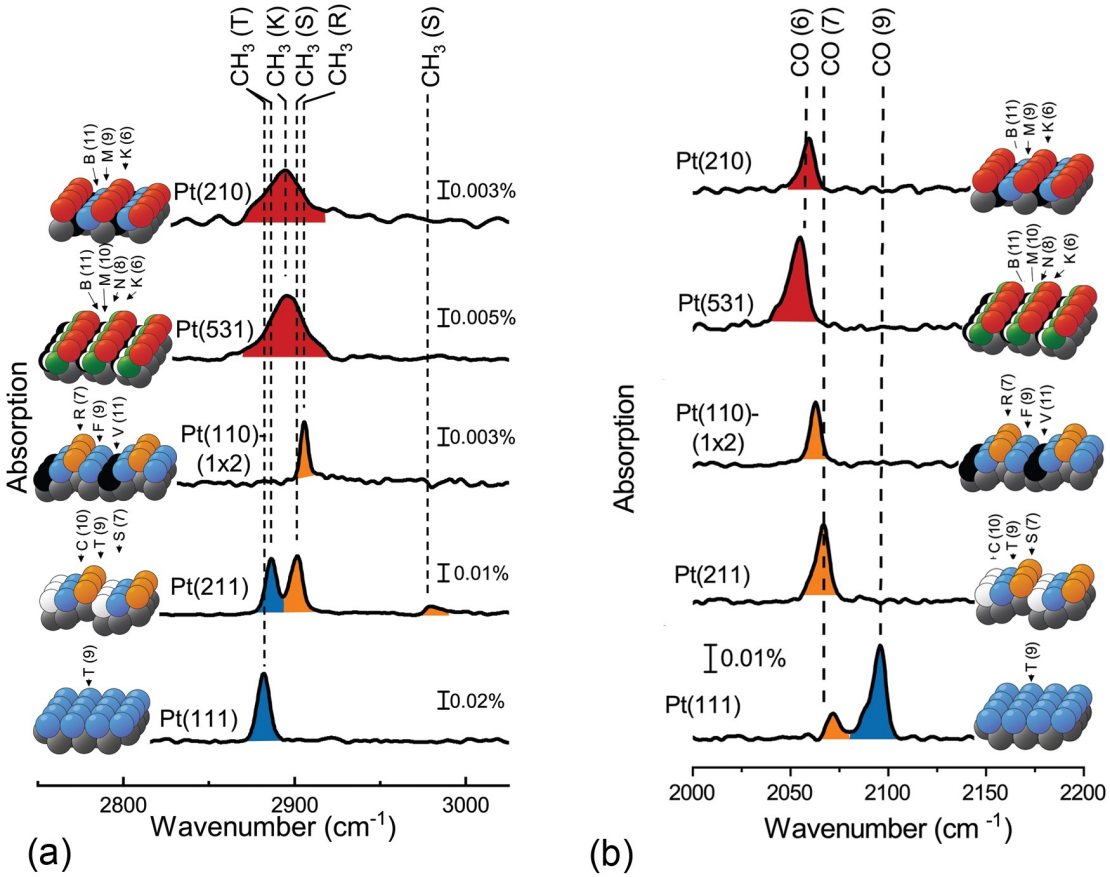

Figure 18: RAIRS detection of (a) methane and (b) CO dissociation products on specific Pt planes at T_s = 120–150 K with incident kinetic energies E_{KIN} = 62–65 kJ mol^{-1}. The vibrations of products adsorbed on terrace (T), step (S), ridge (R), corner (C), and kink (K) sites Pt are indicated by the color code. The coordination numbers of the different surface sites are given in parentheses. Adapted with permission from Gutierrez-Gonzalez and Beck, *Phys. Chem. Chem. Phys.* **22** 2020 17448-17459. Copyright 2020 Royal Society of Chemistry.

View Article Online
DOI: 10.1039/D2CP01458K

A very illustrative example of the reactive specificity of particular surface site to dissociation of adsorbed species is RAIRS monitoring of adsorption of CO and dissociation of CH_4 on various Pt surfaces, cut along different Miller indices. CO has been widely used to detect and identify the presence of different absorption sites on single crystal metal surfaces due to its large dynamic dipole moment, which leads to highly sensitive surface-site-resolved detection of adsorbed CO by RAIRS (Fig. 18 b).[250,253] Actually, frequency of adsorbed CO is almost linear function of the coordination number of the atom of the substrate, which binds the CO molecule.[254]

Dissociation of CH_4 was also extensively studied by RAIRS.[255–260] It is shown that the adsorbed CO forms terraces on the surface of Pt, which are site-dependent. Fig. 18 (a) shows the three different types of surface atoms on Pt(211), referred to as steps (orange), terraces (blue) and corners (white) with coordination numbers 7, 9, and 10 respectively.[252] It is observed that dissociation of CH_4 on Pt(531) and Pt(210) requires a lower energy with respect of CH_4 molecules on Pt(211) and Pt(110). The broad RAIRS feature, observed on Pt(210) and Pt(531), is due to methane dissociation products adsorbed on the kink sites. Currently, there is no satisfactory explanation why CH_4 dissociation on the kink sites leads to a broader $\tilde{\nu}$(CH) band than for terrace and step sites.

An important advantage of RAIRS is its noninvasivity. Contrary to high-energy electrons or X-rays, the IR radiation does not perturb chemisorption, which allows real time, in-situ monitoring of the product uptake as the sorption proceeds. For example, RAIRS spectra clearly shows the dose-dependent evolution of the adsorbed CH_4 layer on the surface of Pt(211).[252] RAIRS time sequence can be converted into site-specific uptake curves for adsorbed CH_3 as a function of incident dose of CH_4. Thus, RAIRS enables a highly controlled approach for surface-site-resolved studies of dissociation of small molecules on metal surfaces, by providing highly accurate and precise experimental evidence for quantum state-specific reactant preparation and detection of surface-site-specific products. In this way, RAIRS measurements provide a simultaneous information on reaction probability and mechanism,

View Article Online
DOI: 10.1039/D2CP01458K

energy barrier heights and the transition state geometry for dissociation on the different surface sites of a given surface. Thus, these measurements provide valuable information to test first principles theoretical models that aim to describe and predict gas/surface reactivity at the microscopic level including the role of different atoms of the surface of the catalyst, which is of crucial importance for understanding the catalytic action of metals.

Heterogeneous Catalysis on Non-Metallic Surfaces

The interest for surface phenomena is not limited to metals. It is actually of high interest to investigate surface interactions of semiconductive or insulating materials with various molecules. Beyond catalysis, they are also interesting with respect of various applications in energy storage and conversion, molecular electronics, gas sensing etc.

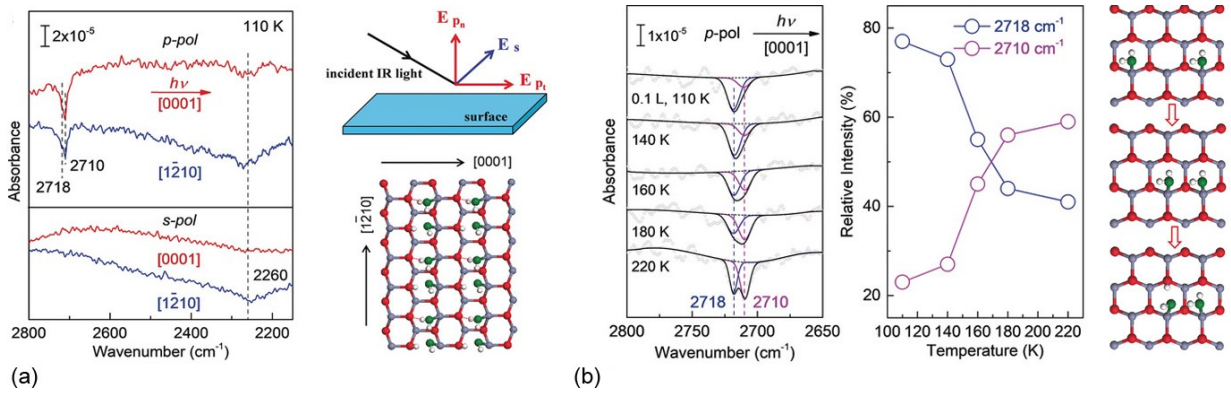

Figure 19: RAIRS spectra of adsorption of D_2O on the ZnO(10$\bar{1}$0) surface at 110 K with DFT-optimized structure of a water monolayer and the hydrogen bonds formed on the non-polar (Zn grey, O_s red, O_w green, H white). All spectra were measured with p-polarized light incident along the [0001] azimuth. (a) Polarization- and azimuth-resolved RAIRS spectra obtained after saturation adsorption. Orientation of the s- and p-polarized components for the incident light are depicted on the scheme of geometry of the experiment. (b) Polarization-resolved RAIRS spectra obtained after exposing the clean surface to D_2O and gradual heating to the indicated temperatures. The averaged data were deconvoluted by fitting individual components with Gaussian curves. The blue and magenta lines illustrate $D_f{}^{16}$OD and 16 O_wD species, respectively. Graph shows relative intensity of OD groups as a function of temperature. Adapted from Yu et al. *Angew. Chem. Int. Ed.* **58** (2019) 17751-17757, published as open access article under CC BY license.

For example, hydration processes at ZnO surfaces are relevant for numerous catalytic

View Article Online
DOI: 10.1039/D2CP01458K

reactions, such as production of CH_3OH from syngas and the water-gas shift reaction, which produces H_2.[261–266] The structural evolution of water on the anisotropic mixed-terminated $ZnO(10\bar{1}0)$ surface was investigated by polarization-, azimuth-, and temperature-dependent RAIRS over a large range of coverages.[261] The combined results demonstrate that the hydration process is rather complex in nature and is initiated by the formation of intact water monomers. The thermally induced diffusion of isolated water molecules leads to the formation of dimer species in which an autocatalytic dissociation occurs via proton transfer to the substrate (Fig. 19). Increase of the coverage by water causes building of an extensive hydrogen-bonded network, including the well-ordered 2D OD/D_2O monolayer, anisotropic water bilayer, and isotropic 3D multilayers. The comprehensive results provide detailed insights into the orientation and strength of hydrogen bonds within the 2D and 3D water networks.

CO_2 adsorption on surfaces of various oxides is another highly interesting surface adsorption reaction. First, CO_2 is an abundant chemical feedstock with wide applications in industry. Second, capture and sequestration of CO_2 has recently received enormous attention. In this respect, alkaline-earth oxides such as CaO were found as promising materials: they are abundant in nature, low-cost, and exhibit high CO_2 uptake and good thermal stability.[137,267,268] Although the formation of $CaCO_3$ from CaO and CO_2 belongs to elementary school chemistry, there is still a great interest in understanding the initial stages of CO_2 adsorption by CaO.[269–271] The RAIRS study of the adsorption of CO_2 to well-ordered CaO(001) films grown on Pt(001) and Mo(001) single crystals was recently conducted.[242] The results show that CO_2 first adsorbs as monodentate carbonate CO_3^{2-}. Its adsorption energy decreases by increased coverage due to agglomeration of carbonates in pairs and chains. However, at high exposures, CO_2 desorbs at considerably higher temperatures corresponding to increased adsorption energy. Temperature-programmed desorption and RAIRS spectra revealed a critical role of residual water in the ultra-high vacuum conditions on CO_2 interaction with CaO. H_2O molecules readily dissociate within the carbonate ad-layer formed

View Article Online
DOI: 10.1039/D2CP01458K

at room temperature. Comparative RAIRS measurements show that surface hydroxyls coexist with carbonate species, thus affecting their adsorption geometry rather than forming bicarbonate. Therefore, surface hydroxyls show the stabilizing effect on the carbonate layer.

Assembly of Adsorbed Molecules

An interesting aspect of adsorption of molecules to surfaces is their orientation with respect of the surface plane. Namely, according to the surface selection rule, only vibrational modes with dynamic dipoles with a non-zero component perpendicular to the surface can be detected by RAIRS. As a consequence, the relative intensities of different vibration bands of a given adsorbate can be used to determine its adsorption geometry.[272–274] For example, RAIRS study of the temperature-induced assembly of methanol molecules on Cu(100), Cu(111) and Cu(110) surface, respectively, show significant spectral changes, most importantly in the ν(OH) band, associated with the structural transformation of the hydrogen bonded CH_3OH clusters. Annealing of the CH_3OH layer on Cu(111) converts the hydrogen bonded chains to cyclic hexamers, whereas this transformation is not fully complete on Cu(100) and Cu(110).[275]

Self assembly of the long-chain molecules is of particular interest, since this can be of crucial importance for tuning their reactivity and rearrangements when adsorbed to a surface. For example, the formation and structure of supported bilayer membranes, on the example of 11-mercapto-undecanoic acid on Au surface, has been investigated using sum frequency generation (SFG) vibrational spectroscopy supplemented by RAIRS.[276] It was found that the tethering of the proximal lipid leaflet resulted in an increase in the conformational order of the self-assembled lipid monolayers. Furthermore, a careful spectroscopic analysis has shown that a better ordered and more biologically relevant lipid bilayer was formed when the distal leaflet was added using Langmuir–Blodgett deposition. In another study, self assembly of the monolayers of peptide nucleic acids on gold surfaces was investigated.[277] A combination of RAIRS with X-ray photoelectron spectroscopy (XPS) allows the authors

View Article Online
DOI: 10.1039/D2CP01458K

to affirm that the structure of the self-assembled monolayers is stabilized by intermolecular interactions through noncomplementary adjacent nucleic bases. The results indicate a tilted rather than normal orientation of the molecular chains, which facilitates hydrogen bonding between neighbouring molecules of nucleic acids, thus stabilizing the structure.

The other examples of IR studies of surface adsorption include larger molecules, like porphyrins,[241] which are essential for their functionality at hybrid interfaces. RAIRS spectroscopy revealed numerous mechanistic details of this adsorption. RAIRS was also used to study the interaction and complex chemistry of relevant molecules on model astrophysical surfaces, like acetonitrile on astrophysical dust grains and ices.[278] Additionally, IR spectroscopy provided important information on environmentally relevant processes, like adsorption of water on nylon, as one of the initial steps of nylon decompsition.[279]

Surface-Affected Chemical Transformations

From the conceptual IR spectroscopy point of view, heterogeneous catalytic reactions are just an upgrade of above discussed surface adsorptions. In situ spectroscopy of heterogeneous catalysis by definition requires simultaneous measurement of catalytic performance to identify the structure and composition of species relevant for catalytic process, as well as evolution of adsorbed species. In other words, while the above text describes processes that generally do not involve significant chemical reactions, in the case of heterogeneous catalysis, the focus shifts precisely to surface-affected chemical transformations. For this reason, RAIRS configuration does not meet all the requirements of the experiment. Thus, it is practically impossible to cover all the ingenious experimental setups in the framework of this review, and here only a few of them will be presented as an illustration. The interested readers are invited to consult more detailed reviews focused on this issue.[3,7,20,280–286]

From the fundamental point of view, in situ approach enables identification of changes and interplay of cluster and nanoparticle structures and compositions during ongoing catalytic reactions, thus revealing how molecules interact with surfaces and interfaces.[20] The

View Article Online
DOI: 10.1039/D2CP01458K

case studies cover the full scale from clusters via nanoparticles to meso-scale aggregates, and demonstrate the benefits of specific in situ methods. Restructuration, mobility of ligands and atoms, as well as evolution of surface composition during the reaction have pronounced effects on activity and selectivity. The nanoscale metal oxide interface steers catalytic performance via a long ranging effect. Combining in situ spectroscopic methods with techniques that enable a controlled modulation of concentration provide further mechanistic insights. The obtained fundamental understanding is a prerequisite for improving catalytic performance and for rational design of catalysts. The examples include CO oxidation reaction, accompanied by dynamic structure changes of $Au_{38}(SR)_{24}$ clusters on CeO_2 (Fig. 20)[287] or Co_3O_4,[288] reformation of methane on Ni/ZrO_2,[289] as well as oxidation of CH_3OH by steam reforming on Pd_2Ga/Ga_2O_3 (Fig. 21).[290]

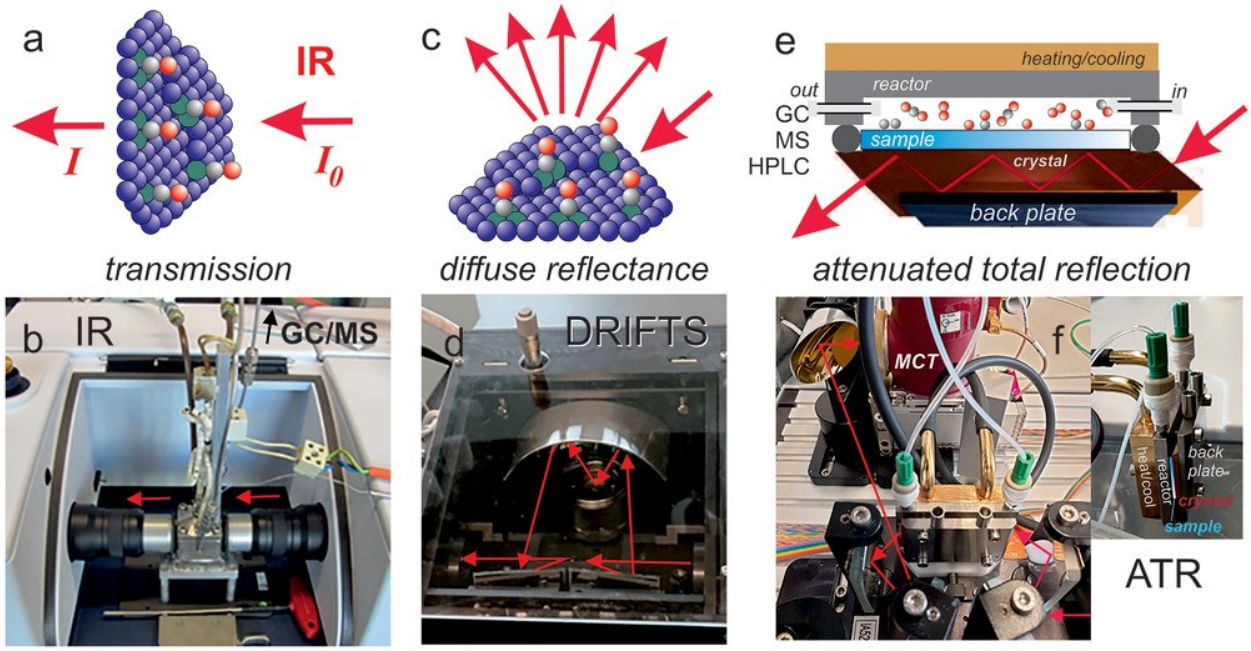

Figure 20: Various IR cells for different geometries of monitoring of catalytic reactions (a) and (b) transmission, (c) and (d) DRIFTS, (e) and (f) ATR mode. Cell design and IR beam paths are shown in the lower row (b,d,f). For transmission and diffuse reflectance, catalyst powders are pressed to pellets or into small crucibles, respectively, for ATR the crystals are coated with thin catalyst films. Reprinted from Rupprechter et al. *Small* **17** (2021) 2004289, published as open access article under CC BY license.

IR spectroscopy is extensively applied in practically all steps of of preparation, treatment

View Article Online
DOI: 10.1039/D2CP01458K

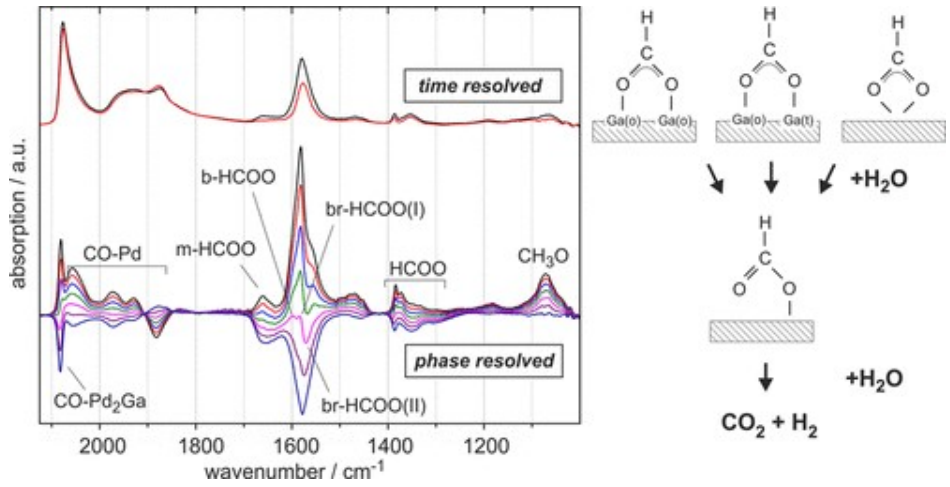

Figure 21: Averaged time-resolved DRIFTS spectra recorded at the end of each half-period of $CH_3OH/CH_3OH + H_2O$ modulation on the Pd_2Ga/Ga_2O_3 surface (top) and corresponding phase-resolved spectra in a phase angle range of 060° calculated using phase-sensitive detection. Schematic representation of mechanistic findings from in situ concentration modulation FTIR are depicted. Reprinted with permission from Haghofer et al. *ACS Catal.* 2 (2012) 2305–2315. Copyright 2012 American Chemical Society.

and utilization of heterogeneous catalysts.[291] For sure, one of the most interesting and important applications of IR spectroscopy in heterogeneous catalysis is monitoring of the catalytic reactions, in order to detect and characterize the intermediates and their evolution across the reaction coordinate, thus enabling a reconstruction of mechanistic details at molecular level.[164,283,292–304] Although the majority of the work is focused on simple compounds, catalytic conversion of complex species are also traced. The examples include catalytic hydroformylation of ethylene on the Rh/Al_2O_3 surface.[305] In this study, the authors applied the rapid-scan technique,[306] which enabled a millisecond-range time resolution, thus providing the resolution of high intermediates, together with kinetic data for individual species (Fig. 22).

DRIFTS technique is also frequently used for monitoring of solid-gas catalytic reactions.[9] One of the chronologically oldest examples is its application to study the oxidation of CO on Rh/Al_2O_3 catalyst.[309] In this study, the catalytic activity was correlated with surface coverage, which leaded the authors toward the conclusion that CO occupies the oxidized Rh sites, which is the predominant intermediate. Further, DRIFTS was accompanied by

View Article Online
DOI: 10.1039/D2CP01458K

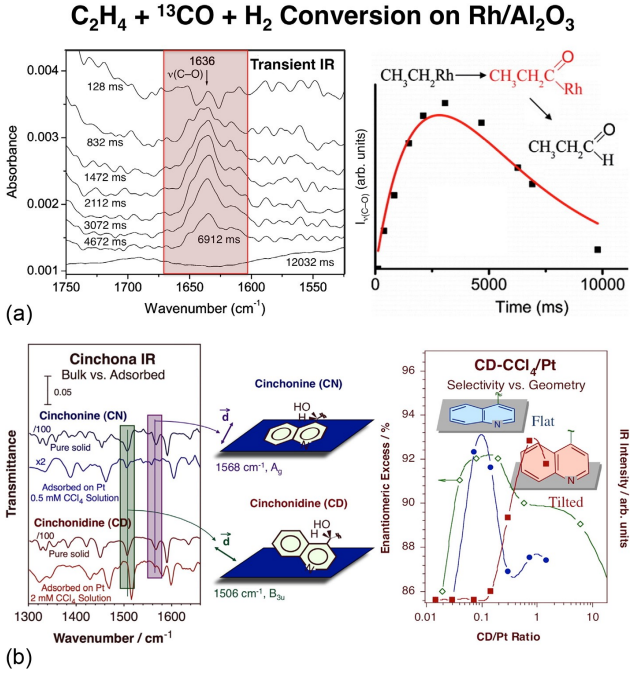

Figure 22: (a) Example of the use of in situ IR to follow the formation and consumption of surface intermediates during catalysis.[305] IR spectra acquired at different times after the start of an ethylene hydroformylation reaction promoted by a Rh/alumina catalyst and plot of the peak signal intensity of that feature as a function of time to show its transient nature and to calculate the kinetic parameters of the reaction. (b) In situ IR characterization of the adsorption geometry of chiral modifiers from solution onto platinum surfaces, and correlation with their catalytic modification efficiency. Left: Low and high coverage spectra for cinchonine (CN, top) and cinchonidine (CD, bottom).[307] Center: Orientation of the aromatic ring of the adsorbed molecules relative to the surface plane, estimated from the relative intensities of the different peaks in the IR spectra [39]. Right: correlation between ring orientation and the enantioselectivity excess obtained during the hydrogenation of ethyl pyruvate.[308] Optimum performance is seen at the intermediate CD concentrations that favor adsorption with the aromatic ring flat on the surface. Adapted from Zaera, *J. Catal.* **404** (2021) 900-910, published as open access article under CC BY license.

View Article Online
DOI: 10.1039/D2CP01458K

gas chromatography with mass spectrometry to understand the selectivity of H_2 in preferential oxidation process on Au/Fe_2O_3 catalyst.[310] Another interesting example includes an innovative design of DRIFTS cell, which minimize dead volume, thus providing a faster and more reliable response to changes in gas composition (Fig. 23).[311] It is utilised to investigate CO oxidation on Pt/CeO_2 catalyst by time-resolved spectroscopy using a steady-state isotope transient kinetic analysis. DRIFTS, in combination with multiple-reflection IR gas cell, was applied to investigate photocatalytic oxidation of ethanol to acetone on nanocrystalline TiO_2. This study has shown a formation of both formate and acetate intermediate on the TiO_2 surface, while acetaldehyde is formed in gas phase.[312]

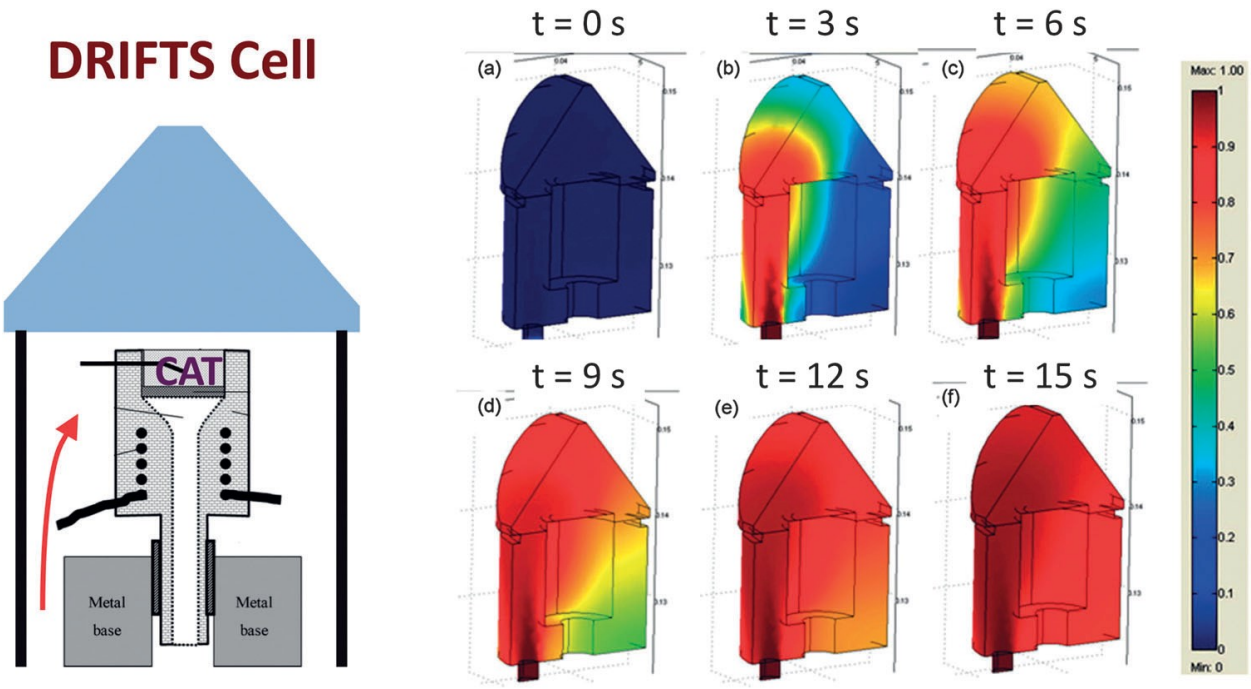

Figure 23: Schematic representation of a high temperature/high pressure DRIFTS cell design for homogeneous flow through the catalyst in short time periods[311] and flow dynamics images acquired for the distribution of gas in the volume of the DRIFTS cell as a function of time. Reprinted with permission from Zaera *Chem. Soc. Rev.* **43** (2014) 7624-7663. Copyright 2014 Royal Society of Chemistry.

A more challenging issue is to apply IR spectroscopy for monitoring of heterogeneous catalytic reactions in liquid medium.[313] However, in this field it is crucial to minimize the path of the IR radiation through the solvent, and here the strengths of the ATR technique

View Article Online
DOI: 10.1039/D2CP01458K

come to the fore.[314–316] The illustrative example is so-called Orito reaction, where enantioselectivity of hydrogenation of α-keto esters is promoted by Pt. In situ IR monitoring of this reaction has shown that the adsorption geometry changes with surface coverage, which is related to concentration in solution. The optimal configuration of the adsorbed cinchona is that when the aromatic rings are oriented parallel to the surface, which is enabled at low concentrations. Tilted orientation, obtained at higher concentrations, is detrimental to enantioselectivity of the catalytic process (Fig. 22 b).[308,317]

Electrochemical Processes

A very interesting application of ATR IR spectroscopy is its utilisation to investigate the processes relevant to water splitting.[2] Since the catalycally active layer can be grown on the top surface of ATR crystal, this technique provides a robust and stable platform for in situ monitoring of the relevant catalytic processes (Fig. 24). The rationale of the method lies in the fact that the incident radiation, totally reflected on the interface between ATR crystal and sample, partially penetrates into the sample by the evanescent wave, and the typical depth of penetration is $\sim 2\,\mu m$. This is deep enough for acquisition of the spectroscopic information on the layer of the solution in contact with catalytically active layer. Thus, the acquired spectrum contains information on both the thin film of catalyser and on solution in contact with it (Fig. 24 c). The simplicity of the setup provides a potential for its development to a routine method for the characterization of liquid-solid interfaces in water splitting. Two types of setups are developed. The separated setup consists of the sample surface, pressed with the active surface onto the ATR crystal. It was used to study photoelectrochemical cells.[318,319] In another design, the surface to be measured is deposited on top of the ATR crystal, so this is an integrated setup.[2] These setups are, for now, checked on example of hematite-catalysed water splitting reaction.

Surface processes play a crucial role in a number of other important chemical processes, such as electrochemical reactions,[166,282,320] processes on membranes[320–322] and cor-

View Article Online
DOI: 10.1039/D2CP01458K

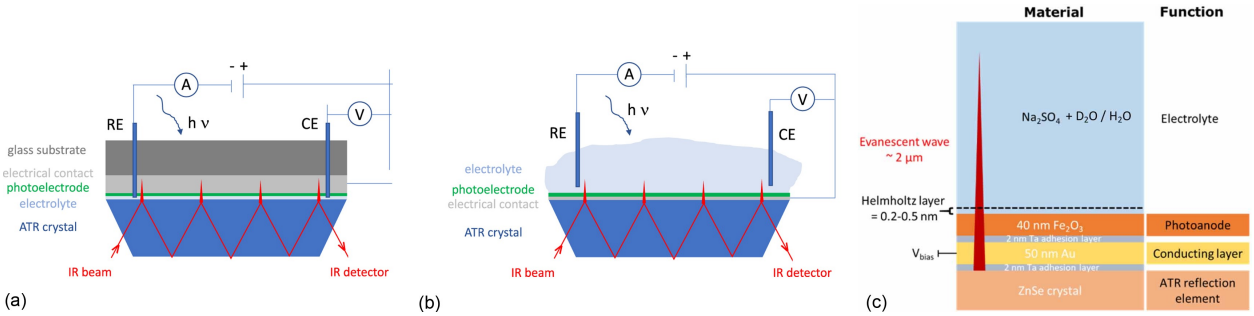

Figure 24: (a) Separated and (b) integrated for setup for in situ ATR-FTIR water splitting measurements. (WE—working electrode, CE—counter electrode, RE—reference electrode, A—ampermeter, V–voltmeter). (c) Sample design and penetration of the evanescent wave in an integrated measurement setup. Adapted from Bieberle-Hütter et al. *J. Phys. D: Appl. Phys.* **54** (2021) 133001, published as open access article under CC BY license.

rosion.[323–325]

Corrosion is natural deterioration a material, which undergoes as a result of interaction of its exposed surface with environment, most commonly atmosphere or water. It is chemical or electrochemical process that converts a material into chemically more stable species such as oxide, hydroxide, carbonate, sulfide etc. Corrosion commonly occurs locally, especially at weak parts of the sample, for instance where grain boundaries and defects are situated, and the nanoscale of initial and localized corrosion makes it difficult to understand and predict,[326] so sensitive techniques with a high spatial resolution are required to investigate the fundamental mechanisms under the hood of corrosion. Among them, IR spectroscopy is especially interesting, since it provides a chemical and structural information on molecular level of corroded surfaces, as well as chemical factor that catalyse or inhibit the corrosion process.[323,327] However, a drawback of the classical IR microspectroscopy is limited spatial resolution, which is nowadays resolved by combining IR spectroscopy with AFM, that overcomes the diffraction limit, hence improving the spatial resolution down to 10 nm.[328] By this approach, it is possible to simultaneously obtain valuable information on nanoscale topography and present chemical species and their evolution. Typical experimental designs involve RAIRS or ATR, and they are presented in Fig. 25. For example, steel corrosion inhibition by polyphosphonates, which is marketed, although not fully understood, was investigated

View Article Online
DOI: 10.1039/D2CP01458K

by combination of RAIRS-AFM and bulk ATR IR spectroscopy.[329] It has been shown that cathodic inhibition dominates at the galvanised steel cut edge in the presence of dissolved strontium aluminium polyphosphate inhibitor, which is caused by rapid precipitation of thick film to cathodic regions. EDX elemental analysis and the AFM-IR technique shown that the rapid formation of a cathodic film is in fact due to the presence of highly soluble strontium carbonate impurities in the commercially available pigment, which leads to the capture of zinc ions in the form of a zinc carbonate layer (Fig. 25 d-e).

Electrochemical processes are of crucial importance for energy storage, conversion, electrocatalysis, photoelectrocatalysis, sensorics and a variety of other applications. Thus, their detailed understanding continuously attracts a vivid research interest. Classical electrochemical methods provide important information about the thermodynamics and kinetics of electron transfer across interfaces, and in many cases enable identification of chemical species via the measurement of redox potentials. However, the molecular information is limited by this classical approach, so additional characterisation tools are needed for a complete picture of physical and chemical processes at interfaces that govern the electrochemical processes. Obviously, there is a huge room in this respect for a variety of applications of IR spectroscopy. It enables not only detection and identification of unknown molecular species but, particularly in the case of solid–liquid interfaces, reveals important, information-rich insights into the nature of surface adsorbates, such as the binding mode, bond strength and molecular orientation.[330]

Various cells for in situ IR spectroscopy, usually based on ATR, are designed to investigate various processes responsible for action of batteries. The examples include cells that enable monitoring of decomposition of lithium sulfide battery electrolytes, compatible with various cathodes and anodes,[331,332] A very important utilisation of IR spectroscopy in the field of lithium sulfide batteries includes chemical identification of polysulfide species.[332,333] For instance, in situ ATR-IR study indicates the evolution of polysulfide species and triflate anion coordination states during cycling.[333] The transport kinetics and the degree of polysulfide

View Article Online
DOI: 10.1039/D2CP01458K

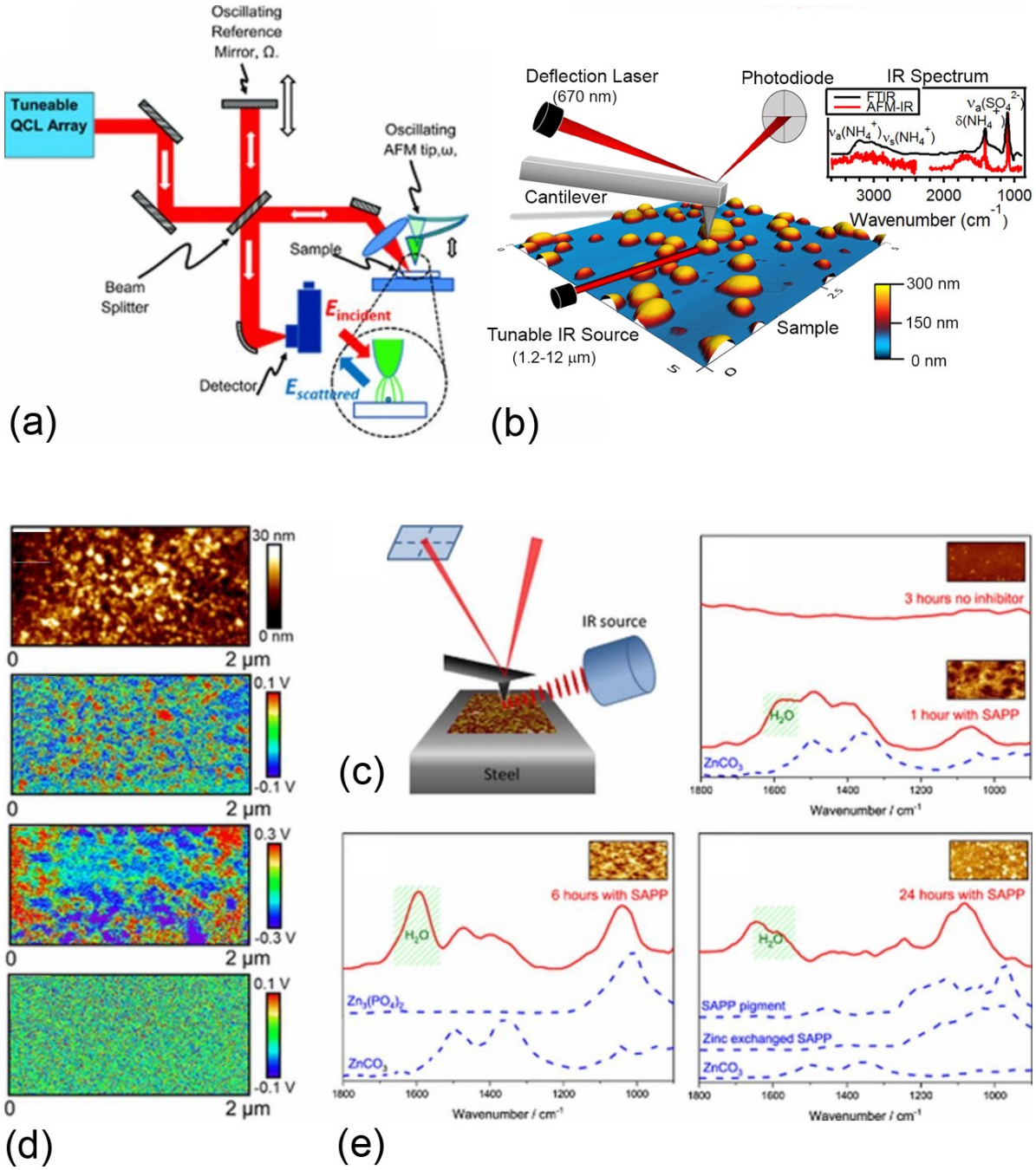

Figure 25: Schematic diagram of (a) scanning near-field optical microscopy (s-SNOM); (b) general scheme of AFM-FTIR (Reprinted with permission from Bondy et al. *Anal. Chem.* **89** (2017) 8594–8598. Copyright 2017 American Chemical Society); (c) The AFM-FTIR setup; (d) Height image of a 100 nm thick microtomed section of epoxy phenolic resin cured with a catalyst at 150 °C for 10 min and corresponding maps of peak-to-peak IR-induced deflection following irradiation at 1116 cm^{-1}; (e) AFM-IR spectra, gathered from the steel cathode after immersion in NaCl with or without the addition of saturated concentrations of an inhibitor (red solid lines). Bulk ATR-IR spectra (blue dashed lines) are shown for comparison. Adapted from Zhao and Johnson *J. Electrochem. Soc.* **166** (2019) C3456, published as open access article under CC BY license.

View Article Online
DOI: 10.1039/D2CP01458K

dissolution in either polymer or ionic liquid electrolytes is clearly demonstrated. Moreover, the authors further pointed out that this in situ IR monitoring has a high potential to be applied in assisting the design of novel functional electrolytes, additives, and new systems for lithium sulfide batteries, such as polymeric and all-solid-state electrolytes. Further, a combination of in situ IR and Raman spectroscopy gives a real-time information of adsorbed species on the interface of the electrode of the a lithium oxide battery system, and reveal the in-depth reaction mechanism on the electrode-electrolyte interface.[320]

The power of surface-enhanced Raman spectroscopy (SERS) ignites the development of analogous IR technique, SEIRS.[330,334] This is especially interesting due to the limitations of the Raman spectroscopy. Although the two techniques share a great deal in common, they are significanly different in their practical implementation, which makes IR spectroscopy the method of choice in a variety of electrochemically-relevant applications. The SEIRS effect is based on amplification of the electromagnetic field due to localised surface plasmons and chemical effects in operation.[334–336] SEIRS allows sub-monolayer detection of molecules adsorbed at surfaces and, as demonstrated by the pioneering work of the Osawa group, can provide a valuable tool for investigating electrochemical interfaces in situ.[335] Although SEIRS is far less powerful than SERS, and for this reason it is not widely applied, the recent developments in surface Raman scattering techniques could in principle be extended to SEIRS, so there is no doubt scope for further innovation.[330] The most common configuration of the electrochemical SEIRS experiment is to use the ATR, with the working electrode deposited as a thin film on the surface of a bevelled prism and the IR beam is reflected off the interior wall of this prism (Fig. 26). In this way, the incident IR beam does not pass directly through the electrolyte solution, but instead the evanescent wave penetrates into solution, thus minimising the losses.[337]

Despite its limitations, that are not yet satisfactory overcame, in-situ IR spectroscopy, especially in its ATR-SEIRS incarnation, where IR beam targets the working electrode,[338–340] is relatively frequently employed to investigate the electrochemical capacitors.[166] Its first use in

View Article Online
DOI: 10.1039/D2CP01458K

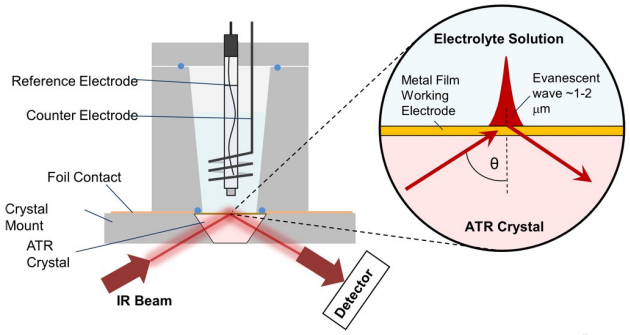

Figure 26: Schematic depiction of ATR configuration commonly employed for electrochemical surface-enhanced IR absorption spectroscopy (EC-SEIRAS). Adapted from Wain and O'Connell *Adv. Phys.* **2** (2017) 188-209, published as an open access article under CC BY license.

this respects was a measurement of ion dynamics of an ionic liquid 1-ethyl-3-methylimidazolium triflate, in a functioning capacitor and RuO_2 as a pseudocapacitor.[338] Since then, it revealed new insights onto the charging mechanism of electrochemical capacitors and clearly demonstrates the role of surface chemistry of carbon electrodes in the charge storage mechanism.[341–343] A very interesting and important application of IR spectroscopy to follow the degradation of battery electrodes include the monitoring of generation of solid electrolyte interface on the surface of anodes of lithium batteries, which supresses cycling thus causing passivation of the battery.[344–349]

Other Examples

2D materials find a wide range of applications in the field of electrochemical devices, since they have large active surface area, they are often semiconductors with tunable band gaps.[350] IR spectroscopy is here especially interesting as a tool for characterisation of phase transformations of the electrodes made of 2D materials, identification and chemical reactions of active sites, as well as characterisation of the role of intercallated species.

Development of efficient procedures for CO_2 capture is initiated by aspirations to reduce its concentration in the atmosphere by chemical or electrochemical methods, and thus to contribute mitigation of climate change by realizing various versions of so called net-zero

View Article Online
DOI: 10.1039/D2CP01458K

energetic scenarios. IR spectroscopy is especially interesting technique in this regard, since it enables elucidation of very accurate information on binding and chemical transformartions of CO_2 molecule on the surface of electrode or catalyser.[17,351,352] For this purpose, ATR mode is ideally suited.[23,353,354] Metal electrodes made of silver, gold or platinum can further amplify the signal, practically enabling SEIRS,[355,356] (Fig. 27) which enabled detailed insight into the mechanism of CO_2 transformations to usable products, through identification and quantification of intermediates.[357–359] Beyond the studies of dependence of metal type to electrocatalytic transformation of CO_2, it is shown that activity and selectivity strongly depends on the exposed surface of the metal.[360–362] Recent advancement of the ATR-SEIRS have led to studies involving the real catalytic systems, apart from the model electrode surfaces. In one of the experiments, Au film was chemically deposited on the basal plane of a hemicylindrical Si ATR element, covered by the layer of Zn.[363] This setup enabled monitoring of the Li-tuned electrochemically Zn-catalysed CO_2 reduction reaction with time resolution of 2 s. Such a high time resolution enabled an accurate detection and quantification of reaction intermediates, thus revealing the mechanism of interfacial reduction of CO_2 to CO at the molecular level.

Diffusion

Recent breakthroughs in the field of solid-state chemistry, especially mechanochemistry and ageing reactions undoubtedly show that solids are much more dynamic systems, more susceptible to mutual chemical changes, compared to the until recently ingrained opinion.

Although examples of such reactions have only recently multiplied, for example unexpectedly fast and furious reaction of NaH with NH_3BH_3[195] (still unexplored by IR spectroscopy), a classical cocrystallization of diphenylamine and benzophenone was only recently thoroughly studied by IR spectroscopy.[194] In this example, eutectic liquid intermediate is responsible for promotion of the reaction by transporting the reactants. To investigate mechanistic details

View Article Online
DOI: 10.1039/D2CP01458K

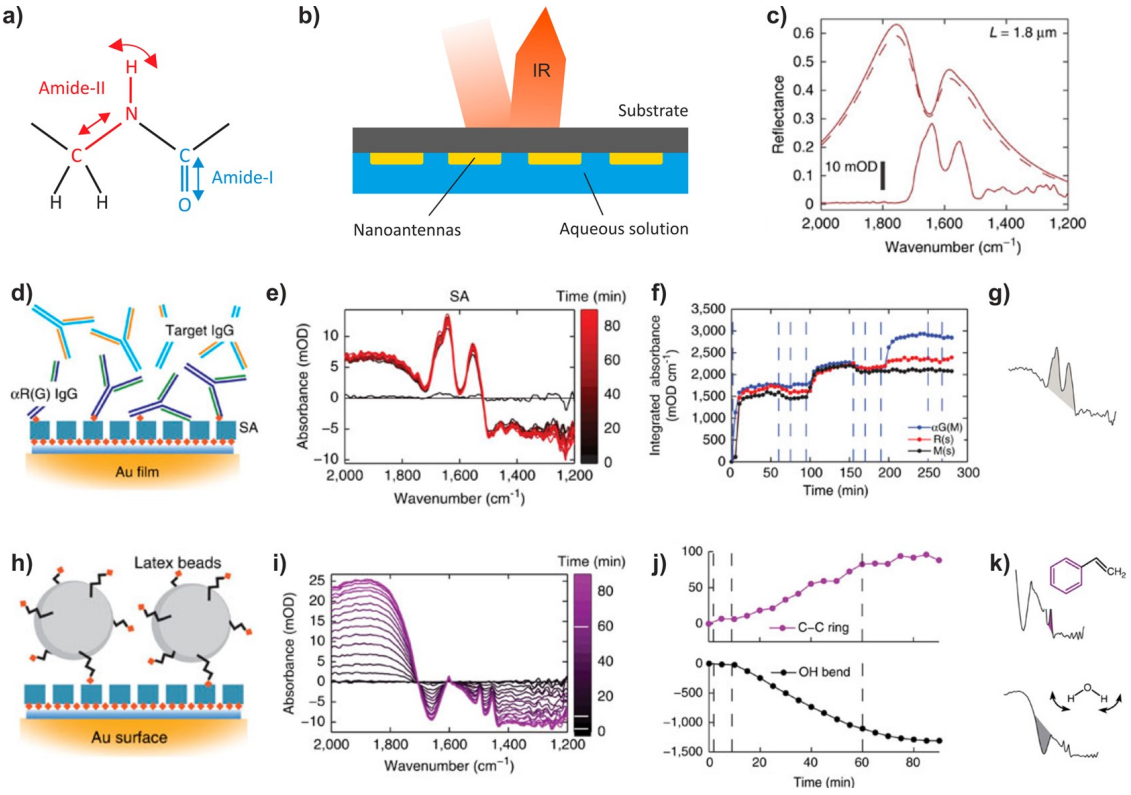

Figure 27: (a) Molecular structure of the amide group and vibrational modes as indicated by arrows. (b) Schematic illustration of the plasmon internal reflection (PIR) (not to scale). (c) Reflectance spectra before (dashed) and after (solid) streptavidin (SA) binding for the $L = 2.2\,\mu$m antenna array sampled in an aqueous media. The absorbance is displayed at the bottom of the panel (solid line) with units indicated by the scale bar. (d) Schematic of protein-binding interactions measured. The gold antennas (Au film) are covered with a self-assembled monolayer of a biotin-labeled alkanethiol (blue and red dots), to which SA binds. They are further functionalized with G(M) IgG, which allows for a selective adsorption of the respective target IgG (see text). (e) Time series of spectra taken during SA. (f) Peak integral (integrated absorbance) evolution over time during the protein-binding measurements for the three samples. Abbreviations are as follows: G(M), antigoat (mouse host) IgG; R(s), rabbit IgG; M(s), mouse IgG. Vertical lines indicate the rinsing process. In all experiments, for each step the protein solution is introduced and allowed to flow for 60 min (first horizontal line). Each step is followed by a 15 min rinse with a detergent (second vertical line), then pure buffer (third vertical line). (g) Amide band peak integral used to assess protein binding. (h) Schematic of the biotin-labeled latex bead ((b)LB)SA binding (compare labeling in (d)). (i) Time-series absorbance spectra during the (b)LB-binding steps. The vibrational features at 1450 and 1490 cm1 are associated with the benzene ring; the vibrational feature at 1650 cm1 originates from the OH vibration in H2O (see also (k)). (j) Evolution of the peak integrals (integrated absorbance, units of mOD (optical density) cm1) over time during (b)LB-binding steps. Vertical dashed lines indicate the rinsing process. (k) Specific chemical structures and their corresponding IR fingerprints (peak integrals) used to monitor their presence during the flow experiments. Reprinted with permission from Neubrech et al. *Chem. Rev.* **117** (2017) 5110–5145. Copyright 2017 American Chemical Society.

View Article Online
DOI: 10.1039/D2CP01458K

of this reaction, an extremely simple experimental setup, consisting of a glass tube vertically placed on the single-reflection ATR element was constructed, which enabled an effective separation of the two sides of the benzophenone-diphenylamine melting phase diagram. IR spectroscopic monitoring enabled a detailed observation of all stages of the cocrystallization process. It consists of a series of mechanisms including molecular diffusion, formation of eutectic phase, and cocrystallization through an amorphous phase. The cocrystallization itself is enabled by continuous feeding of eutectic phase by solvation of the starting phases, which then flow through and combine together in liquid phase. The overall process is evidently driven by hydrogen-bonding interactions of NH···O=C type, while the melting of individual starting phases and their efficient transport through liquid is improved by the difference in conformational flexibility. Isothermal and nonisothermal monitoring shows that the melting of cocrystal and its recrystallization are not single-step processes. By heating, the system passes through an amorphous phase. By cooling, the liquid phase recrystallizes to cocrystal, but this process requires some time, which can be very long. In this respect, more similar IR spectroscopic studies are needed to resolve generalities in solid-state transformations that involve formation of eutectic liquid intermediate. (Fig. 28)

Additionally, IR spectroscopy was employed to monitor the diffusion and transport of low molecular weight compounds and tu provide the predictive thermodynamic description of sorption processes in polymers.[18] The examples include exploration of structure and dynamics of H_2O molecules in polymeric matrices,[364] as well as diffusion of acetone, methyl ethyl ketone and benzene polyethylene,[365] which is aimed to demonstrate the feasibility and accuracy of the ATR measurement of diffusion coefficients.

View Article Online
DOI: 10.1039/D2CP01458K

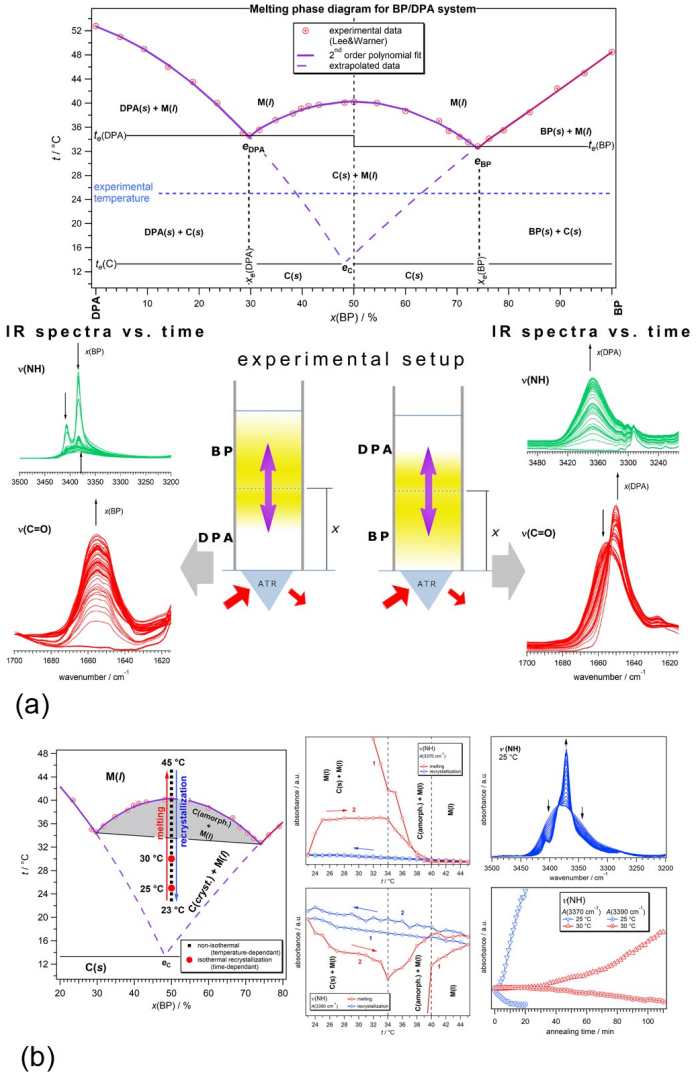

Figure 28: (a) Scheme of the isothermal experiment. Melting phase diagram for benzophenone - diphenylamine (BP/DPA) system. The experimental setup, consisting of a glass tube vertically placed on the ATR element of an IR spectrometer, practically enables a spectroscopic consideration of two separated two-component phase diagrams, which reflect the experimentally observed events along the reaction coordinate. On their contact, the reactants melt and the front of liquid intermediate phase travels along the column in both directions with respect to the original contact surface, as indicated by violet arrows. As a result, IR spectra, here represented by ν(NH) (green) and ν(CO) regions (red) of the corresponding systems, are obtained. (b) Nono-isothermal transmission IR spectroscopic monitoring of melting and recrystallization of the BP/DPA cocrystal. A nonisothermal experiment in the 2345 °C range is denoted by black dots in the phase diagram, while red dots indicate temperatures at which recrystallization was followed over time. The gray region arbitrarily indicates the amorphous phase that precedes melting of cocrystal. Two cycles of nonisothermal melting recrystallization are indicated by the hysteretic temperature dependence of IR absorbances of individual contributions of ν(NH). The same spectral features are followed to monitor the isothermal recrystallization over time. Reprinted with permission from Biliskov *Cryst. Growth Des.* **21** (2021) 1434–1442. Copyright 2021 American Chemical Society.

View Article Online
DOI: 10.1039/D2CP01458K

Other Chemical Processes

Monitoring of thermal decomposition processes is one of the most classical fields of utilisation of in situ IR spectroscopy. The accessories that satisfy the needs for these experiments are now widely commercially accessible from various providers. Most basically, chemical identity of the sample is completely changed upon decomposition, which generally causes dramatic changes of IR spectra with respect of applied perturbation, most commonly temperature. Another perturbation causing decomposition could be presence of reactive chemicals, radiation or time. More generally, decomposition can be defined as a chemical alteration caused by exposure of the sample to environmental conditions over time.

Since the products of decomposition frequently involve gas phase, IR spectroscopy can be used to follow the evolution of both solid and gaseous products. The approach is thus similar to those described for monitoring of gas sorption and desorption processes. Although decomposition can be caused by different chemical and physical agents, thermal decomposition is most widely investigated. The commercially available accessories include variable-temperature ATR plates, heating jackets for transmission measurements, variable-temperature DRIFTS chambers, high-pressure high-temperature cells, TG instruments coupled to IR spectrometers equipped with gas cells etc. The variety of available equipment, together with high flexibility of IR spectroscopy enable accurate IR spectroscopic insight into practically all the chemical processes that involve changes in covalent bonds, hydrogen bonding network and intra- and intermolecular rearrangements governed by various intermolecular interactions. In this respect, a highly helpful review with a throughout discussion of design and characteristics of numberous cells for in situ vibrational spectroscopic reaction monitoring should be emphasized here.[366] The opportunities are practically infinite, limited only by the creativity of the researcher.

In line with this comment, it is clear that it is impossible to cover all the applications of IR spectroscopy to monitor the decomposition processes. This paper will brought only a few illustrative examples, without intention to cover all possible concepts. Actually, surprisingly

View Article Online
DOI: 10.1039/D2CP01458K

low number of reviews on methodology itself are available,[367–369] so the interested reader should itself screen the specialized reviews and primary publications in accordance to his/her field of interest.

The use of IR spectroscopy to monitor non-thermal decompositions and chemical alterations of materials involve the study of UV aging of asphalt involving carbon nanotubes/polystyrene composite,[370] as well as alteration of microplastics,[371] discharge-initiated decomposition of SF_6,[372] and environmental degradation of various real-world materials.[373,374]

The experiments in transmission mode usually require the use of alkaline helogenide matrix material, most commonly KBr. However, in some cases such a matrix can influence the sample, thus one should always take into account this possibility and critically consider the obtained results. One of the relatively recent examples is an investigation of thermal decomposition of ammonia borane NH_3BH_3.[75] In this study, decomposition of NH_3BH_3 was monitored in both transmission and ATR mode, and comparison of the obtained results undoubtedly shows that interaction with KBr significantly affect the mechanistic pathway of technologically relevant thermal decomposition of this material, considered for solid-state hydrogen storage. As usual, KBr pellets were used for transmission measurements, while ATR measurements were done for both neat NH_3BH_3 and $NH_3BH_3 : KBr = 1 : 1$ mixture. While neat NH_3BH_3 shows a two-step decomposition, its mixtures with KBr is a one-step process in the same temperature range (Fig. 29). Although KBr does not affect the chemical identity of NH_3BH_3, it dramatically affects its thermal decomposition, which is especially pronounced by partial solvation of KBr in molten highly polar NH_3BH_3. Additionally, thermally induced dimerization of NH_3BH_3, crucial step in its decomposition, is evidently promoted by ionic species such as KBr.

In another study, thermal decomposition of a series of derivatives of NH_3BH_3, namely $Li_2Ca(NH_2BH_3)_4$ and $Na_2Ca(NH_2BH_3)_4$, was monitored by transmission IR spectroscopy, supported by mass spectrometry for evolved gas analysis.[195] From Fig. 30, it is evident that $Na_2Ca(NH_2BH_3)$ decomposes through a two-step mechanism, while $Li_2Ca(NH_2BH_3)$

View Article Online
DOI: 10.1039/D2CP01458K

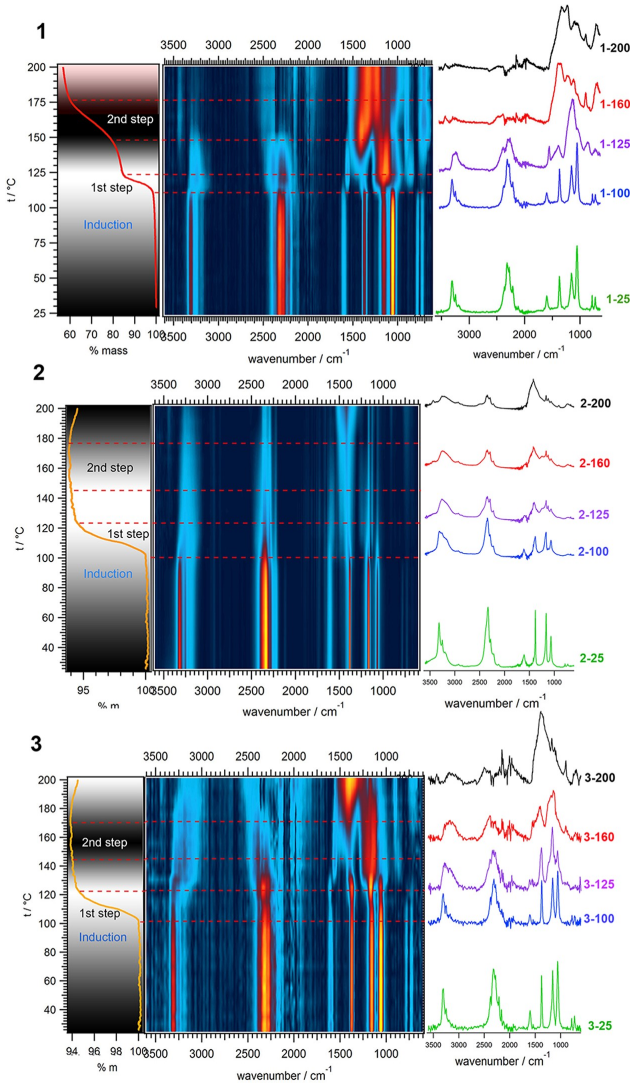

Figure 29: Comparison of variable-temperature IR spectra with TG/DTA for ATR spectra of neat NH_3BH_3 (**1**), transmission spectra of KBr pellet of NH_3BH_3 (**2**) and ATR spectra of 1 : 1 mixture of KBr and NH_3BH_3 (**3**). These measurements clearly indicate high influence of KBr to thermal decomposition of NH_3BH_3. Reprinted with permission from Biliškov et al. *J. Phys. Chem. C*. Copyright 2016 American Chemical Society.

View Article Online
DOI: 10.1039/D2CP01458K

goes straight forward to product. Although both species are similar, their crystal structures are significantly different. These findings and their comparison with familiar systems indicate that generally all sodium-containing amidoboranes follow two competitive thermal dehydrogenation pathways.

In this domain, the advantages provided by 2D correlation analysis have come to the fore.[105,375–390] Although in principle just another method of visualisation of measured data, it provides a good insight into perturbation-induced evolution of the chemical system, by emphasizing changes in the background, and indicating the ranges of perturbation where the changes occur, which facilitates further analysis.

Challenges, Perspectives and Horizons

Although very simple and flexible in its performance and simultaneously very sophisticated in the wealth of provided information, IR spectroscopy is still most frequently used only as a routine technique for characterisation of chemical products. In this light, it is a pity that researchers often overlook the benefits of this widespread and widely available technique. Examples of its utilisation from the text so far clearly illustrates its high flexibility and usability through a huge range of chemical and physical problems. Today, availability of highly sophisticated instrumentation from one side, together with advances in dedicated online accessible software[61] enables really unique opportunities, which are limited exclusively by researcher's creativity. I hope these examples will be inspiring enough for at least some further research. Finally, now I would like to give an overview of the problems and challenges for the further development and applications of the method. This discussion is by no means exhaustive, but should be experienced exclusively as the author's perspective.

View Article Online
DOI: 10.1039/D2CP01458K

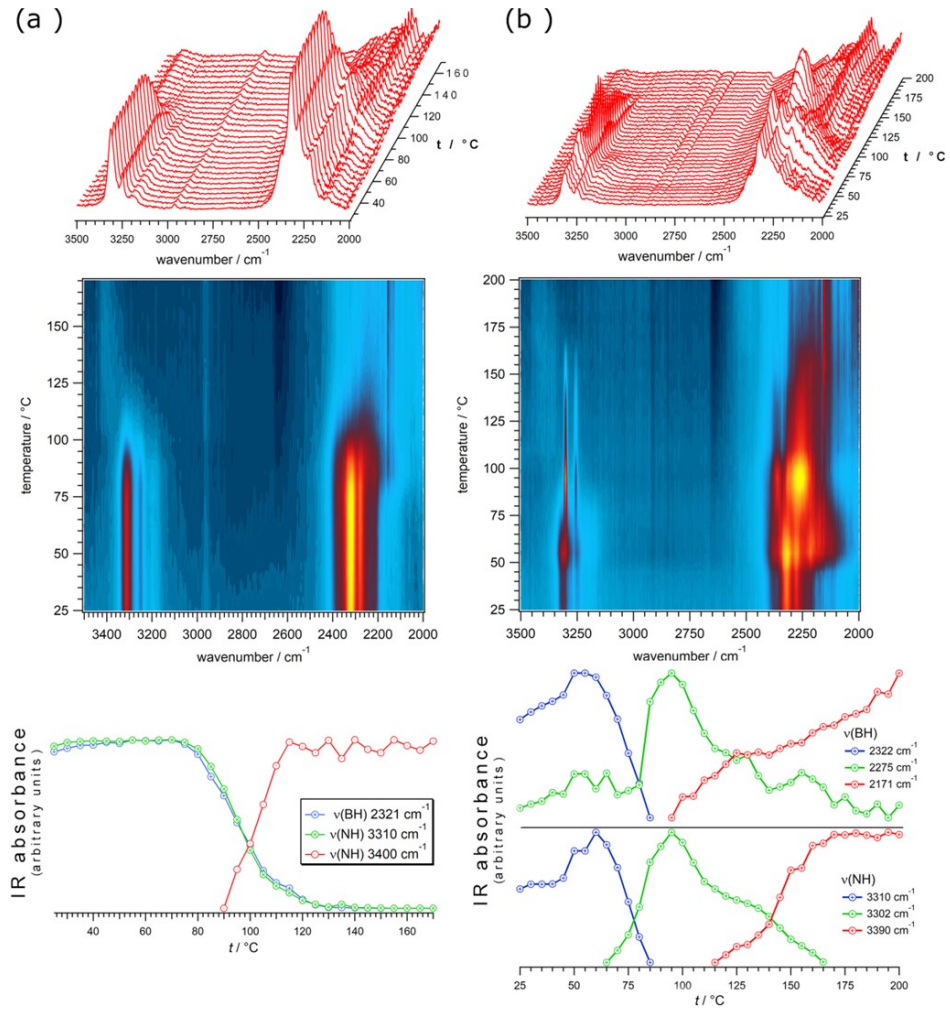

Figure 30: Temperature-dependent IR spectra of (a) $Li_2Ca(NH_2BH_3)_4$ and (b) $Na_2Ca(NH_2BH_3)_4$ in the 35002000 cm^{-1} spectral and room temperature to 200 °C temperature range at 2 °C min^{-1} heating rate. Reaction profiles for different ν(NH) and ν(BH) bands are shown on the bottom. The profiles show absorbances normalized with respect to their maximal values and are obtained by fitting the envelopes to Lorentzian profile functions. Reprinted with permission from Milanović et al. *ACS Sust. Chem. Eng.* **9** (2021) 2089–2099. Copyright 2021 American Chemical Society.

View Article Online
DOI: 10.1039/D2CP01458K

Development of new accessories

Needless to say, ever arising problems solvable by IR spectroscopy inspire new techniques and approaches, which are enabled by design and development of new accessories and instrumentation. In some cases just a very simple setup can do the required job well.[194] This is especially enabled by recent development and a dramatic drop in price of 3D printing, which in turn enabled a quick and simple making of devices in accordance to the researcher's own needs and ideas.[391,392]

However, a vast majority of new challenges require a very sophisticated, often multiinstrumental approaches. The use of synchrotron radiation enables until recently unattainable spatial and temporal resolutions, which in turn enables accurate real time monitoring of various solid-state systems by their detailed mapping.[393] This is especially true for surface and interface phenomena, where there is plenty of room for further developments.[57,394–398] The development in the field of femtosecond IR spectroscopy is also promising a deep insight into ultrafast dynamics of solid-state systems, and significant breakthroughs are also to be expected here.[399–401]

Microspectroscopy

The brilliance of synchrotron radiation now enables analysis of hitherto elusive processes over a wide spectral region of electromagnetic radiation, including IR.[10,124,393,402–405] High intensities enable very accurate microspectroscopy. In this respect, especially interesting is synchrotron-based infrared microspectroscopy (SIRMS) with its very high signal-to-noise ratio, high spatial resolution, extended measurement conditions and high sensitivity. Altogether, this provides a platform for the investigations of the very small amounts of material that need to be used in various investigations performed by use of IR spectroscopy. In recent review, Kong and Liu presented well organised parameters of available IR beamlines, together with other useful information.[10] However, the greatest challenge of using IR microspectroscopies to analyse and monitor the changes of submicrometer particles has been

View Article Online
DOI: 10.1039/D2CP01458K

the diffraction limited resolution of IR light (Abbe limit), which is typically $2 - 20\,\mu m$.[406] Recent development of commercial infrared focal plane array (FPA) detectors[407,408] has enabled rapid acquisition of chemical images with fields of view greater than $100 \times 100\,\mu m^2$. Although the imaged pixel size of FPA detectors can be less than $1 \times 1\,\mu m^2$, the spatial resolution remains limited by diffraction, and can only be marginally improved beyond the Abbe limit through oversampling and point spread function deconvolution techniques. By combining simultaneous single-particle measurements of physical properties by atomic force microscopy (AFM) with chemical composition as obtained by IR spectroscopy, AFM-IR overcomes size limitations with imaging capabilities on the scale of $\sim 50\,nm$ chemical resolution (Fig. 25).[409–414]

The current AFM-IR technique is relatively simple and it uses an IR tunable pulsed laser to induce a photothermal effect in the sample and an AFM to detect the resulting mechanical expansion via the cantilever tip that is in contact with the sample. To relax the excess of stress induced by the local increase of temperature of the sample, the absorbing region expands and pushes the cantilever tip in contact with the sample surface. So, the idea of AFM-IR is not to detect the induced photothermal heat but to detect the thermal expansion with an AFM tip, using the high sensitivity of the AFM system to vertical height changes of the sample (tens of picometers) and its excellent lateral resolution (10–20 nm). For sure, this principle enables the best spatial resolution, currently achievable by IR spectroscopy. However, the local radiation-induced heating of the sample could be seen as a potential drawback of the technique, since it could modify the sample, which in turn can cause a deviation from its realistic chemical nature. It could be expected that further development of IR spectroscopic techniques will in some way overcome this drawback.

Still unexplored chemical processes

The importance of solid-state chemical reactions is growing, since they often result in targetted products, without presence of byproducts in significant amounts. Crucial for these

View Article Online
DOI: 10.1039/D2CP01458K

processes are usually diffusion and interpenetrations of reactants, which can be, in some cases, unexpectedly fast.[194,195,415] These phenomena are still unsatisfactory understood. Especially in combination with molecular dynamics, IR spectroscopy can provide a deep and detailed insight into the mechanisms of these important processes, that open up a new perspective on solid state dynamics.

A very interesting and important, still unexplored field of potential utilisation of IR spectroscopy for in situ monitoring of chemical reactions comprises mechanochemistry, especially ball milling as the most commonly used mechanochemical method. By it origin very old, literally prehistoric, mechanochemistry only relatively recently attracted a significant interest of chemists and chemical industry. In practice, ball milling reactions are carried out by addition of one or more steel balls to reaction mixture closed in reaction vessel. Mill shakes the vessel, which causes rapid moving of the balls inside the vessel, and the mechanical energy of the balls is transferred to reaction mixture and converted to chemical energy. Very recently, a series of publications on resonant acoustic mixing starts to appear, which even does not require balls to convert mechanical energy to chemical system, which is very promising with respect of energy efficiency and greenness of the chemical process.[416] One of the most important benefits of mechanochemistry is its inherently solvent-free means of chemical and materials transformations, which sets it to the frontline of developing Green Chemistry concepts aimed towards an environmentally friendlier chemical and pharmaceutical industry.[417–419] The range of chemical transformations achieved by mechanochemistry has been rapidly expanding in the last two decades, and it is now present in entire preparative chemistry with high perspective for a wide industrial implementation.[382,420–430]

Regardless of their ever-growing importance and prevalence, mechanochemical reactions remained some kind of black box. Only a recent implementation of various techniques for in situ monitoring of ball milling reactions enables an insight under the hood of rapidly moving mechanochemical milling vessels.[195,431–440] Monitoring of ball milling reactions enables a significant progress of understanding of their mechanistic pathways and kinetics, influence of

View Article Online
DOI: 10.1039/D2CP01458K

additives and environmental conditions. However, due to serious technical problems facing the design of appropriate equipment, IR spectroscopy did not enter this playground yet. Its introduction would enable a deeper insight into the intra- and intermolecular background of mechanochemical processes, since it is more than any other method sensitive to intermolecular interactions and changes in local microenvironment. The use of IR spectroscopy in the field of mechanochemistry is still limited to ex situ routine spectroscopy. By the best of our knowledge, the first example of the use of IR spectroscopy to monitor the ball milling reactions was described very recently by Rathmann et al.[441] Actually, they connected an FTIR spectrometer to the milling jar by a gas capillary, and combine the IR spectroscopy with EGA-MS to analyse the composition of gas phase inside the milling jar. However, solid phase transformations, essential for full mechanistic understanding of the mechanochemical reactions, still remain unattainable to IR spectroscopy, but the development in this direction is to be expected soon.

Concluding Remarks

Although practically ubiquitous technique, available in most of the chemical laboratories, and simultaneously very rich in information on intra- and intermolecular arrangement of the matter on molecular scale, IR spectroscopy is frequently underutilized, used merely as a routine method for quick characterisation of obtained products. However, all the possibilities offered by this technique, simple and flexible in its application, and rich in information on chemical systems, are often neglected by researchers. Thus, this tutorial review serves as a reminder or introduction to fundamental and practical aspect of this technique, which could provide crucial information on not only solids, but also liquids and gases. Specifically, it is focused on solids, with an emphasis on those of relevance in contemporary materials science. Although many examples were beyond the scope of this review, here is brought a variety of unique illustrative and, the author hopes, inspiring examples in the field, along with the

View Article Online
DOI: 10.1039/D2CP01458K

various techniques involved in data acquisition and their analysis.

Today, IR spectroscopy is successfully coupled with various techniques and integrated in most sophisticated facilities, that enable a deep and detailed insight into the molecular processes underlying the chemical and physical phenomena, which are fundamental for action of materials. Whilst the author does not suggest in any way that IR spectroscopy alone will ever replace other available methods that enable investigation of matter on its molecular level, he underlines its power in providing a unique insight into intra- and intermolecular forces and molecular environment through direct measurement of vibrations of functional groups.

On a shorter term, the author anticipates that the implementation of in situ IR spectroscopy to address various chemical and physical problems. However, on the longer term, the development of new technologies, such as 3D printing, automation, robotics, machine learning and artificial intelligence, and their implementation to IR spectroscopy will revolutionise its applications and enable its penetration even deeper under the hood of matter. This, in the author's humble opinion, is the next frontier of IR spectroscopy and its utilisation.

Conflict of interest

The author declares no conflicts of interest.

Acknowledgement

This review was written under the financial support in the framework of H2020-MSCA-IF-894705 (GrindCore) action. Additionally, the author wishes to thank COST action CA18112, and to reviewers for valuable comments.

View Article Online
DOI: 10.1039/D2CP01458K

References

(1) Kraka, E.; Zou, W.; Tao, Y. Decoding chemical information from vibrational spectroscopy data: Local vibrational mode theory. *WIREs Comp. Mol. Sci.* **2020**, *10*, e1480.

(2) Bieberle-Hütter, A.; Bronneberg, A.; George, K.; Van De Sanden, M. Operando attenuated total reflection Fourier-transform infrared (ATR-FTIR) spectroscopy for water splitting. *J. Phys. D: Appl. Phys.* **2021**, *54*.

(3) Feng, K.; Wang, Y.; Guo, M.; Zhang, J.; Li, Z.; Deng, T.; Zhang, Z.; Yan, B. In-situ/operando techniques to identify active sites for thermochemical conversion of CO_2 over heterogeneous catalysts. *J. En. Chem.* **2021**, *62*, 153–171.

(4) Murgida, D. In Situ Spectroelectrochemical Investigations of Electrode-Confined Electron-Transferring Proteins and Redox Enzymes. *ACS Omega* **2021**, *6*, 3435–3446.

(5) Nunes, C.; Reva, I.; Fausto, R. Chapter 1: Direct Observation of Tunnelling Reactions by Matrix Isolation Spectroscopy. *RSC Theor. Comp. Chem. Ser.* **2021**, *2021-January*, 1–60.

(6) Chen, B. Exploring nanomechanics with high-pressure techniques. *Matter and Radiation at Extremes* **2020**, *5*.

(7) Wöll, C. Structure and chemical properties of oxide nanoparticles determined by surface-ligand IR spectroscopy. *ACS Catal.* **2020**, *10*, 168–176.

(8) Alodhayb, A.; Khan, F.; Etayash, H.; Thundat, T. Review - Nanomechanical Calorimetric Infrared Spectroscopy using Bi-Material Microfluidic Cantilevers. *J. Electrochem. Soc.* **2020**, *167*.

(9) Zaera, F. New advances in the use of infrared absorption spectroscopy for the characterization of heterogeneous catalytic reactions. *Chem. Soc. Rev.* **2014**, *43*, 7624–7663.

View Article Online
DOI: 10.1039/D2CP01458K

(10) Kong, L.; Liu, G. Synchrotron-based infrared microspectroscopy under high pressure: An introduction. *Matter and Radiation at Extremes* **2021**, *6*, 068202.

(11) Kratz, C.; Furchner, A.; Sun, G.; Rappich, J.; Hinrichs, K. Sensing and structure analysis by in situ IR spectroscopy: from mL flow cells to microfluidic applications. *J. Phys. Cond. Matt.* **2020**, *32*, 393002.

(12) Grabow, K.; Bentrup, U. Homogeneous catalytic processes monitored by combined in situ ATR-IR, UV-VIS, and Raman spectroscopy. *ACS Catalysis* **2014**, *4*, 2153–2164.

(13) Mittal, V.; Mashanovich, G.; Wilkinson, J. Perspective on Thin Film Waveguides for on-Chip Mid-Infrared Spectroscopy of Liquid Biochemical Analytes. *Anal. Chem.* **2020**, *92*, 10891–10901.

(14) Napier, B. et al. Ultra-broadband infrared gas sensor for pollution detection: The TRIAGE project. *J. Phys. Photonics* **2021**, *3*.

(15) Giechaskiel, B.; Clairotte, M. Fourier transform infrared (FTIR) spectroscopy for measurements of vehicle exhaust emissions: A review. *Appl. Sci. (Switzerland)* **2021**, *11*.

(16) Drenchev, N.; Chakarova, K.; Lagunov, O.; Mihaylov, M.; Ivanova, E.; Strauss, I.; Hadjiivanov, K. In situ FTIR spectroscopy as a tool for investigation of gas/solid interaction: Water-enhanced CO_2 adsorption in UiO-66 metal-organic framework. *J. Visual. Exp.* **2020**, *2020*.

(17) Kas, R.; Ayemoba, O.; Firet, N. J.; Middelkoop, J.; Smith, W. A.; Cuesta, A. In-Situ Infrared Spectroscopy Applied to the Study of the Electrocatalytic Reduction of CO_2: Theory, Practice and Challenges. *ChemPhysChem* **2019**, *20*, 2904–2925.

(18) Mensitieri, G.; Scherillo, G.; Panayiotou, C.; Musto, P. Towards a predictive thermodynamic description of sorption processes in polymers: The synergy between theo-

View Article Online
DOI: 10.1039/D2CP01458K

retical EoS models and vibrational spectroscopy. *Mater. Sci. Eng. R: Reports* **2020**, *140*.

(19) Mudunkotuwa, I.; Minshid, A.; Grassian, V. ATR-FTIR spectroscopy as a tool to probe surface adsorption on nanoparticles at the liquid-solid interface in environmentally and biologically relevant media. *Analyst* **2014**, *139*, 870–881.

(20) Rupprechter, G. Operando Surface Spectroscopy and Microscopy during Catalytic Reactions: From Clusters via Nanoparticles to Meso-Scale Aggregates. *Small* **2021**, *17*.

(21) Li, X.; Wang, S.; Li, L.; Sun, Y.; Xie, Y. Progress and Perspective for in Situ Studies of CO_2 Reduction. *J. Am. Chem. Soc.* **2020**, *142*, 9567–9581.

(22) Jin, L.; Seifitokaldani, A. In situ spectroscopic methods for electrocatalytic CO_2 reduction. *Catalysts* **2020**, *10*.

(23) Zhang, Y.; Guo, S.-X.; Zhang, X.; Bond, A.; Zhang, J. Mechanistic understanding of the electrocatalytic CO_2 reduction reaction – New developments based on advanced instrumental techniques. *Nano Today* **2020**, *31*.

(24) Ring, E. F. J. The discovery of infrared radiation in 1800. *Imaging Sci. J.* **2000**, *48*, 1–8.

(25) Rogalski, A. History of infrared detectors. *Opto-Electronics Rev.* **2012**, *20*, 279–308.

(26) Herschel, J. F. W. I. On the chemical action of the rays of the solar spectrum on preparations of silver and other substances, both metallic and non-metallic, and on some photographic processes. *Phil. Trans. Royal Soc. London* **1840**, *130*, 1–59.

(27) Langley, S. P. The Bolometer and Radiant Energy. *Proc. Am. Acad. Arts Sci.* **1880**, *16*, 342–358.

View Article Online
DOI: 10.1039/D2CP01458K

(28) Barr, E. The infrared pioneers—III. Samuel Pierpont Langley. *Infrared Phys.* **1963**, *3*, 195–206.

(29) Coblentz, W. W. Reminiscences of Early Investigations of Infrared Absorption Spectra. *Appl. Spectrosc.* **1953**, *7*, 109–111.

(30) Barnes, R. B.; Bonner, L. G. The Early History and the Methods of Infrared Spectroscopy. *Am. J. Phys.* **1936**, *4*, 181–189.

(31) Wilson, E. B.; Decius, J. C.; Cross, P. C. *Molecular Vibrations: The Theory of Infrared and Raman Vibrational Spectra*; Dover Publications: London, 1980.

(32) Einstein, A. On the Theory of Light Production and Light Absorption. *Ann. Phys* **1906**, *20*, 199–206.

(33) Einstein, A. Strahlungs-Emission und Absorption nach der Quantentheorie. *Deutsche Phys. Gesellschaft* **1916**, *18*, 318–323.

(34) Michelson, A. A. XXX. On the application of interference methods to spectroscopic measurements.—II. *Phil. Mag.* **1892**, *34*, 280–299.

(35) Michelson, A. A. XXVIII. Visibility of interference-fringes in the focus of a telescope. *Phil. Mag.* **1891**, *31*, 256–259.

(36) Lord Rayleigh 2nd, R. XLVII. On the interference bands of approximately homogeneous light; in a letter to Prof. A. Michelson. *Phil. Mag.* **1892**, *34*, 407–411.

(37) Griffiths, P. R. The Early Days of Commercial FT-IR Spectrometry: A Personal Perspective. *Appl. Spectrosc.* **2017**, *71*, 329–340.

(38) Connes, P. Early history of Fourier transform spectroscopy. *Infrared Phys.* **1984**, *24*, 69–93.

View Article Online
DOI: 10.1039/D2CP01458K

(39) Griffiths, P. R.; de Haseth, J. A. *Fourier Transform Infrared Spectrometry*, 2nd ed.; John Wiley & Sons, Inc.: Hoboken, New Jersey, 2006.

(40) Jiang, E. Y. *Advanced FT-IR Spectroscopy - Principles, Experiments and Applications Based on Research-Grade Nicolet FT-IR Spectrometers*; Thermo Electron Corporation, 2008.

(41) Jiang, E. Y. Phase-, Time-, and Space-Resolved Step-Scan FT-IR Spectroscopy: Principles and Applications to Dynamic and Heterogenous Systems. *Spectrosc.* **2002**, *17*, 22–34.

(42) Mezzetti, A.; Schnee, J.; Lapini, A.; Di Donato, M. Time-resolved infrared absorption spectroscopy applied to photoinduced reactions: how and why. *Photochem. Photobiol. Sci.* **2022**, *21*, 557–584.

(43) Dittmar, R. M.; Chao, J. L.; Palmer, R. A. Photoacoustic Depth Profiling of Polymer Laminates by Step-Scan Fourier Transform Infrared Spectroscopy. *Appl. Spectrosc.* **1991**, *45*, 1104–1110.

(44) Jiang, E.; Grenov, A. Extension of two-dimensional global phase difference correlation analysis to step-scan FT-IR photoacoustic spectral depth profiling of layered systems. *J. Mol. Struct.* **2006**, *799*, 188–195.

(45) Wang, H.; Palmer, R. A.; Manning, C. J. Study of Impulse Polymer Rheo-Optics by Step-Scan FT-IR Time-Resolved Spectroscopy. *Appl. Spectrosc.* **1997**, *51*, 1245–1250.

(46) Uhmann, W.; Becker, A.; Taran, C.; Siebert, F. Time-Resolved FT-IR Absorption Spectroscopy Using a Step-Scan Interferometer. *Appl. Spectrosc.* **1991**, *45*, 390–397.

(47) Offenbach, I.; Gupta, S.; Chung, T.; Weiss, R.; Cakmak, M. Real-Time Infrared-Mechano-Optical Behavior and Structural Evolution of Polypropylene and Hydroxyl-

View Article Online
DOI: 10.1039/D2CP01458K

Functionalized Polypropylene during Uniaxial Deformation. *Macromolecules* **2015**, *48*, 6294 – 6305.

(48) Gregoriou, V. G.; Daun, M.; Schauer, M. W.; Chao, J. L.; Palmer, R. A. Modification of a research-grade FT-IR spectrometer for optional step-scan operation. *Appl. Spectrosc.* **1993**, *47*, 1311 – 1316.

(49) Palmer, R. A.; Smith, G. D.; Chen, P. Breaking the nanosecond barrier in FTIR time-resolved spectroscopy. *Vib. Spectrosc.* **1999**, *19*, 131 – 141.

(50) Smith, G. D.; Palmer, R. A. *Handbook of Vibrational Spectroscopy*; John Wiley Sons, Ltd, 2006; p 121–144.

(51) Ganim, Z.; Hoi, S.; Smith, A.; Deflores, L.; Jones, K.; Tokmakoff, A. Amide I two-dimensional infrared spectroscopy of proteins. *Acc. Chem. Res.* **2008**, *41*, 432–441.

(52) Hetmańczyk, J.; Hetmańczyk, Ł.; Gassowska, K. Phase transition, structure and reorientational dynamics of H_2O ligands and ReO_4 anions in $[Ba(H_2O)_3](ReO_4)_2 \cdot H_2O$. *J. Mol. Struct.* **2019**, *1188*, 173–184.

(53) Nihonyanagi, S.; Yamaguchi, S.; Tahara, T. Ultrafast Dynamics at Water Interfaces Studied by Vibrational Sum Frequency Generation Spectroscopy. *Chem. Rev.* **2017**, *117*, 10665–10693.

(54) Hong, Z.; Rezvani, S.; Zhang, Q.; Lu, P. Ultrafast Mid-IR laser pulses generation via chirp manipulated optical parametric amplification. *Appl. Sci. (Switzerland)* **2018**, *8*.

(55) Fang, C.; Tang, L.; Chen, C. Unveiling coupled electronic and vibrational motions of chromophores in condensed phases. *J. Chem. Phys.* **2019**, *151*.

(56) Liao, R.; Tian, H.; Liu, W.; Li, R.; Song, Y.; Hu, M. Dual-comb generation from a single laser source: Principles and spectroscopic applications towards mid-IR - A review. *J. Phys Photonics* **2020**, *2*.

View Article Online
DOI: 10.1039/D2CP01458K

(57) Wang, J.; Wang, K.; Shen, Y.; Han, Z.; Li, F.; He, Z.; Wang, D.-w.; Sokolov, A. V.; Scully, M. O. Femtosecond Time-Resolved Infrared-Resonant Third-Order Sum-Frequency Spectroscopy. *ACS Photonics* **2021**, *8*, 1137–1142.

(58) Herzberg, G.; Crawford, B. L. Infrared and Raman Spectra of Polyatomic Molecules. *J. Phys. Chem.* **1946**, *50*, 288–288.

(59) Cannon, C. The nature of hydrogen bonding: A review of published work and discussion. *Spectrochim. Acta* **1958**, *10*, 341–368.

(60) Bratos, S. Profiles of hydrogen stretching ir bands of molecules with hydrogen bonds: A stochastic theory. I. Weak and medium strength hydrogen bonds. *J. Chem. Phys.* **1975**, *63*, 3499–3509.

(61) Jablonka, K. M.; Patiny, L.; Smit, B. Making Molecules Vibrate: Interactive Web Environment for the Teaching of Infrared Spectroscopy. *J. Chem. Educ.* **2022**, *99*, 561–569.

(62) Socrates, G. *Infrared and Raman Characteristic Group Frequencies: Tables and Charts*, 3rd ed.; 2004.

(63) Silverstein, R. M.; Webster, F. X.; Kiemle, D. J.; Bryce, D. L. *Spectrometric Identification of Organic Compounds*, 8th ed.; 2014.

(64) Nakamoto, K. *Infrared and Raman Spectra of Inorganic and Coordination Compounds: Part A: Theory and Applications in Inorganic Chemistry*, 6th ed.; 2008.

(65) Nakamoto, K. *Infrared and Raman Spectra of Inorganic and Coordination Compounds: Part B: Applications in Coordination, Organometallic, and Bioinorganic Chemistry*, 6th ed.; 2008.

(66) Maddams, W. F. The Scope and Limitations of Curve Fitting. *Appl. Spectrosc.* **1980**, *34*, 245–267.

View Article Online
DOI: 10.1039/D2CP01458K

(67) Antoon, M. K.; D'Esposito, L.; Koenig, J. L. Factor Analysis Applied to Fourier Transform Infrared Spectra. *Appl. Spectrosc.* **1979**, *33*, 351–357.

(68) Malinowski, E. R. *Factor Analysis in Chemistry*, 3rd ed.; Wiley: New York, 2002.

(69) Jones, C. W.; Tao, F. F.; Garland, M. V. Introduction to Special Issue on Operando and In Situ Studies of Catalysis. *ACS Catalysis* **2012**, *2*, 2444–2445.

(70) Koo, B. M.; Corte, D. A. D.; Chazalviel, J.; Maroun, F.; Rosso, M.; Ozanam, F. Lithiation Mechanism of Methylated Amorphous Silicon Unveiled by Operando ATR-FTIR Spectroscopy. *Adv. En. Mater.* **2018**, *8*, 1702568.

(71) He, X.; Larson, J.; Bechtel, H.; Kostecki, R. In situ infrared nanospectroscopy of the local processes at the Li/polymer electrolyte interface. *Nature Commun.* **2022**, *13*.

(72) King, J.; Liu, C.; Chuang, S. In situ infrared approach to unravel reaction intermediates and pathways on catalyst surfaces. *Res. Chem. Intermed.* **2019**, *45*, 5831–5847.

(73) Gauglitz, G.; Vo-Dinh, T. *Handbook of Spectroscopy, Vol. 1*; Wiley-VCH: Weinheim, Germany, 2003.

(74) Liu, X.; Hou, L.; Wang, H. Investigations into the mid-infrared Christiansen effect of the dispersive materials. *Infrared Phys. Technol.* **2002**, *43*, 401–405.

(75) Biliškov, N.; Vojta, D.; Kótai, L.; Szilágyi, I. M.; Hunyadi, D.; Pasinszki, T.; Flinčec Grgac, S.; Borgschulte, A.; Züttel, A. High Influence of Potassium Bromide on Thermal Decomposition of Ammonia Borane†. *J. Phys. Chem. C* **2016**, *120*, 25276–25288.

(76) Delgado, A.; Paroli, R.; Beaudoin, J. Comparison of IR techniques for the characterization of construction cement minerals and hydrated products. *Appl. Spectrosc.* **1996**, *50*, 970–976.

(77) Ritter, D.; Weiser, K. Suppression of interference fringes in absorption measurements on thin films. *Optics Commun.* **1986**, *57*, 336–338.

View Article Online
DOI: 10.1039/D2CP01458K

(78) Poelman, D.; Smet, P. F. Methods for the determination of the optical constants of thin films from single transmission measurements: a critical review. *J. Phys. D: Appl. Phys.* **2003**, *36*, 1850–1857.

(79) Raof, N. H. A.; Ng, S. S.; Hassan, H. A.; Hassan, Z. Kramers-Kronig Analysis of Infrared Reflectance Spectra for Quaternary $In_xAl_yGa_{1xy}N$ Alloy. *AIP Conf. Proc.* **2010**, *1250*, 337–340.

(80) Biliškov, N. Infrared optical constants, molar absorption coefficients, dielectric constants, molar polarisabilities, transition moments and dipole moment derivatives of liquid N,N-dimethylformamide–carbon tetrachloride mixtures. *Spectrochim. Acta A* **2011**, *79*, 302–307.

(81) Okamura, H. In *Optical Techniques for Solid-State Materials Characterization*; Prasankumar, R., Taylor, A. J., Eds.; CRC Press: Boca Raton, FL, 2011; pp 111–150.

(82) Mendelsohn, R.; Flach, C. R. *Peptide-Lipid Interactions*; Curr. Topics in Membranes; Academic Press, 2002; Vol. 52; pp 57–88.

(83) Mendelsohn, R.; Mao, G.; Flach, C. R. Infrared reflection–absorption spectroscopy: Principles and applications to lipid–protein interaction in Langmuir films. *Biochim. Biophys. Acta - Biomembranes* **2010**, *1798*, 788–800.

(84) Brand, I. Application of Polarization Modulation Infrared Reflection Absorption Spectrosocpy Under Electrochemical Control for Structural Studies of Biomimetic Assemblies. *Z. Phys. Chem.* **2016**, *230*, 133–183.

(85) Blume, A.; Kerth, A. Peptide and protein binding to lipid monolayers studied by FT-IRRA spectroscopy. *Biochim. Biophys. Acta - Biomembranes* **2013**, *1828*, 2294–2305.

(86) Wang, Y.; Wöll, C. IR spectroscopic investigations of chemical and photochemical

View Article Online
DOI: 10.1039/D2CP01458K

reactions on metal oxides: bridging the materials gap. *Chem. Soc. Rev.* **2017**, *46*, 1875–1932.

(87) Ito, M. Structures of water at electrified interfaces: Microscopic understanding of electrode potential in electric double layers on electrode surfaces. *Surface Sci. Rep.* **2008**, *63*, 329–389.

(88) Dluhy, R.; Shanmukh, S.; Morita, S. The application of two-dimensional correlation spectroscopy to surface and interfacial analysis. *Surf. Interf. Anal.* **2006**, *38*, 1481–1496.

(89) Stefaniu, C.; Brezesinski, G.; Möhwald, H. Langmuir monolayers as models to study processes at membrane surfaces. *Adv. Colloid Interf. Sci.* **2014**, *208*, 197–213.

(90) Bardwell, J. A.; Dignam, M. J. Routine determination of the absorption and dispersion spectra of solids with a Fourier-transform infrared spectrometer. *Anal. Chim. Acta* **1985**, *172*, 101–110.

(91) Roessler, D. M. Kramers-Krönig analysis of reflection data. *Br. J. Appl. Phys.* **1965**, *16*, 1119–1123.

(92) Roessler, D. M. Kramers - Krönig analysis of non-normal incidence reflection. *Br. J. Appl. Phys.* **1965**, *16*, 1359–1366.

(93) Roessler, D. M. Kramers - Krönig analysis of reflectance data: III. Approximations, with reference to sodium iodide. *Br. J. Appl. Phys.* **1966**, *17*, 1313–1317.

(94) Brendel, R. The concept of effective film thickness for the determination of bond concentrations from IR spectra of weakly absorbing thin films on silicon. *J. Appl. Phys.* **1991**, *69*, 7395–7399.

(95) Edgar, R. F.; Stay, B. J. Techniques For Suppressing Optical Interference Errors In

View Article Online
DOI: 10.1039/D2CP01458K

Infrared Film Thickness Gauging. Infrared Technology and Applications. 1986; pp 316 – 321.

(96) Farrington, P. J.; Hill, D. J. T.; O'Donnell, J. H.; Pomery, P. J. Suppression of Interference Fringes in the Infrared Spectra of Thin Polymer Films. *Appl. Spectrosc.* **1990**, *44*, 901–903.

(97) Gamsky, C.; Howes, G.; Taylor, J. Infrared Reflection Absorption Spectroscopy of Photoresist Films on Silicon Wafers: Measuring Film Thickness and Removing Interference Fringes. *Anal. Chem.*

(98) Dahm, D. J. *Interpreting Diffuse Reflectance and Transmittance: A Theoretical Introduction to Absorption Spectroscopy of Scattering Materials*; IM Publications LLP, 2007.

(99) Sun, S.; Zhang, F. In *Semiconductor Photocatalysis: Materials, Mechanisms and Applications*; Cao, W., Ed.; Intechopen: London, UK, 2016; Chapter Insights into the Mechanism of Photocatalytic Degradation of Volatile Organic Compounds on TiO_2 by Using In-situ DRIFTS, pp 185–206.

(100) Fahrenfort, J. Attenuated total reflection: A new principle for the production of useful infra-red reflection spectra of organic compounds. *Spectrochim. Acta* **1961**, *17*, 698–709.

(101) Harrick, N. J. *Internal Reflection Spectroscopy*, 1st ed.; Interscience: New York, 1967.

(102) Harrick, N. J.; Beckmann, K. H. In *Characterization of Solid Surfaces*; Kane, P. F., Larrabee, G. B., Eds.; Springer US: Boston, MA, 1974; pp 215–245.

(103) Siesler, H. W. In *Oriented Polymer Materials*; Fakirov, S., Ed.; John Wiley & Sons, 1996; pp 138–166.

View Article Online
DOI: 10.1039/D2CP01458K

(104) Siesler, H. W.; Hoffmann, G. G.; Kolomiets, O.; Pfeifer, F.; Zahedi, M. In *Vibrational Spectroscopy of Polymers: Principles and Practice*; Everall, N. J., Chalmers, J. M., Griffiths, P. R., Eds.; John Wiley & Sons, Ltd, 2007.

(105) Unger, M.; Siesler, H. W. In Situ Orientation Studies of a Poly(3-hydroxybutyrate)/Poly(ϵ-caprolactone) Blend by Rheo-Optical Fourier Transform Infrared Spectroscopy and Two-Dimensional Correlation Spectroscopic Analysis. *Appl. Spectrosc.* **2009**, *63*, 1351–1355.

(106) Shen, J.; Kashimoto, M.; Matsumoto, T.; Mori, A.; Nishino, T. Structural deformation of elastic polythiophene with disiloxane moieties under stretching. *Polymer J.* **2020**, *52*, 1273–1278.

(107) Kimura, S.-i.; Okamura, H. Infrared and Terahertz Spectroscopy of Strongly Correlated Electron Systems under Extreme Conditions. *J. Phys. Soc. Jpn.* **2013**, *82*, 021004.

(108) Aoki, K.; Yamawaki, H.; Sakashita, M.; Fujihisa, H. Infrared absorption study of the hydrogen-bond symmetrization in ice to 110 GPa. *Phys. Rev. B* **1996**, *54*, 15673–15677.

(109) Goncharov, A. F.; Gregoryanz, E.; Mao, H.-k.; Liu, Z.; Hemley, R. J. Optical Evidence for a Nonmolecular Phase of Nitrogen above 150 GPa. *Phys. Rev. Lett.* **2000**, *85*, 1262–1265.

(110) Zha, C.-s.; Liu, Z.; Ahart, M.; Boehler, R.; Hemley, R. J. High-Pressure Measurements of Hydrogen Phase IV Using Synchrotron Infrared Spectroscopy. *Phys. Rev. Lett.* **2013**, *110*, 217402.

(111) Spaulding, D. K.; Weck, G.; Loubeyre, P.; Datchi, F.; Dumas, P.; Hanfland, M. Pressure-induced chemistry in a nitrogen-hydrogen host–guest structure. *Nature Commun.* **2014**, *5*, 5739.

View Article Online
DOI: 10.1039/D2CP01458K

(112) Mao, H. K.; Hemley, R. J. The high-pressure dimension in earth and planetary science. *Proceedings of the National Academy of Sciences* **2007**, *104*, 9114–9115.

(113) Thompson, E. C.; Davis, A. H.; Brauser, N. M.; Liu, Z.; Prakapenka, V. B.; Campbell, A. J. Phase transitions in -FeOOH at high pressure and ambient temperature. *Amer. Mineral.* **2020**, *105*, 1769–1777.

(114) Montgomery, W.; Tuff, J.; Kohn, S.; Jones, R. Reactions between organic acids and montmorillonite clay under Earth-forming conditions. *Chem. Geol.* **2011**, *283*, 171–176.

(115) Koch-Müller, M.; Jahn, S.; Birkholz, N.; Ritter, E.; Schade, U. Phase transitions in the system $CaCO_3$ at high P and T determined by in situ vibrational spectroscopy in diamond anvil cells and first-principles simulations. *Phys. Chem. Minerals* **2016**, *43*, 545–561.

(116) Ross, N. L.; Detrie, T. A.; Liu, Z. High-Pressure Raman and Infrared Spectroscopic Study of Prehnite. *Minerals* **2020**, *10*, 312–318.

(117) Shieh, S. R.; Duffy, T. S.; Liu, Z.; Ohtani, E. High-pressure infrared spectroscopy of the dense hydrous magnesium silicates phase D and phase E. *Phys. Earth Planet. Interiors* **2009**, *175*, 106–114.

(118) Syassen, K.; Sonnenschein, R. Microoptic double beam system for reflectance and absorption measurements at high pressure. *Rev. Sci. Inst.* **1982**, *53*, 644–650.

(119) Nanba, T. High-pressure solid-state spectroscopy at UVSOR by Infrared Synchrotron Radiation. *Nouv. Cim. D* **1998**, *20*, 397–413.

(120) Hemley, R.; Goncharov, A.; Lu, R.; Struzhkin, V.; Li, M.; Mao, H. High-pressure synchrotron infrared spectroscopy at the National Synchrotron Light Source. *Nuov. Cim. D* **1998**, *20*, 539–551.

View Article Online
DOI: 10.1039/D2CP01458K

(121) Beyer, R.; Dressel, M. Piston pressure cell for low-temperature infrared investigations. *Rev. Sci. Instr.* **2015**, *86*, 053904.

(122) Tran, M. K.; Levallois, J.; Akrap, A.; Teyssier, J.; Kuzmenko, A. B.; Lévy-Bertrand, F.; Tediosi, R.; Brandt, M.; Lerch, P.; van der Marel, D. Versatile setup for optical spectroscopy under high pressure and low temperature. *Rev. Sci. Instr.* **2015**, *86*, 105102.

(123) Voute, A.; Deutsch, M.; Kalinko, A.; Alabarse, F.; Brubach, J. B.; Capitani, F.; Chapuis, M.; Ta Phuoc, V.; Sopracase, R.; Roy, P. New high-pressure/low-temperature set-up available at the AILES beamline. *Vib. Spectrosc.* **2016**, *86*, 17–23.

(124) Okamura, H.; Ikemoto, Y.; Moriwaki, T.; Nanba, T. Infrared spectroscopy techniques for studying the electronic structures of materials under high pressure. *Japan. J. Appl. Phys.* **2017**, *56*, 05FA11.

(125) Goncharov, A. F.; Kong, L.; Mao, H. K. High-pressure integrated synchrotron infrared spectroscopy system at the Shanghai Synchrotron Radiation Facility. *Rev. Sci. Instr.* **2019**, *90*, 093905.

(126) Almodovar, C. A.; Su, W. W.; Strand, C. L.; Sur, R.; Hanson, R. K. High-pressure, high-temperature optical cell for mid-infrared spectroscopy. *J. Quant. Spectrosc. Rad. Transfer* **2019**, *231*, 69–78.

(127) Piermarini, G. J. Alvin Van Valkenburg and the diamond anvil cell. *High Press. Res.* **1993**, *11*, 279–284.

(128) Bassett, W. A. Diamond anvil cell, 50th birthday. *High Press. Res.* **2009**, *29*, 163–186.

(129) Eggert, J. H.; Goettel, K. A.; Silvera, I. F. Ruby at high pressure. I. Optical line shifts to 156 GPa. *Phys. Rev. B* **1989**, *40*, 5724–5732.

View Article Online
DOI: 10.1039/D2CP01458K

(130) Mishra, M. K.; Ghalsasi, P.; Deo, M. N.; Bhatt, H.; Poswal, H. K.; Ghosh, S.; Ganguly, S. In situ high pressure study of an elastic crystal by FTIR spectroscopy. *CrystEngComm* **2017**, *19*, 7083–7087.

(131) Ganguly, S.; Chinnasamy, R.; Parikh, S.; Kiran, M. S. R. N.; Ramamurty, U.; Bhatt, H.; Deo, M. N.; Ghosh, S.; Ghalsasi, P. Understanding Structural Variations in Elastic Organic Crystals by in Situ High-Pressure Fourier Transform Infrared Spectroscopy and Nanoindentation Study. *Cryst. Growth Des.* **2019**, *19*, 2114–2122.

(132) Matsunami, M.; Okamura, H.; Ochiai, A.; Nanba, T. Pressure Tuning of an Ionic Insulator into a Heavy Electron Metal: An Infrared Study of YbS. *Phys. Rev. Lett.* **2009**, *103*, 237202.

(133) Smith, K. A.; Ramkumar, S. P.; Harms, N. C.; Clune, A. J.; Cheong, S.-W.; Liu, Z.; Nowadnick, E. A.; Musfeldt, J. L. Pressure-induced phase transition and phonon softening in $h - Lu_{0.6}Sc_{0.4}FeO_3$. *Phys. Rev. B* **2021**, *104*, 094109.

(134) Chellappa, R. S.; Somayazulu, M.; Struzhkin, V. V.; Autrey, T.; Hemley, R. J. Pressure-induced complexation of $NH_3BH_3NH_3BH_3$. *J. Chem. Phys.* **2009**, *131*, 224515.

(135) Lin, Y.; Mao, W. L.; Drozd, V.; Chen, J.; Daemen, L. L. Raman spectroscopy study of ammonia borane at high pressure. *J. Chem. Phys.* **2008**, *129*, 234509.

(136) Lin, Y.; Welchman, E.; Thonhauser, T.; Mao, W. L. The structure and unconventional dihydrogen bonding of a pressure-stabilized hydrogen-rich $(NH_3BH_3) \cdot (H_2)_x$ $(x = 1.5)$ compound. *J. Mater. Chem. A* **2017**, *5*, 7111–7117.

(137) Wang, S.; Mao, W. L.; Autrey, T. Bonding in boranes and their interaction with molecular hydrogen at extreme conditions. *J. Chem. Phys.* **2009**, *131*, 144508.

View Article Online
DOI: 10.1039/D2CP01458K

(138) Najiba, S.; Chen, J. High-pressure study of lithium amidoborane using Raman spectroscopy and insight into dihydrogen bonding absence. *Proc. Nat. Acad. Sci.* **2012**, *109*, 19140–19144.

(139) Chellappa, R. S.; Chandra, D.; Gramsch, S. A.; Hemley, R. J.; Lin, J.-F.; Song, Y. Pressure-Induced Phase Transformations in LiAlH4. *J. Phys. Chem. B* **2006**, *110*, 11088–11097.

(140) Chellappa, R. S.; Chandra, D.; Somayazulu, M.; Gramsch, S. A.; Hemley, R. J. Pressure-Induced Phase Transitions in $LiNH_2$. *J. Phys. Chem. B* **2007**, *111*, 10785–10789.

(141) George, L.; Drozd, V.; Couvy, H.; Chen, J.; Saxena, S. K. An extended high pressure-temperature phase diagram of $NaBH_4$. *J. Chem. Phys.* **2009**, *131*, 074505.

(142) Marizy, A.; Geneste, G.; Garbarino, G.; Loubeyre, P. High pressure polymorphism of LiBH4 and of NaBH4. *RSC Adv.* **2021**, *11*, 25274–25283.

(143) Park, J. H.; Sudarshan, T. S. *Chemical Vapor Deposition*; ASM International, 2001.

(144) Mahan, J. E. *Physical Vapor Deposition of Thin Films*; Wiley-VCH, 2000.

(145) Cao, G. *Nanostructures & Nanomaterials: Synthesis, Properties & Applications*; Imperial College Press: London, 2004.

(146) Yang, E. H.; Datta, D.; Ding, J.; Hader, G. *Synthesis, Modelling and Characterization of 2D Materials and their Heterostructures*; Elsevier: Amsterdam, 2020.

(147) Zaera, F. Infrared and molecular beam studies of chemical reactions on solid surfaces. *Int. Rev. Phys. Chem.* **2002**, *21*, 433–471.

(148) Soonmin, H. Analysis of Thin Films by Infrared Spectroscopy: Review. *Ind. J. Nat. Sci.* **2020**, *10*, 27593–27599.

View Article Online
DOI: 10.1039/D2CP01458K

(149) Du, Y.; Li, L.; Wang, X.; Qiu, H. A Newly Designed Infrared Reflection Absorption Spectroscopy System for In Situ Characterization from Ultrahigh Vacuum to Ambient Pressure. *Appl. Spectrosc.* **2018**, *72*, 122–128.

(150) Chadwick, H.; Beck, R. D. Quantum state resolved gas–surface reaction dynamics experiments: a tutorial review. *Chem. Soc. Rev.* **2016**, *45*, 3576–3594.

(151) Tiznado, H.; Bouman, M.; Kang, B. C.; Lee, I.; Zaera, F. Mechanistic details of atomic layer deposition (ALD) processes for metal nitride film growth. *J. Mol. Catal. A* **2008**, *281*, 35–43.

(152) Kan, B. C.; Boo, J. H.; Lee, I.; Zaera, F. Thermal Chemistry of Tetrakis(ethylmethylamido)titanium on Si(100) Surfaces. *J. Phys. Chem. A* **2009**, *113*, 3946–3954.

(153) Guo, L.; Zaera, F. Spatial resolution in thin film deposition on silicon surfaces by combining silylation and UV/ozonolysis. *Nanotechnol.* **2014**, *25*, 504006.

(154) Hoffmann, H.; Griffiths, P.; Zaera, F. A RAIRS study on the surface chemistry of ethyl iodide on Pt(111). *Surf. Sci.* **1992**, *262*, 141–150.

(155) Motyka, M.; Sek, G.; Misiewicz, J.; Bauer, A.; Dallner, M.; Höfling, S.; Forchel, A. Fourier transformed Photoreflectance and photoluminescence of mid infrared GaSb-based type II quantum wells. *Appl. Phys. Exp.* **2009**, *2*.

(156) Nan, C.; Yue, W.; Tao, L.; Yang, X. Fourier transform infrared nano-spectroscopy: Mechanism and applications. *Appl. Spectrosc. Rev.* **2021**, *56*, 531–552.

(157) Patoka, P.; Ulrich, G.; Nguyen, A. E.; Bartels, L.; Dowben, P. A.; Turkowski, V.; Rahman, T. S.; Hermann, P.; Kästner, B.; Hoehl, A.; Ulm, G.; Rühl, E. Nanoscale plasmonic phenomena in CVD-grown MoS_2 monolayer revealed by ultra-broadband

View Article Online
DOI: 10.1039/D2CP01458K

synchrotron radiation based nano-FTIR spectroscopy and near-field microscopy. *Opt. Express* **2016**, *24*, 1154–1164.

(158) Dai, S. et al. Tunable Phonon Polaritons in Atomically Thin van der Waals Crystals of Boron Nitride. *Sci.* **2014**, *343*, 1125–1129.

(159) Yang, J.; Mayyas, M.; Tang, J.; Ghasemian, M. B.; Yang, H.; Watanabe, K.; Taniguchi, T.; Ou, Q.; Li, L. H.; Bao, Q.; Kalantar-Zadeh, K. Boundary-Induced Auxiliary Features in Scattering-Type Near-Field Fourier Transform Infrared Spectroscopy. *ACS Nano* **2020**, *14*, 1123–1132.

(160) Szostak, R.; Silva, J. C.; Turren-Cruz, S.-H.; Soares, M. M.; Freitas, R. O.; Hagfeldt, A.; Tolentino, H. C. N.; Nogueira, A. F. Nanoscale mapping of chemical composition in organic-inorganic hybrid perovskite films. *Sci. Adv.* **2019**, *5*, eaaw6619.

(161) Wang, C.-F.; Habteyes, T. G.; Luk, T. S.; Klem, J. F.; Brener, I.; Chen, H.-T.; Mitrofanov, O. Observation of Intersubband Polaritons in a Single Nanoantenna Using Nano-FTIR Spectroscopy. *Nano Lett.* **2019**, *19*, 4620–4626.

(162) Paul, G.; Bisio, C.; Braschi, I.; Cossi, M.; Gatti, G.; Gianotti, E.; Marchese, L. Combined solid-state NMR, FT-IR and computational studies on layered and porous materials. *Chem. Soc. Rev.* **2018**, *47*, 5684–5739.

(163) Delgado, R. M. Structure and Stability of Gas Adsorption Complexes in Periodic Porous Solids as Studied by VTIR Spectroscopy: An Overview. *Appl. Sci.* **2020**, *10*.

(164) Kornienko, N. Operando spectroscopy of nanoscopic metal/covalent organic framework electrocatalysts. *Nanoscale* **2021**, *13*, 1507–1514.

(165) Hadjiivanov, K. I.; Panayotov, D. A.; Mihaylov, M. Y.; Ivanova, E. Z.; Chakarova, K. K.; Andonova, S. M.; Drenchev, N. L. Power of Infrared and Ra-

View Article Online
DOI: 10.1039/D2CP01458K

man Spectroscopies to Characterize Metal-Organic Frameworks and Investigate Their Interaction with Guest Molecules. *Chem. Rev.* **2021**, *121*, 1286–1424.

(166) Pal, B.; Yasin, A.; Kaur, R.; Tebyetekerwa, M.; Zabihi, F.; Yang, S.; Yang, C.-C.; Sofer, Z.; Jose, R. Understanding electrochemical capacitors with in-situ techniques. *Renew. Sust. En. Rev.* **2021**, *149*, 111418.

(167) Li, Z.; Zhu, G.; Lu, G.; Qiu, S.; Yao, X. Ammonia Borane Confined by a MetalOrganic Framework for Chemical Hydrogen Storage: Enhancing Kinetics and Eliminating Ammonia. *J. Amer. Chem. Soc.* **2010**, *132*, 1490–1491.

(168) Hiraoka, T.; Shigeto, S. Interactions of water confined in a metal–organic framework as studied by a combined approach of Raman, FTIR, and IR electroabsorption spectroscopies and multivariate curve resolution analysis. *Phys. Chem. Chem. Phys.* **2020**, *22*, 17798–17806.

(169) Möslein, A. F.; Gutiérrez, M.; Cohen, B.; Tan, J.-C. Near-Field Infrared Nanospectroscopy Reveals Guest Confinement in Metal–Organic Framework Single Crystals. *Nano Lett.* **2020**, *20*, 7446–7454.

(170) Martinez, V.; Karadeniz, B.; Biliškov, N.; Lončarić, I.; Muratović, S.; Žilić, D.; Avdoshenko, S. M.; Roslova, M.; Popov, A. A.; Užarević, K. Tunable Fulleretic Sodalite MOFs: Highly Efficient and Controllable Entrapment of C_{60} Fullerene via Mechanochemistry. *Chem. Mater.* **2020**, *32*, 10628–10640.

(171) Ngo, D.; Liu, H.; Chen, Z.; Kaya, H.; Zimudzi, T.; Gin, S.; Mahadevan, T.; Du, J.; Kim, S. Hydrogen bonding interactions of H2O and SiOH on a boroaluminosilicate glass corroded in aqueous solution. *NPJ Mater. Degrad.* **2020**, *4*.

(172) Delgado, M. Structure and stability of gas adsorption complexes in periodic porous solids as studied by VTIR spectroscopy: An overview. *Appl. Sci.* **2020**, *10*.

View Article Online
DOI: 10.1039/D2CP01458K

(173) Ahmed, A. Zeolite-encapsulated transition metal chelates: Synthesis and characterization. *Rev. Inorg. Chem.* **2014**, *34*, 153–175.

(174) Sreenivasulu, B.; Sreedhar, I.; Suresh, P.; Raghavan, K. Development Trends in Porous Adsorbents for Carbon Capture. *Env. Sci. Technol.* **2015**, *49*, 12641–12661.

(175) Liu, J.; Qian, W.; He, Y. F.; Wang, R. M. Mechanisms on formation of hierarchically porous carbon and its adsorption behaviors. *Water Sci. Technol.* **2016**, *74*, 266–275.

(176) Qezelsefloo, E.; Khalili, S.; Jahanshahi, M.; Peyravi, M. Adsorptive removal of CO_2 on Nitrogen-doped porous carbon derived from polyaniline: Effect of chemical activation. *Mater. Chem. Phys.* **2020**, *239*, 122304.

(177) Chen, Y.; Zhang, X.; Chen, W.; Yang, H.; Chen, H. The structure evolution of biochar from biomass pyrolysis and its correlation with gas pollutant adsorption performance. *Biores. Technol.* **2017**, *246*, 101–109.

(178) Lim, J. K.; Liu, T.; Jeong, J.; Shin, H.; Jang, H. J.; Cho, S. P.; Park, J. S. In situ syntheses of silver nanoparticles inside silver citrate nanorods via catalytic nanoconfinement effect. *Coll. Surf. A* **2020**, *605*, 125343.

(179) Ozaki, Y.; Beć, K. B.; Morisawa, Y.; Yamamoto, S.; Tanabe, I.; Huck, C. W.; Hofer, T. S. Advances, challenges and perspectives of quantum chemical approaches in molecular spectroscopy of the condensed phase. *Chem. Soc. Rev.* **2021**, *50*, 10917–10954.

(180) Iqbal, Z.; Owens, F. J. *Vibrational spectroscopy of phase transitions*; U.S. Department of Energy, 1984.

(181) Sherwood, P. M. A. *Vibrational Spectroscopy of Solids*; Cambridge University Press, 2011.

View Article Online
DOI: 10.1039/D2CP01458K

(182) Bellur Atici, E.; Karlığa, B. Quantitative determination of two polymorphic forms of imatinib mesylate in a drug substance and tablet formulation by X-ray powder diffraction, differential scanning calorimetry and attenuated total reflectance Fourier transform infrared spectroscopy. *J. Pharm. Biomed. Anal.* **2015**, *114*, 330–340.

(183) Le Pevelen, D.; Tranter, G. In *Encyclopedia of Spectroscopy and Spectrometry (Third Edition)*, 3rd ed.; Lindon, J. C., Tranter, G. E., Koppenaal, D. W., Eds.; Academic Press: Oxford, 2017; pp 750–761.

(184) Noda, O. Y., Isao *Two-Dimensional Correlation Spectroscopy – Applications in Vibrational and Optical Spectroscopy*; John Willey & Sons: Hoboken, USA, 2004.

(185) Šašić, S.; Katsumoto, Y.; Sato, H.; Ozaki, Y. Applications of Moving Window Two-Dimensional Correlation Spectroscopy to Analysis of Phase Transitions and Spectra Classification. *Anal. Chem.* **2003**, *75*, 4010–4018.

(186) Zimmermann, B.; Baranović, G. Determination of Phase Transition Temperatures by the Analysis of Baseline Variations in Transmittance Infrared Spectroscopy. *Appl. Spectrosc.* **2009**, *63*, 1152–1161.

(187) Zimmermann, B.; Baranović, G. Thermal analysis of paracetamol polymorphs by FT-IR spectroscopies. *J. Pharm. Biomed. Anal.* **2011**, *54*, 295–302.

(188) Zimmermann, B.; Vrsaljko, D. IR spectroscopy based thermal analysis of polymers. *Polymer Test.* **2010**, *29*, 849–856.

(189) Mihelj, T.; Vojta, D.; Tomašić, V. The diversity in thermal behavior of novel catanionic cholates: The dominant effect of quaternary ammonium centers. *Thermochim. Acta* **2014**, *584*, 17–30.

(190) Vojta, D.; Vrankić, M.; Bertmer, M.; Schaumann, G. Dehydration of -oxalic acid dihydrate: Structural, spectroscopic and thermal study with implications on the dis-

View Article Online
DOI: 10.1039/D2CP01458K

ruption of water molecular bridges in soil organic matter. *Thermochim. Acta* **2016**, *643*, 73–82.

(191) Vojta, D.; Višnjevac, A.; Leka, Z.; Kosović, M.; Vazdar, M. Temperature-induced release of crystal water in the Co, Mo and Pt complexes of N,N-diacetatedithiocarbamate. FTIR spectroscopy and quantum chemical study. *J. Mol. Struct.* **2016**, *1103*, 245–253.

(192) Tomašić, V.; Biliškov, N.; Mihelj, T.; Štefanić, Z. Thermal behaviour and structural properties of surfactant-Picrate compounds: The effect of the ammonium headgroup number. *Thermochim. Acta* **2013**, *569*, 25–35.

(193) Mihelj, T.; Tomašić, V.; Biliškov, N. 18-crown-6-sodium cholate complex: Thermochemistry, structure, and stability. *Langmuir* **2014**, *30*, 6274–6285.

(194) Biliškov, N. In Situ Monitoring of a Quasi Solid-State Diffusion-Driven Cocrystallization in the Diphenylamine-Benzophenone System. *Cryst. Growth Des.* **2021**, *21*, 1434–1442.

(195) Milanović, I.; Biliškov, N.; Užarević, K.; Lukin, S.; Etter, M.; Halasz, I. Mechanochemical Synthesis and Thermal Dehydrogenation of Novel Calcium-Containing Bimetallic Amidoboranes. *ACS Sust. Chem. Eng.* **2021**, *9*, 2089–2099.

(196) Köhler, M. H.; Schardt, M.; Rauscher, M. S.; Koch, A. W. Gas Measurement Using Static Fourier Transform Infrared Spectrometers. *Sensors* **2017**, *17*.

(197) Coenen, K.; Gallucci, F.; Mezari, B.; Hensen, E.; van Sint Annaland, M. An in-situ IR study on the adsorption of CO_2 and H_2O on hydrotalcites. *J. CO_2 Util.* **2018**, *24*, 228–239.

(198) Köck, E.-M.; Kogler, M.; Bielz, T.; Klötzer, B.; Penner, S. In Situ FT-IR Spectroscopic

View Article Online
DOI: 10.1039/D2CP01458K

Study of CO_2 and CO Adsorption on Y_2O_3, ZrO_2, and Yttria-Stabilized ZrO_2. *J. Phys. Chem. C* **2013**, *117*, 17666–17673.

(199) Collins, S. E.; Baltanás, M. A.; Bonivardi, A. L. Infrared Spectroscopic Study of the Carbon Dioxide Adsorption on the Surface of Ga_2O_3 Polymorphs. *J. Phys. Chem. B* **2006**, *110*, 5498–5507.

(200) Breunig, M.; Dorner, M.; Senker, J. Ultramicroporous polyimides with hierarchical morphology for carbon dioxide separation. *J. Mater. Chem. A* **2021**, *9*, 12797–12806.

(201) Cueto-Díaz, E.; Castro-Muiz, A.; Suárez-García, F.; Gálvez-Martínez, S.; Torquemada-Vico, M.; Valles-González, M.; Mateo-Martí, E. Aptes-based silica nanoparticles as a potential modifier for the selective sequestration of CO_2 gas molecules. *Nanomater.* **2021**, *11*.

(202) Hua, J.; Duan, Z.; Gao, C.; Xie, X.; Qiao, Z.; Feng, T.; Ma, X. A 3,5-Connected 3D Nickel-Mixed Ligands Coordination Polymer with Selective Adsorption of Carbon Dioxide. *Russ. J. Coord. Chem.* **2021**, *47*, 646–652.

(203) Hua, J.; Yang, C.; Zhang, X.; Chen, N.; Hu, B.; Bian, Y.; Ma, X. A three dimensional cobalt-mixed ligands framework with selective adsorption of carbon dioxide. *Inorg. Nano-Metal Chem.* **2021**,

(204) Lourenço, M.; Fontana, M.; Jagdale, P.; Pirri, C.; Bocchini, S. Improved CO_2 adsorption properties through amine functionalization of multi-walled carbon nanotubes. *Chem. Eng. J.* **2021**, *414*.

(205) Pazdera, J.; Berger, E.; Lercher, J.; Jentys, A. Conversion of CO_2 to methanol over bifunctional basic-metallic catalysts. *Catal. Commun.* **2021**, *159*.

(206) Sugamata, K.; Kobayashi, S.; Iihama, T.; Minoura, M. Gas Adsorption in R2-MOF-5 Difunctionalized with Alkyl Groups. *Eur. J. Inorg. Chem.* **2021**, *2021*, 3185–3190.

View Article Online
DOI: 10.1039/D2CP01458K

(207) Zheng, Y.; Wang, X.; Liu, C.; Yu, B.; Li, W.; Wang, H.; Sun, T.; Jiang, J. Triptycene-supported bimetallic salen porous organic polymers for high efficiency CO_2 fixation to cyclic carbonates. *Inorg. Chem. Front.* **2021**, *8*.

(208) Kiani, A.; Sakurovs, R.; Grigore, M.; Keshavarz, A.; White, S. The Use of Infrared Spectroscopy to Determine Methane Emission Rates from Coals at Atmospheric Pressures. *Energy & Fuels* **2019**, *33*, 238–247.

(209) Creci, S.; Wang, X.; Carlsson, P.-A.; Martinelli, A.; Skoglundh, M. Methoxy ad-species in MFI zeotypes during methane exposure and methanol desorption followed by in situ IR spectroscopy. *Catal. Today* **2021**, *369*, 123–128.

(210) Wang, K.; Du, F.; Wang, G. The influence of methane and CO_2 adsorption on the functional groups of coals: Insights from a Fourier transform infrared investigation. *J. Nat. Gas Sci. Eng.* **2017**, *45*, 358–367.

(211) Kundu, T.; Shah, B. B.; Bolinois, L.; Zhao, D. Functionalization-Induced Breathing Control in Metal–Organic Frameworks for Methane Storage with High Deliverable Capacity. *Chem. Mater.* **2019**, *31*, 2842–2847.

(212) Mauron, P.; Gaboardi, M.; Remhof, A.; Bliersbach, A.; Sheptyakov, D.; Aramini, M.; Vlahopoulou, G.; Giglio, F.; Pontiroli, D.; Riccó, M.; Züttel, A. Hydrogen Sorption in $Li_{12}C_{60}$. *J. Phys. Chem. C* **2013**, *117*, 22598–22602.

(213) Stripp, S. T. In Situ Infrared Spectroscopy for the Analysis of Gas-processing Metalloenzymes. *ACS Catal.* **2021**, *11*, 7845–7862.

(214) Liao, Y.; Picot, P.; Lainé, M.; Brubach, J.-B.; Roy, P.; Thill, A.; Le Caër, S. Tuning the properties of confined water in standard and hybrid nanotubes: An infrared spectroscopic study. *Nano Res.* **2018**, *11*, 4759–4773.

View Article Online
DOI: 10.1039/D2CP01458K

(215) Biswas, R.; Bagchi, B. Anomalous water dynamics at surfaces and interfaces: synergistic effects of confinement and surface interactions. *J. Phys.: Cond. Matter* **2017**, *30*, 013001.

(216) Manna, U.; Halder, S.; Das, G. Ice-like Cyclic Water Hexamer Trapped within a Halide Encapsulated Hexameric Neutral Receptor Core: First Crystallographic Evidence of a Water Cluster Confined within a Receptor-Anion Capsular Assembly. *Cryst. Growth Des.* **2018**, *18*, 1818–1825.

(217) Köhler,; Bordin, J. R.; de Matos, C. F.; Barbosa, M. C. Water in nanotubes: The surface effect. *Chem. Eng. Sci.* **2019**, *203*, 54–67.

(218) Zhang, Y.-L.; Liu, Y.-Q.; Han, D.-D.; Ma, J.-N.; Wang, D.; Li, X.-B.; Sun, H.-B. Quantum-Confined-Superfluidics-Enabled Moisture Actuation Based on Unilaterally Structured Graphene Oxide Papers. *Adv. Mater.* **2019**, *31*, 1901585.

(219) Chen, L.; He, X.; Liu, H.; Qian, L.; Kim, S. H. Water Adsorption on Hydrophilic and Hydrophobic Surfaces of Silicon. *J. Phys. Chem. C* **2018**, *122*, 11385–11391.

(220) Uhlig, M.; Garcia, R. In Situ Atomic-Scale Imaging of Interfacial Water under 3D Nanoscale Confinement. *Nano Lett.* **2021**, *21*, 5593–5598.

(221) Moučka, F.; Zamfir, S.; Bratko, D.; Luzar, A. Molecular polarizability in open ensemble simulations of aqueous nanoconfinements under electric field. *J. Chem. Phys.* **2019**, *150*.

(222) Knight, A.; Kalugin, N.; Coker, E.; Ilgen, A. Water properties under nano-scale confinement. *Sci. Rep.* **2019**, *9*.

(223) Ghasemi, M.; Ramsheh, S.; Sharma, S. Quantitative Assessment of Thermodynamic Theory in Elucidating the Behavior of Water under Hydrophobic Confinement. *J. Phys. Chem. B* **2018**, *122*, 12087–12096.

View Article Online
DOI: 10.1039/D2CP01458K

(224) Sammon, C.; Mura, C.; Yarwood, J.; Everall, N.; Swart, R.; Hodge, D. FTIR-ATR studies of the structure and dynamics of water molecules in polymeric matrixes. A comparison of PET and PVC. *J. Phys. Chem. B* **1998**, *102*, 3402–3411.

(225) Zhang, L.; Hu, J.-S.; Huang, X.-H.; Song, J.; Lu, S.-Y. Particle-in-box nanostructured materials created via spatially confined pyrolysis as high performance bifunctional catalysts for electrochemical overall water splitting. *Nano En.* **2018**, *48*, 489–499.

(226) Rueda, M.; Sanz-Moral, L. M.; Segovia, J. J.; Martín, A. Improvement of the kinetics of hydrogen release from ammonia borane confined in silica aerogel. *Micropor. Mesopor. Mater.* **2017**, *237*, 189–200.

(227) Hassanpour, M.; Jafari, H.; Sharifi, S.; Rezaie, J.; Lighvan, Z.; Mahdavinia, G.; Gohari, G.; Akbari, A. Salicylic acid-loaded chitosan nanoparticles (SA/CTS NPs) for breast cancer targeting: Synthesis, characterization and controlled release kinetics. *J. Mol. Struct.* **2021**, *1245*.

(228) Maleki, M.; Hadian, Z.; Abdi, K.; Koohy-Kamaly, P.; Bahmanyar, F. Study of the Physicochemical Properties and Antimicrobial Activities of Nanoparticles Containing -Cyclodextrin and Geranial. *J. Nanostr.* **2021**, *11*, 189–201.

(229) Nkanga, C.; Krause, R. Encapsulation of Isoniazid-conjugated Phthalocyanine-In-Cyclodextrin-In-Liposomes Using Heating Method. *Sci. Rep.* **2019**, *9*.

(230) Nyamekye, C.; Bobbitt, J.; Zhu, Q.; Smith, E. The evolution of total internal reflection Raman spectroscopy for the chemical characterization of thin films and interfaces. *Anal. Bioanal. Chem.* **2020**,

(231) Guerrero-Pérez, M.; Patience, G. Experimental methods in chemical engineering: Fourier transform infrared spectroscopy—FTIR. *Can. J. Chem. Eng.* **2020**, *98*, 25–33.

View Article Online
DOI: 10.1039/D2CP01458K

(232) Kubota, J.; Ma, Z.; Zaera, F. In Situ Characterization of Adsorbates in SolidLiquid Interfaces by ReflectionAbsorption Infrared Spectroscopy. *Langmuir* **2003**, *19*, 3371–3376.

(233) Bewick, A.; Pons, S. *Advances in Infrared and Raman Spectroscopy*; Wiley: Heyden, New York, 1985; Vol. 12; Chapter Infrared Spectroscopy of the Electrode-Electrolyte Solution Interface, pp 1–63.

(234) Hoffmann, F. M. Infrared reflection-absorption spectroscopy of adsorbed molecules. *Surf. Sci. Rep.* **1983**, *3*, 107–192.

(235) Chabal, Y. Surface infrared spectroscopy. *Surf. Sci. Rep.* **1988**, *8*, 211–357.

(236) Chabal, Y.; Hines, M.; Feijóo, D.; Hines, M.; Feijóo, D. Characterization of silicon surfaces and interfaces by optical vibrational spectroscopy. *J. Vac. Sci. Technol. A* **1995**, *13*, 1719–1727.

(237) Greenler, R. G. Infrared Study of Adsorbed Molecules on Metal Surfaces by Reflection Techniques. *J. Chem. Phys.* **1966**, *44*, 310–315.

(238) Attia, S.; Schauermann, S. Coverage-Dependent Adsorption Geometry of Acetophenone on Pt(111). *J. Phys. Chem. C* **2020**, *124*, 557–566.

(239) Blaumeiser, D.; Schuschke, C.; Fromm, L.; Taccardi, N.; Schötz, S.; Eschenbacher, R.; Bühlmeyer, H.; Xu, T.; Bauer, T.; Wasserscheid, P.; Görling, A.; Libuda, J. CO Permeability and Wetting Behavior of Ionic Liquids on Pt(111): An IRAS and PM-IRAS Study from Ultrahigh Vacuum to Ambient Pressure. *J. Phys. Chem. C* **2021**, *125*, 15301–15315.

(240) Hofman, M.; Scoullos, E.; Robbins, J.; Ezeonu, L.; Potapenko, D.; Yang, X.; Podkolzin, S.; Koel, B. Acetic Acid Adsorption and Reactions on Ni(110). *Langmuir* **2020**, *36*, 8705–8715.

View Article Online
DOI: 10.1039/D2CP01458K

(241) Wähler, T.; Schuster, R.; Libuda, J. Self-Metalation of Anchored Porphyrins on Atomically Defined Cobalt Oxide Surfaces: In situ Studies by Surface Vibrational Spectroscopy. *Chem. Eur. J.* **2020**, *26*, 12445–12453.

(242) Weng, X.; Cui, Y.; Shaikhutdinov, S.; Freund, H.-J. CO_2 Adsorption on CaO(001): Temperature-Programmed Desorption and Infrared Study. *J. Phys. Chem. C* **2019**, *123*, 1880–1887.

(243) Widdascheck, F.; Kothe, M.; Thussing, S.; Jakob, P.; Witte, G. Evolution of TiOPc Films on Au(111): From Seed Layer to Crystalline Multilayers. *J. Phys. Chem. C* **2020**, *124*, 14664–14671.

(244) Pickering, H. L.; Eckstrom, H. C. Heterogeneous Reaction Studies by Infrared Absorption. *J. Phys. Chem.* **1959**, *63*, 512–518.

(245) Hollins, P.; Pritchard, J. Infrared studies of chemisorbed layers on single crystals. *Prog. Surf. Sci.* **1985**, *19*, 275–349.

(246) Barner, B. J.; Green, M. J.; Saez, E. I.; Corn, R. M. Polarization modulation Fourier transform infrared reflectance measurements of thin films and monolayers at metal surfaces utilizing real-time sampling electronics. *Anal. Chem.* **1991**, *63*, 55–60.

(247) Golden, W. G.; Saperstein, D. D.; Severson, M. W.; Overend, J. Infrared reflection-absorption spectroscopy of surface species: a comparison of Fourier transform and dispersion methods. *J. Phys. Chem.* **1984**, *88*, 574–580.

(248) Agrawal, V. K.; Trenary, M. An infrared study of NO adsorption at defect sites on Pt(111). *Surf. Sci.* **1991**, *259*, 116–128.

(249) The influence of surface defects on the infrared spectra of adsorbed species. *Surf. Sci. Rep.* **1992**, *16*, 51–94.

View Article Online
DOI: 10.1039/D2CP01458K

(250) Mukerji, R.; Bolina, A.; Brown, W. A RAIRS and TPD investigation of the adsorption of CO on Pt211. *Surf. Sci.* **2003**, *527*, 198–208.

(251) Vattuone, L.; Savio, L.; Rocca, M. Bridging the structure gap: Chemistry of nanostructured surfaces at well-defined defects. *Surf. Sci. Rep.* **2008**, *63*, 101–168.

(252) Gutiérrez-González, A.; Beck, R. Quantum state and surface-site-resolved studies of methane chemisorption by vibrational spectroscopies. *Phys. Chem. Chem. Phys.* **2020**, *22*, 17448–17459.

(253) Walsh, A. J.; van Lent, R.; Auras, S. V.; Gleeson, M. A.; Berg, O. T.; Juurlink, L. B. F. Step-type and step-density influences on CO adsorption probed by reflection absorption infrared spectroscopy using a curved Pt(1 1 1) surface. *J. Vac. Sci. Technol. A* **2017**, *35*, 03E102.

(254) Brandt, R. K.; Sorbello, R. S.; Greenler, R. G. Site-specific, coupled-harmonic-oscillator model of carbon monoxide adsorbed on extended, single-crystal surfaces and on small crystals of platinum. *Surf. Sci.* **1992**, *271*, 605–615.

(255) Chadwick, H.; Guo, H.; Gutiérrez-González, A.; Menzel, J. P.; Jackson, B.; Beck, R. D. Methane dissociation on the steps and terraces of Pt(211) resolved by quantum state and impact site. *J. Chem. Phys.* **2018**, *148*, 014701.

(256) Chadwick, H.; Gutiérrez-González, A.; Migliorini, D.; Beck, R. D.; Kroes, G.-J. Incident Angle Dependence of CHD3 Dissociation on the Stepped Pt(211) Surface. *J. Phys. Chem. C* **2018**, *122*, 19652–19660.

(257) Chadwick, H.; Gutiérrez-González, A.; Beck, R. D.; Kroes, G.-J. Transferability of the SRP32-vdW specific reaction parameter functional to CHD_3 dissociation on Pt(110)-(2×1). *J. Chem. Phys.* **2019**, *150*, 124702.

View Article Online
DOI: 10.1039/D2CP01458K

(258) Chadwick, H.; Gutiérrez-González, A.; Beck, R. D.; Kroes, G.-J. CHD_3 Dissociation on the Kinked Pt(210) Surface: A Comparison of Experiment and Theory. *J. Phys. Chem. C* **2019**, *123*, 14530–14539.

(259) Chen, L.; Ueta, H.; Bisson, R.; Beck, R. D. Vibrationally bond-selected chemisorption of methane isotopologues on Pt(111) studied by reflection absorption infrared spectroscopy. *Faraday Discuss.* **2012**, *157*, 285–295.

(260) Gutiérrez-González, A.; Torio, M.; Busnengo, H.; Beck, R. Site Selective Detection of Methane Dissociation on Stepped Pt Surfaces. *Top. Catal.* **2019**, *62*, 859–873.

(261) Yu, X.; Schwarz, P.; Nefedov, A.; Meyer, B.; Wang, Y.; Wöll, C. Structural Evolution of Water on ZnO($10\bar{1}0$): From Isolated Monomers via Anisotropic H-Bonded 2D and 3D Structures to Isotropic Multilayers. *Angew. Chem. Int. Ed.* **2019**, *58*, 17751–17757.

(262) Behrens, M.; Studt, F.; Kasatkin, I.; Kühl, S.; Hävecker, M.; Abild-Pedersen, F.; Zander, S.; Girgsdies, F.; Kurr, P.; Kniep, B.-L.; Tovar, M.; Fischer, R. W.; Nrskov, J. K.; Schl¨ ogl, R. The Active Site of Methanol Synthesis over $Cu/ZnO/Al_2O_3$ Industrial Catalysts. *Science* **2012**, *336*, 893–897.

(263) Kuld, S.; Thorhauge, M.; Falsig, H.; Elkjær, C. F.; Helveg, S.; Chorkendorff, I.; Sehested, J. Quantifying the promotion of Cu catalysts by ZnO for methanol synthesis. *Science* **2016**, *352*, 969–974.

(264) Kattel, S.; Ramírez, P. J.; Chen, J. G.; Rodriguez, J. A.; Liu, P. Active sites for CO¡sub¿2¡/sub¿ hydrogenation to methanol on Cu/ZnO catalysts. *Science 355*.

(265) Studt, F.; Behrens, M.; Kunkes, E. L.; Thomas, N.; Zander, S.; Tarasov, A.; Schumann, J.; Frei, E.; Varley, J. B.; Abild-Pedersen, F.; Nrskov, J. K.; Schlögl, R. The Mechanism of CO and CO_2 Hydrogenation to Methanol over Cu-Based Catalysts. *ChemCatChem* **2015**, *7*, 1105–1111.

View Article Online
DOI: 10.1039/D2CP01458K

(266) Lunkenbein, T.; Schumann, J.; Behrens, M.; Schlögl, R.; Willinger, M. G. Formation of a ZnO Overlayer in Industrial Cu/ZnO/Al_2O_3 Catalysts Induced by Strong Metal–Support Interactions. *Angew. Chem. Int. Ed.* **2015**, *54*, 4544–4548.

(267) Grasa, G.; González, B.; Alonso, M.; Abanades, J. C. Comparison of CaO-Based Synthetic CO2 Sorbents under Realistic Calcination Conditions. *Energy & Fuels* **2007**, *21*, 3560–3562.

(268) Choi, S.; Drese, H., Jeffrey; Jones, W., Christopher Adsorbent Materials for Carbon Dioxide Capture from Large Anthropogenic Point Sources. *ChemSusChem* **2009**, *2*, 796–854.

(269) Freund, H.-J.; Roberts, M. Surface chemistry of carbon dioxide. *Surf. Sci. Rep.* **1996**, *25*, 225–273.

(270) Taifan, W.; Boily, J.-F.; Baltrusaitis, J. Surface chemistry of carbon dioxide revisited. *Surf. Sci. Rep.* **2016**, *71*, 595–671.

(271) Burghaus, U. Surface science perspective of carbon dioxide chemistry—Adsorption kinetics and dynamics of CO2 on selected model surfaces. *Catal. Today* **2009**, *148*, 212–220.

(272) Zaera, F.; Hoffmann, H.; Griffiths, P. Determination of molecular chemisorption geometries using reflection-absorption infrared spectroscopy: alkyl halides on Pt(111). *Journal of Electron Spectroscopy and Related Phenomena* **1990**, *54-55*, 705–715.

(273) Hinrichs, K. In *Surface and Thin Film Analysis: A Compendium of Principles, Instrumentation, and Applications*, 2nd ed.; Friedbacher, G., Bubert, H., Eds.; 2011; Chapter Reflection Absorption IR Spectroscopy (RAIRS), pp 367–375.

(274) Sheppard, N. In *Encyclopedia of Spectroscopy and Spectrometry*, third edition ed.;

View Article Online
DOI: 10.1039/D2CP01458K

Lindon, J. C., Tranter, G. E., Koppenaal, D. W., Eds.; Academic Press: Oxford, 2017; pp 455–462.

(275) David, R. B.; Yaacov, A. B.; Eren, B. Effect of Surface Orientation on Methanol Adsorption and Thermally Induced Structural Transformations on Copper Surfaces. *J. Phys. Chem. C* **2021**, *125*, 6099–6107.

(276) Casford, M. T. L.; Ge, A.; Kett, P. J. N.; Ye, S.; Davies, P. B. The Structure of Lipid Bilayers Adsorbed on Activated Carboxy-Terminated Monolayers Investigated by Sum Frequency Generation Spectroscopy. *J. Phys. Chem. B* **2014**, *118*, 3335–3345.

(277) Mateo-Martí, E.; Briones, C.; Román, E.; Briand, E.; Pradier, C. M.; Martín-Gago, J. A. Self-Assembled Monolayers of Peptide Nucleic Acids on Gold Surfaces: A Spectroscopic Study. *Langmuir* **2005**, *21*, 9510–9517.

(278) Ingman, E.; Shepherd, A.; Brown, W. Using surface science techniques to investigate the interaction of acetonitrile with dust grain analogue surfaces behaviour of acetonitrile and water on a graphitic surface. *Johnson Matthey Technol. Rev.* **2021**, *65*, 600–614.

(279) Iwamoto, R.; Murase, H. Infrared spectroscopic study of the interactions of nylon-6 with water. *J. Polymer Sci. B: Polymer Phys.* **2003**, *41*, 1722–1729.

(280) Concepción, P. In *Infrared Spectroscopy - Principles, Advances, and Applications*; El-Azazy, M., Ed.; IntechOpen, 2018.

(281) Bianchi, D. A contribution to the experimental microkinetic approach of gas/solid heterogeneous catalysis: Measurement of the individual heats of adsorption of coadsorbed species by using the AEIR method. *Catalysts* **2018**, *8*.

(282) Kim, J.; Kim, H.-E.; Lee, H. Single-Atom Catalysts of Precious Metals for Electrochemical Reactions. *ChemSusChem* **2018**, *11*, 104–113.

View Article Online
DOI: 10.1039/D2CP01458K

(283) Luo, L.; Hernandez, R.; Zhou, X.-D.; Yan, H. Heterogeneous catalysis at metal-oxide interfaces using in situ and operando spectroscopy: From nanoparticles to single-atom sites. *Appl. Catal. A* **2021**, *624*.

(284) Mudiyanselage, K.; Stacchiola, D. J. *In-situ Characterization of Heterogeneous Catalysts*; John Wiley Sons, Ltd, 2013; Chapter 8, pp 209–239.

(285) Newton, M. A.; Fernández-García, M. *In-situ Characterization of Heterogeneous Catalysts*; John Wiley Sons, Ltd, 2013; Chapter 14, pp 369–409.

(286) Stavitski, E. *In-situ Characterization of Heterogeneous Catalysts*; John Wiley Sons, Ltd, 2013; Chapter 9, pp 241–265.

(287) Pollitt, S.; Truttmann, V.; Haunold, T.; Garcia, C.; Olszewski, W.; Llorca, J.; Barrabés, N.; Rupprechter, G. The Dynamic Structure of $Au_{38}(SR)_{24}$ Nanoclusters Supported on CeO_2 upon Pretreatment and CO Oxidation. *ACS Catal.* **2020**, *10*, 6144–6148.

(288) Lukashuk, L.; Yigit, N.; Rameshan, R.; Kolar, E.; Teschner, D.; Hävecker, M.; Knop-Gericke, A.; Schlögl, R.; Föttinger, K.; Rupprechter, G. Operando Insights into CO Oxidation on Cobalt Oxide Catalysts by NAP-XPS, FTIR, and XRD. *ACS Catal.* **2018**, *8*, 8630–8641.

(289) Wolfbeisser, A.; Sophiphun, O.; Bernardi, J.; Wittayakun, J.; Föttinger, K.; Rupprechter, G. Methane dry reforming over ceria-zirconia supported Ni catalysts. *Catal. Today* **2016**, *277*, 234–245.

(290) Haghofer, A.; Ferri, D.; Föttinger, K.; Rupprechter, G. Who Is Doing the Job? Unraveling the Role of Ga_2O_3 in Methanol Steam Reforming on Pd_2Ga/Ga_2O_3. *ACS Catal.* **2012**, *2*, 2305–2315.

View Article Online
DOI: 10.1039/D2CP01458K

(291) Zaera, F. In-situ and operando spectroscopies for the characterization of catalysts and of mechanisms of catalytic reactions. *J. Catal.* **2021**, *404*, 900–910.

(292) Chansai, S.; Burch, R.; Hardacre, C.; Breen, J.; Meunier, F. The use of short time-on-stream in situ spectroscopic transient kinetic isotope techniques to investigate the mechanism of hydrocarbon selective catalytic reduction (HC-SCR) of NO_x at low temperatures. *J. Catal.* **2011**, *281*, 98–105.

(293) Saavedra, J.; Doan, H. A.; Pursell, C. J.; Grabow, L. C.; Chandler, B. D. The critical role of water at the gold-titania interface in catalytic CO oxidation. *Science* **2014**, *345*, 1599–1602.

(294) Kale, M. J.; Christopher, P. Utilizing Quantitative in Situ FTIR Spectroscopy To Identify Well-Coordinated Pt Atoms as the Active Site for CO Oxidation on Al_2O_3-Supported Pt Catalysts. *ACS Catal.* **2016**, *6*, 5599–5609.

(295) Zaera, F. Gold-Titania Catalysts for Low-Temperature Oxidation and Water Splitting. *Topics. Catal.* **2018**, *61*.

(296) Abdel-Mageed, A.; Chen, S.; Fauth, C.; Häring, T.; Bansmann, J. Fundamental Aspects of Ceria Supported Au Catalysts Probed by In Situ/Operando Spectroscopy and TAP Reactor Studies. *ChemPhysChem* **2021**, *22*, 1302–1315.

(297) Fan, W.; Tahir, M. Current Trends and Approaches to Boost the Performance of Metal Organic Frameworks for Carbon Dioxide Methanation through Photo/Thermal Hydrogenation: A Review. *Ind. Eng. Chem. Res.* **2021**, *60*, 13149–13179.

(298) Liu, Y.; Wu, Z.; Kuhlenbeck, H.; Freund, H.-J. Surface Action Spectroscopy: A Review and a Perspective on a New Technique to Study Vibrations at Surfaces. *Chem. Rec.* **2021**, *21*, 1270–1283.

View Article Online
DOI: 10.1039/D2CP01458K

(299) Chen, L.; Wang, Y.; Wang, X.; Wang, Q.; Li, B.; Li, S.; Zhang, S.; Li, W. Brnsted acid enhanced hexagonal cerium phosphate for the selective catalytic reduction of NO with NH_3: In situ DRIFTS and DFT investigation. *J. Hazard. Mater.* **2022**, *424*.

(300) Henry, B.; Samokhvalov, A. Hygroscopic metal-organic framework MIL-160(Al): In-situ time-dependent ATR-FTIR and gravimetric study of mechanism and kinetics of water vapor sorption. *Spectrochim. Acta A* **2022**, *267*.

(301) Jothinathan, L.; Cai, Q.; Ong, S.; Hu, J. Fe-Mn doped powdered activated carbon pellet as ozone catalyst for cost-effective phenolic wastewater treatment: Mechanism studies and phenol by-products elimination. *J. Hazard. Mater.* **2022**, *424*.

(302) Li, X.; Li, H.; Huang, Y.; Cao, J.; Huang, T.; Li, R.; Zhang, Q.; Lee, S.-C.; Ho, W. Exploring the photocatalytic conversion mechanism of gaseous formaldehyde degradation on TiO2–x-OV surface. *J. Hazard. Mater.* **2022**, *424*.

(303) Rajabi, S.; Nasiri, A.; Hashemi, M. Enhanced activation of persulfate by $CuCoFe_2O_4$@MC/AC as a novel nanomagnetic heterogeneous catalyst with ultrasonic for metronidazole degradation. *Chemosphere* **2022**, *286*.

(304) Schröder, C.; Haugg, P.; Baumann, A.-K.; Schmidt, M.; Smyczek, J.; Schauermann, S. Competing Reaction Pathways in Heterogeneously Catalyzed Hydrogenation of Allyl Cyanide: The Chemical Nature of Surface Species. *Chem. Eur. J.* **2021**, *27*, 17240–17254.

(305) Sivasankar, N.; Frei, H. Direct Observation of Kinetically Competent Surface Intermediates upon Ethylene Hydroformylation over Rh/Al2O3 under Reaction Conditions by Time-Resolved Fourier Transform Infrared Spectroscopy. *J. Phys. Chem. C* **2011**, *115*, 7545–7553.

(306) Johnson, T. J.; Simon, A.; Weil, J. M.; Harris, G. W. Applications of Time-Resolved

View Article Online
DOI: 10.1039/D2CP01458K

Step-Scan and Rapid-Scan FT-IR Spectroscopy: Dynamics from Ten Seconds to Ten Nanoseconds. *Appl. Spectrosc.* **1993**, *47*, 1376–1381.

(307) Lai, J.; Ma, Z.; Mink, L.; Mueller, L. J.; Zaera, F. Influence of Peripheral Groups on the Physical and Chemical Behavior of Cinchona Alkaloids. *J. Phys. Chem. B* **2009**, *113*, 11696–11701.

(308) Kubota, J.; Zaera, F. Adsorption geometry of modifiers as key in imparting chirality to platinum catalysts. *J. Am. Chem. Soc.* **2001**, *123*.

(309) Cavers, M.; Davidson, J.; Harkness, I.; Rees, L.; McDougall, G. Spectroscopic Identification of the Active Site for CO Oxidation on Rh/Al2O3 by Concentration Modulation in situ DRIFTS. *J. Catal.* **1999**, *188*, 426–430.

(310) Schubert, M. M.; Häring, T. P.; Bräth, G.; Gasteiger, H. A.; Behm, R. J. New DRIFTS Cell Design for the Simultaneous Acquisition of IR Spectra and Kinetic Data Using On-Line Product Analysis. *Appl. Spectrosc.* **2001**, *55*, 1537–1543.

(311) Meunier, F.; Goguet, A.; Shekhtman, S.; Rooney, D.; Daly, H. A modified commercial DRIFTS cell for kinetically relevant operando studies of heterogeneous catalytic reactions. *Appl. Catal. A* **2008**, *340*, 196–202.

(312) Dynamic phenomena during the photocatalytic oxidation of ethanol and acetone over nanocrystalline TiO2: simultaneous FTIR analysis of gas and surface species. *J. Catal. 219*.

(313) Zaera, F. Surface chemistry at the liquid/solid interface. *Surf. Sci.* **2011**, *605*, 1141–1145.

(314) Meemken, F.; Müller, P.; Hungerbühler, K.; Baiker, A. Simultaneous probing of bulk liquid phase and catalytic gas-liquid-solid interface under working conditions using attenuated total reflection infrared spectroscopy. *Rev. Sci. Instr.* **2014**, *85*, 084101.

View Article Online
DOI: 10.1039/D2CP01458K

(315) Zaera, F. Probing Liquid/Solid Interfaces at the Molecular Level. *Chem. Rev.* **2012**, *112*, 2920–2986.

(316) Mojet, B. L.; Ebbesen, S. D.; Lefferts, L. Light at the interface: the potential of attenuated total reflection infrared spectroscopy for understanding heterogeneous catalysis in water. *Chem. Soc. Rev.* **2010**, *39*, 4643–4655.

(317) Infrared absorption spectroscopy characterization of liquid–solid interfaces: The case of chiral modification of catalysts. *Surf. Sci.* **2018**, *669*, 16–24.

(318) Zandi, O.; Hamann, T. Determination of photoelectrochemical water oxidation intermediates on haematite electrode surfaces using operando infrared spectroscopy. *Nature Chem.* **2016**, *8*, 778–783.

(319) Zhang, Y.; Zhang, H.; Liu, A.; Chen, C.; Song, W.; Zhao, J. Rate-Limiting O–O Bond Formation Pathways for Water Oxidation on Hematite Photoanode. *J. Am. Chem. Soc.* **2018**, *140*, 3264–3269.

(320) Chen, C.; Song, M.; Lu, L.; Yue, L.; Huang, T.; Yu, A. Application of In Situ Raman and Fourier Transform Infrared Spectroelectrochemical Methods on the Electrode-Electrolyte Interface for LithiumOxygen Batteries. *Batteries and Supercaps* **2021**, *4*, 850–859.

(321) Zhang, L.; Qian, T.; Zhu, X.; Hu, Z.; Wang, M.; Zhang, L.; Jiang, T.; Tian, J.-H.; Yan, C. In situ optical spectroscopy characterization for optimal design of lithium-sulfur batteries. *Chem. Soc. Rev.* **2019**, *48*, 5432–5453.

(322) Cowan, A.; Hardwick, L. Advanced Spectroelectrochemical Techniques to Study Electrode Interfaces Within Lithium-Ion and Lithium-Oxygen Batteries. *Ann. Rev. Anal. Chem.* **2019**, *12*, 323–346.

View Article Online
DOI: 10.1039/D2CP01458K

(323) Hosseinpour, S.; Johnson, M. Vibrational spectroscopy in studies of atmospheric corrosion. *Materials* **2017**, *10*.

(324) Qian, Z.; Wang, S.; Ye, X.; Liu, Z.; Wu, Z. Corrosion resistance and wetting properties of silica-based superhydrophobic coatings on AZ31B Mg alloy surfaces. *Appl. Surf. Sci.* **2018**, *453*, 1–10.

(325) Zhao, W.; Magnus Johnson, C. Nano infrared microscopy: Obtaining chemical information on the nanoscale in corrosion studies. *J. Electrochem. Soc.* **2019**, *166*, C3456–C3460.

(326) Frankel, G.; Sridhar, N. Understanding localized corrosion. *Mater. Today* **2008**, *11*, 38–44.

(327) Hosseinpour, S.; Hedberg, J.; Baldelli, S.; Leygraf, C.; Johnson, M. Initial Oxidation of Alkanethiol-Covered Copper Studied by Vibrational Sum Frequency Spectroscopy. *J. Phys. Chem. C* **2011**, *115*, 23871–23879.

(328) Hillenbrand, R.; Keilmann, F. Material-specific mapping of metal/semiconductor/dielectric nanosystems at 10 nm resolution by backscattering near-field optical microscopy. *Appl. Phys. Lett.* **2002**, *80*, 25–27.

(329) Morsch, S.; Emad, S.; Farren, L.; Goodall, M.; Lyon, S.; Gibbon, S. The Unexpected Role of Carbonate Impurities in Polyphosphate Corrosion Inhibition. *Sci. Rep.* **2018**, *8*.

(330) Wain, A.; O'connell, M. Advances in surface-enhanced vibrational spectroscopy at electrochemical interfaces. *Adv. Phys.* **2017**, *2*, 188–209.

(331) Matsui, M.; Deguchi, S.; Kuwata, H.; Imanishi, N. In-operando FTIR Spectroscopy for Composite Electrodes of Lithium-ion Batteries. *Electrochem.* **2015**, *83*, 874–878.

View Article Online
DOI: 10.1039/D2CP01458K

(332) Saqib, N.; Ohlhausen, G. M.; Porter, J. M. In operando infrared spectroscopy of lithium polysulfides using a novel spectro-electrochemical cell. *J. Power Sources* **2017**, *364*, 266–271.

(333) Saqib, N.; Silva, C. J.; Maupin, C. M.; Porter, J. M. A Novel Optical Diagnostic for In Situ Measurements of Lithium Polysulfides in Battery Electrolytes. *Appl. Spectrosc.* **2017**, *71*, 1593–1599.

(334) Aroca, R. F.; Ross, D. J.; Domingo, C. Surface-Enhanced Infrared Spectroscopy. *Appl. Spectrosc.* **2004**, *58*, 324A–338A.

(335) Osawa, M. Dynamic Processes in Electrochemical Reactions Studied by Surface-Enhanced Infrared Absorption Spectroscopy (SEIRAS). *Bull. Chem. Soc. Jpn.* **1997**, *70*, 2861–2880.

(336) Hillenbrand, R.; Taubner, T.; Keilmann, F. Phonon-enhanced light-matter interaction at the nanometre scale. *Nature* **2002**, *418*, 159–162.

(337) Xu, Q.; Berná,; Pobelov, I. V.; Rodes, A.; Feliu, J. M.; Wandlowski, T.; Kuzume, A. ATR-SEIRAS study of CO adsorption and oxidation on Rh modified Au($111-25\,\mathrm{nm}$) film electrodes in 0.1M H_2SO_4. *Electrochim. Acta* **2015**, *176*, 1202–1213.

(338) Richey, F. W.; Elabd, Y. A. In Situ Molecular Level Measurements of Ion Dynamics in an Electrochemical Capacitor. *J. Phys. Chem. Lett.* **2012**, *3*, 3297–3301.

(339) Richey, F. W.; Dyatkin, B.; Gogotsi, Y.; Elabd, Y. A. Ion Dynamics in Porous Carbon Electrodes in Supercapacitors Using in Situ Infrared Spectroelectrochemistry. *J. Am. Chem. Soc.* **2013**, *135*, 12818–12826.

(340) Elabd, Y.; Baschetti, M.; Barbari, T. Time-Resolved Fourier Transform Infrared/Attenuated Total Reflection Spectroscopy for the Measurement of Molecular Diffusion in Polymers. *J. Polymer Sci. B* **2003**, *41*, 2794–2807.

View Article Online
DOI: 10.1039/D2CP01458K

(341) Merlet, C.; Rotenberg, B.; Madden, P.; Taberna, P.-L.; Simon, P.; Gogotsi, Y.; Salanne, M. On the molecular origin of supercapacitance in nanoporous carbon electrodes. *Nature Mater.* **2012**, *11*.

(342) Richey, F. W.; Tran, C.; Kalra, V.; Elabd, Y. A. Ionic Liquid Dynamics in Nanoporous Carbon Nanofibers in Supercapacitors Measured with in Operando Infrared Spectroelectrochemistry. *J. Phys. Chem. C* **2014**, *118*, 21846–21855.

(343) Liu, Y.; Ghaffari, M.; Zhao, R.; Lin, J.-H.; Lin, M.; Zhang, Q. M. Enhanced Electromechanical Response of Ionic Polymer Actuators by Improving Mechanical Coupling between Ions and Polymer Matrix. *Macromol.* **2012**, *45*, 5128–5133.

(344) Ding, J.-F.; Xu, R.; Yan, C.; Li, B.-Q.; Yuan, H.; Huang, J.-Q. A review on the failure and regulation of solid electrolyte interphase in lithium batteries. *J. En. Chem.* **2021**, *59*, 306–319.

(345) Gao, Y.; Yan, Z.; Gray, J.; He, X.; Wang, D.; Chen, T.; Huang, Q.; Li, Y.; Wang, H.; Kim, S.; Mallouk, T.; Wang, D. Polymer–inorganic solid–electrolyte interphase for stable lithium metal batteries under lean electrolyte conditions. *Nat. Mater.* **2019**, *18*, 384–389.

(346) Zhang, X.; Dong, P.; Song, M.-K. MetalOrganic Frameworks for High-Energy Lithium Batteries with Enhanced Safety: Recent Progress and Future Perspectives. *Batt. Supercaps.* **2019**, *2*, 591–626.

(347) Kwak, W.-J.; Park, J.; Nguyen, T. T.; Kim, H.; Byon, H. R.; Jang, M.; Sun, Y.-K. A dendrite- and oxygen-proof protective layer for lithium metal in lithium–oxygen batteries. *J. Mater. Chem. A* **2019**, *7*, 3857–3862.

(348) Zhuang, G. V.; Xu, K.; Jow, T. R.; Ross, P. N. Study of SEI Layer Formed on Graphite Anodes in PC/LiBOB Electrolyte Using IR Spectroscopy. *Electrochem. Solid-State Lett.* **2004**, *7*, A224.

View Article Online
DOI: 10.1039/D2CP01458K

(349) Zhuang, G. V.; Yang, H.; Blizanac, B.; Ross, P. N. A Study of Electrochemical Reduction of Ethylene and Propylene Carbonate Electrolytes on Graphite Using ATR-FTIR Spectroscopy. *Electrochem. Solid-State Lett.* **2005**, *8*, A441.

(350) Meng, C.; Das, P.; Shi, X.; Fu, Q.; Müllen, K.; Wu, Z.-S. In Situ and Operando Characterizations of 2D Materials in Electrochemical Energy Storage Devices. *Small Sci.* **2021**, *1*, 2000076.

(351) Adarsh, K. S.; Chandrasekaran, N.; Chakrapani, V. In-situ Spectroscopic Techniques as Critical Evaluation Tools for Electrochemical Carbon dioxide Reduction: A Mini Review. *Front. Chem.* **2020**, *8*, 137.

(352) Bunea, S.; Urakawa, A. *Carbon Dioxide Electrochemistry: Homogeneous and Heterogeneous Catalysis*; The Royal Society of Chemistry, 2021; Chapter 9, pp 347–407.

(353) Yajima, T.; Uchida, H.; Watanabe, M. In-Situ ATR-FTIR Spectroscopic Study of Electro-oxidation of Methanol and Adsorbed CO at PtRu Alloy. *J. Phys. Chem. B* **2004**, *108*, 2654–2659.

(354) Heidary, N.; Ly, K.; Kornienko, N. Probing CO_2 Conversion Chemistry on Nanostructured Surfaces with Operando Vibrational Spectroscopy. *Nano Lett.* **2019**, *19*, 4817–4826.

(355) Neubrech, F.; Huck, C.; Weber, K.; Pucci, A.; Giessen, H. Surface-Enhanced Infrared Spectroscopy Using Resonant Nanoantennas. *Chem. Rev.* **2017**, *117*, 5110–5145.

(356) Papasizza, M.; Cuesta, A. In Situ Monitoring Using ATR-SEIRAS of the Electrocatalytic Reduction of CO_2 on Au in an Ionic Liquid/Water Mixture. *ACS Catal.* **2018**, *8*, 6345–6352.

(357) Gao, D.; Zhou, H.; Cai, F.; Wang, D.; Hu, Y.; Jiang, B.; Cai, W.-B.; Chen, X.; Si, R.;

View Article Online
DOI: 10.1039/D2CP01458K

Yang, F.; Miao, S.; Wang, J.; Wang, G.; Bao, X. Switchable CO_2 electroreduction via engineering active phases of Pd nanoparticles. *Nano Res.* **2017**, *10*, 2181–2191.

(358) Deng, W.; Zhang, L.; Li, L.; Chen, S.; Hu, C.; Zhao, Z.-J.; Wang, T.; Gong, J. Crucial Role of Surface Hydroxyls on the Activity and Stability in Electrochemical CO_2 Reduction. *J. Am. Chem. Soc.* **2019**, *141*, 2911–2915.

(359) Zhu, S.; Jiang, B.; Cai, W.-B.; Shao, M. Direct Observation on Reaction Intermediates and the Role of Bicarbonate Anions in CO_2 Electrochemical Reduction Reaction on Cu Surfaces. *J. Am. Chem. Soc.* **2017**, *139*, 15664–15667.

(360) Rodes, A.; Pastor, E.; Iwasita, T. Structural effects on CO_2 reduction at Pt single-crystal electrodes: Part 1. The Pt(110) surface. *J. Electroanal. Chem.* **1994**, *369*, 183–191.

(361) Rodes, A.; Pastor, E.; Iwasita, T. Structural efects on CO_2 reduction at Pt single-crystal electrodes: Part 2. Pt(111) and vicinal surfaces in the [011] zone. *J. Electroanal. Chem.* **1994**, *373*, 167–175.

(362) Rodes, A.; Pastor, E.; Iwasita, T. Structural effects on CO_2 reduction at Pt single-crystal electrodes: Part 3. Pt(100) and related surfaces. *J. Electroanal. Chem.* **1994**, *377*, 215–225.

(363) Jiang, K.; Wang, H.; Cai, W.-B.; Wang, H. Li Electrochemical Tuning of Metal Oxide for Highly Selective CO_2 Reduction. *ACS Nano* **2017**, *11*, 6451–6458.

(364) Kitano, H.; Gemmei-Ide, M. Structure of water in the vicinity of amphoteric polymers as revealed by vibrational spectroscopy. *J. Biomater. Sci. Polymer Ed.* **2010**, *21*, 1877–1893.

(365) Remizov, A.; Povov, V.; Lavrent'ev, V. *Polymer Science U.S.S.R. (Vysokomol. soyed.)* **1982**, *24*, 1853.

View Article Online
DOI: 10.1039/D2CP01458K

(366) Bravo-Suárez, J.; Srinivasan, P. Design characteristics of in situ and operando ultraviolet-visible and vibrational spectroscopic reaction cells for heterogeneous catalysis. *Catal. Rev.* **2017**, *59*, 295–445.

(367) Wang, Y.; Zhu, Y.; Zhou, Z.; Yang, J.; Pan, Y.; Qi, F. Pyrolysis Study on Solid Fuels: From Conventional Analytical Methods to Synchrotron Vacuum Ultraviolet Photoionization Mass Spectrometry. *Energy and Fuels* **2016**, *30*, 1534–1543.

(368) Pielichowska, K.; Nowicka, K. Analysis of nanomaterials and nanocomposites by thermoanalytical methods. *Thermochim. Acta* **2019**, *675*, 140–163.

(369) Benhammada, A.; Trache, D. Thermal decomposition of energetic materials using TG-FTIR and TG-MS: a state-of-the-art review. *Appl. Spectrosc. Rev.* **2020**, *55*, 724–777.

(370) Zheng, X.; Xu, W.; Xie, S. Study on Ultraviolet Aging Mechanism of Carbon Nanotubes/SBS Composite-Modified Asphalt in Two-Dimensional Infrared Correlation Spectroscopy. *Materials* **2021**, *14*.

(371) Ainali, N. M.; Bikiaris, D. N.; Lambropoulou, D. A. Aging effects on low- and high-density polyethylene, polypropylene and polystyrene under UV irradiation: An insight into decomposition mechanism by Py-GC/MS for microplastic analysis. *J. Anal. Appl. Pyrolys.* **2021**, *158*, 105207.

(372) Mahdi, A. S.; Abdul-Malek, Z.; Naderipour, A.; Ishak, S.; Bin Hussein, M. N. K. Investigation of SF_6 Decomposition Under Partial Discharge Induced by Protrusion Defect. 2021 IEEE International Conference on the Properties and Applications of Dielectric Materials (ICPADM). 2021; pp 139–142.

(373) Li, W.; Zheng, W.; Ren, L.; Li, H.; Zhao, X.; Wang, C.; Li, J. A Comparative Study on the Insulation Ageing of 10 kV XLPE Cable via Accelerated Electrical Test and Accelerated Water Tree Test. *J. El. Eng. Technol.* **2021**,

View Article Online
DOI: 10.1039/D2CP01458K

(374) Jang, E.-S.; Song, E.; Zain Siddiqui, M.; Lim, S.; Shin, G.; Kim, D.; Kim, Y.-M. The effect of seawater aging on the pyrolysis of fishing nets. *Journal of Analytical and Applied Pyrolysis* **2021**, *156*.

(375) Peng, H.; Han, Y.; Liu, T.; Tjiu, W. C.; He, C. Morphology and thermal degradation behavior of highly exfoliated CoAl-layered double hydroxide/polycaprolactone nanocomposites prepared by simple solution intercalation. *Thermochim. Acta* **2010**, *502*, 1–7.

(376) Popescu, M.-C.; Vasile, C. Melting Behavior of Polytetra Hydrofuran/Cholesteryl Palmitate Blends Investigated by Two-Dimensional Infrared Correlation Spectroscopy. *Soft Mater.* **2010**, *8*, 386–406.

(377) Tang, H.; Sun, S.; Wu, J.; Wu, P.; Wan, X. Conformational changes in novel thermotropic liquid crystalline polymer without conventional mesogens: A Raman spectroscopic investigation. *Polymer* **2010**, *51*, 5482–5489.

(378) Zheng, K.; Liu, R.; Huang, Y. A two-dimensional IR correlation spectroscopic study of the conformational changes in syndiotactic polypropylene during crystallization. *Polymer J.* **2010**, *42*, 81–85.

(379) Cheng, Y.-H.; Chen, W.-P.; Shen, Z.; Fan, X.-H.; Zhu, M.-F.; Zhou, Q.-F. Influences of Hydrogen Bonding and Peripheral Chain Length on Mesophase Structures of Mesogen-Jacketed Liquid Crystalline Polymers with Amide Side-Chain Linkages. *Macromol.* **2011**, *44*, 1429–1437.

(380) Pazderka, T.; Kopecký, V. Two-dimensional correlation analysis of Raman optical activity – Basic rules and data treatment. *Vib. Spectrosc.* **2012**, *60*, 193–199.

(381) Chai, F.; Chen, Y.; You, Z.; Xia, Z.; Ge, S.; Sun, Y.; Huang, B. Two Keggin-type heteropolytungstates with transition metal as a central atom: Crystal structure and

View Article Online
DOI: 10.1039/D2CP01458K

magnetic study with 2D-IR correlation spectroscopy. *J. Solid St. Chem.* **2013**, *202*, 161–167.

(382) Wang, G.-W. Mechanochemical organic synthesis. *Chem. Soc. Rev.* **2013**, *42*, 7668–7700.

(383) Wang, L.; Di, S.; Wang, W.; Chen, H.; Yang, X.; Gong, T.; Zhou, S. Tunable Temperature Memory Effect of Photo-Cross-Linked Star PCL–PEG Networks. *Macromol.* **2014**, *47*, 1828–1836.

(384) Hoshina, H.; Ishii, S.; Otani, C. Separation of overlapping vibrational peaks in terahertz spectra using two-dimensional correlation spectroscopy. *J. Mol. Struct.* **2014**, *1069*, 152–156.

(385) Hou, L.; Ma, K.; An, Z.; Wu, P. Exploring the Volume Phase Transition Behavior of POEGA- and PNIPAM-Based Core–Shell Nanogels from Infrared-Spectral Insights. *Macromol.* **2014**, *47*, 1144–1154.

(386) Seo, H.; Chae, B.; Im, J. H.; Jung, Y. M.; Lee, S. W. Imidization induced structural changes of 6FDA-ODA poly(amic acid) by two-dimensional (2D) infrared correlation spectroscopy. *J. Mol. Struct.* **2014**, *1069*, 196–199.

(387) Kim, H. J.; Kim, S. B.; Kim, J. K.; Jung, Y. M.; Ryu, D. Y.; Lavery, K. A.; Russell, T. P. Phase Behavior of a Weakly Interacting Block Copolymer by Temperature-Dependent FTIR Spectroscopy. *Macromolecules* **2006**, *39*, 408–412.

(388) Unger, M.; Morita, S.; Sato, H.; Ozaki, Y.; Siesler, H. W. Variable-Temperature Fourier Transform Infrared Spectroscopic Investigations of Poly(3-Hydroxyalkanoates) and Perturbation-Correlation Moving-Window Two-Dimensional Correlation Analysis. Part II: Study of Poly(ϵ-Caprolactone) Homopolymer and a Poly(3-Hydroxybutyrate)—Poly(ϵ-Caprolactone) Blend. *Appl. Spectrosc.* **2009**, *63*, 1034–1040.

View Article Online
DOI: 10.1039/D2CP01458K

(389) Unger, M.; Sato, H.; Ozaki, Y.; Siesler, H. W. Crystallization Behavior of Poly(3-hydroxybutyrate) (PHB), Poly(ϵ-caprolactone) (PCL) and Their Blend (50 : 50 wt.%) Studied by 2D FT-IR Correlation Spectroscopy. *Macromol. Symp.* **2011**, *305*, 90–100.

(390) Jia, L.; Guo, C.; Yang, L.; Xiang, J.; Tang, Y.; Liu, C.; Liu, H. Mechanism of PEO–PPO–PEO micellization in aqueous solutions studied by two-dimensional correlation FTIR spectroscopy. *J. Colloid Interf. Sci.* **2010**, *345*, 332–337.

(391) Baumgartner, B.; Freitag, S.; Lendl, B. 3D Printing for Low-Cost and Versatile Attenuated Total Reflection Infrared Spectroscopy. *Anal. Chem.* **2020**, *92*, 4736–4741.

(392) Carrasco-Correa, E. J.; Simó-Alfonso, E. F.; Herrero-Martínez, J. M.; Miró, M. The emerging role of 3D printing in the fabrication of detection systems. *TrAC Trends Anal. Chem.* **2021**, *136*, 116177.

(393) Dumas, P.; Martin, M. C.; Carr, G. L. In *Synchrotron Light Sources and Free-Electron Lasers: Accelerator Physics, Instrumentation and Science Applications*; Jaeschke, E. J., Khan, S., Schneider, J. R., Hastings, J. B., Eds.; Springer International Publishing: Cham, 2020; pp 2059–2113.

(394) Lu, H.; Carroll, G. M.; Neale, N. R.; Beard, M. C. Infrared Quantum Dots: Progress, Challenges, and Opportunities. *ACS Nano* **2019**, *13*, 939–953.

(395) Elgayyar, T.; Atwi, R.; Tuel, A.; Meunier, F. C. Contributions and limitations of IR spectroscopy of CO adsorption to the characterization of bimetallic and nanoalloy catalysts. *Catalysis Today* **2021**, *373*, 59–68.

(396) Hu, Y.; López-Lorente, I.; Mizaikoff, B. Graphene-Based Surface Enhanced Vibrational Spectroscopy: Recent Developments, Challenges, and Applications. *ACS Photonics* **2019**, *6*, 2182–2197.

View Article Online
DOI: 10.1039/D2CP01458K

(397) Hayashi, T. Water at Interfaces: Its Behavior and Roles in Interfacial Phenomena. *Chem. Lett.* **2021**, *50*, 1173–1180.

(398) Steinmann, S. N.; Seh, Z. W. Understanding electrified interfaces. *Nature Rev. Mater.* **2021**, *6*, 289–291.

(399) Brahms, C.; Belli, F.; Travers, J. C. Infrared attosecond field transients and UV to IR few-femtosecond pulses generated by high-energy soliton self-compression. *Phys. Rev. Res.* **2020**, *2*, 043037.

(400) Maiuri, M.; Garavelli, M.; Cerullo, G. Ultrafast Spectroscopy: State of the Art and Open Challenges. *J. Am. Chem. Soc.* **2020**, *142*, 3–15.

(401) Pushkin, A.; Migal, E.; Suleimanova, D.; Mareev, E.; Potemkin, F. High-Power Solid-State Near- and Mid-IR Ultrafast Laser Sources for Strong-Field Science. *Photonics* **2022**, *9*.

(402) Bechtel, H. A.; Johnson, S. C.; Khatib, O.; Muller, E. A.; Raschke, M. B. Synchrotron infrared nano-spectroscopy and -imaging. *Surf. Sci. Rep.* **2020**, *75*, 100493.

(403) Ellis, G.; Martin, M. Opportunities and challenges for polymer science using synchrotron-based infrared spectroscopy. *Eur. Polymer J.* **2016**, *81*, 505–531.

(404) Babal, A.; Souza, B.; Möslein, A.; Gutiérrez, M.; Frogley, M.; Tan, J.-C. Broadband Dielectric Behavior of an MIL-100 Metal-Organic Framework as a Function of Structural Amorphization. *ACS Appl. El. Mater.* **2021**, *3*, 1191–1198.

(405) Li, F.; Han, G.-F.; Baek, J.-B. Nanocatalytic Materials for Energy-Related Small-Molecules Conversions: Active Site Design, Identification and Structure–Performance Relationship Discovery. *Acc. Chem. Res.* **2021**,

(406) Carr, G. L. Resolution limits for infrared microspectroscopy explored with synchrotron radiation. *Rev. Sci. Instr.* **2001**, *72*, 1613–1619.

View Article Online
DOI: 10.1039/D2CP01458K

(407) Lewis, E. N.; Treado, P. J.; Reeder, R. C.; Story, G. M.; Dowrey, A. E.; Marcott, C.; Levin, I. W. Fourier Transform Spectroscopic Imaging Using an Infrared Focal-Plane Array Detector. *Anal. Chem.* **1995**, *67*, 3377–3381.

(408) Tang, X.; Hao, Q. Towards dual-band shot-wave and mid-wave infrared focal plane array by using colloidal quantum dots. Seventh Symposium on Novel Photoelectronic Detection Technology and Applications. 2021; pp 168 – 174.

(409) Dazzi, A.; Prater, C. B.; Hu, Q.; Chase, D. B.; Rabolt, J. F.; Marcott, C. AFM-IR: Combining Atomic Force Microscopy and Infrared Spectroscopy for Nanoscale Chemical Characterization. *Appl. Spectrosc.* **2012**, *66*, 1365–1384.

(410) Dazzi, A.; Prater, C. B. AFM-IR: Technology and Applications in Nanoscale Infrared Spectroscopy and Chemical Imaging. *Chem. Rev.* **2017**, *117*, 5146–5173.

(411) Bondy, A. L.; Kirpes, R. M.; Merzel, R. L.; Pratt, K. A.; Banaszak Holl, M. M.; Ault, A. P. Atomic Force Microscopy-Infrared Spectroscopy of Individual Atmospheric Aerosol Particles: Subdiffraction Limit Vibrational Spectroscopy and Morphological Analysis. *Anal. Chem.* **2017**, *89*, 8594–8598.

(412) Graefe, C. T.; Punihaole, D.; Harris, C. M.; Lynch, M. J.; Leighton, R.; Frontiera, R. R. Far-Field Super-Resolution Vibrational Spectroscopy. *Anal. Chem.* **2019**, *91*, 8723–8731.

(413) Xiao, L.; Schultz, Z. D. Spectroscopic Imaging at the Nanoscale: Technologies and Recent Applications. *Anal. Chem.* **2018**, *90*, 440–458.

(414) Mathurin, J.; Deniset-Besseau, A.; Bazin, D.; Dartois, E.; Wagner, M.; Dazzi, A. Photothermal AFM-IR spectroscopy and imaging: Status, challenges, and trends. *J. Appl. Phys.* **2022**, *131*, 010901.

View Article Online
DOI: 10.1039/D2CP01458K

(415) Milanović, I.; Biliškov, N. Mechanochemical pretreatment of ammonia borane: A new procedure for sodium amidoborane synthesis. *Int. J. Hydrogen En.* **2020**, *45*, 7938–7946.

(416) Gonnet, L.; Lennox, C. B.; Do, J.-L.; Malvestiti, I.; Koenig, S. G.; Nagapudi, K.; Friščić, T. Metal-Catalyzed Organic Reactions by Resonant Acoustic Mixing. *Angew. Chem. Int. Ed.* **2022**, *n/a*, e202115030.

(417) Gomollón-Bel, F. Ten Chemical Innovations That Will Change Our World: IUPAC identifies emerging technologies in Chemistry with potential to make our planet more sustainable. *Chem. Int.* **2019**, *41*, 12–17.

(418) Dunn, P. J. Pharmaceutical Green Chemistry process changes – how long does it take to obtain regulatory approval? *Green Chem.* **2013**, *15*, 3099–3104.

(419) Welton, T. Solvents and sustainable chemistry. *Proc. Royal Soc. A* **2015**, *471*, 20150502.

(420) Liu, X.; Li, Y.; Zeng, L.; Li, X.; Chen, N.; Bai, S.; He, H.; Wang, Q.; Zhang, C. A Review on Mechanochemistry: Approaching Advanced Energy Materials with Greener Force. *Adv. Mater.* 2108327.

(421) Friščić, T.; Mottillo, C.; Titi, H. M. Mechanochemistry for Synthesis. *Angew. Chem. Int. Ed.* **2020**, *59*, 1018–1029.

(422) Effaty, F.; Ottenwaelder, X.; Friščić, T. Mechanochemistry in transition metal-catalyzed reactions. *Curr. Op. Green Sust. Chem.* **2021**, *32*, 100524.

(423)

(424) Bolm, C.; Hernández, J. G. Mechanochemistry of Gaseous Reactants. *Angew. Chem.. Int. Ed.* **2019**, *58*, 3285–3299.

View Article Online
DOI: 10.1039/D2CP01458K

(425) Ardila-Fierro, K. J.; Hernández, J. G. Sustainability Assessment of Mechanochemistry by Using the Twelve Principles of Green Chemistry. *ChemSusChem* **2021**, *14*, 2145–2162.

(426) Amrute, A. P.; De Bellis, J.; Felderhoff, M.; Schüth, F. Mechanochemical Synthesis of Catalytic Materials. *Chem. Eur. J.* **2021**, *27*, 6819–6847.

(427) Hwang, S.; Grätz, S.; Borchardt, L. A guide to direct mechanocatalysis. *Chem. Commun.* **2022**,

(428) Tan, D.; Friščić, T. Mechanochemistry for Organic Chemists: An Update. *Eur. J. Org. Chem.* **2018**, *2018*, 18–33.

(429) Tan, D.; García, F. Main group mechanochemistry: from curiosity to established protocols. *Chem. Soc. Rev.* **2019**, *48*, 2274–2292.

(430) Espro, C.; Rodríguez-Padrón, D. Re-thinking organic synthesis: Mechanochemistry as a greener approach. *Curr. Op. Green and Sust. Chem.* **2021**, *30*.

(431) Friščić, T.; Halasz, I.; Beldon, P.; Belenguer, A.; Adams, F.; Kimber, S.; Honkimäki, V.; Dinnebier, R. Real-time and in situ monitoring of mechanochemical milling reactions. *Nature Chem.* **2013**, *5*, 66–73.

(432) Juribašić, M.; Užarević, K.; Gracin, D.; Ćurić, M. Mechanochemical C–H bond activation: rapid and regioselective double cyclopalladation monitored by in situ Raman spectroscopy. *Chem. Commun.* **2014**, *50*, 10287–10290.

(433) Gracin, D.; v Strukil, V.; Friščić, T.; Halasz, I.; Užarević, K. Laboratory real-time and in situ monitoring of mechanochemical milling reactions by Raman spectroscopy. *Angew. Chem. Int. Ed.* **2014**, *53*, 6193–6197.

(434) Užarević, K.; Halasz, I.; Friščić, T. Real-Time and in Situ Monitoring of

View Article Online
DOI: 10.1039/D2CP01458K

Mechanochemical Reactions: A New Playground for All Chemists. *J. Phys. Chem. Lett.* **2015**, *6*, 4129–4140.

(435) Julien, P.; Užarević, K.; Katsenis, A.; Kimber, S.; Wang, T.; Farha, O.; Zhang, Y.; Casaban, J.; Germann, L.; Etter, M.; Dinnebier, R.; James, S.; Halasz, I.; Friščić, T. In Situ Monitoring and Mechanism of the Mechanochemical Formation of a Microporous MOF-74 Framework. *J. Am. Chem. Soc.* **2016**, *138*, 2929–2932.

(436) Lukin, S.; Stolar, T.; Tireli, M.; Blanco, M.; Babić, D.; sˇ cić, F.

(437) Užarević, K.; Ferdelji, N.; Mrla, T.; Julien, P.; Halasz, B.; Friščić, T.; Halasz, I. Enthalpy vs. friction: Heat flow modelling of unexpected temperature profiles in mechanochemistry of metal-organic frameworks. *Chem. Sci.* **2018**, *9*, 2525–2532.

(438) Ardila-Fierro, K.; Lukin, S.; Etter, M.; Užarević, K.; Halasz, I.; Bolm, C.; Hernández, J. Direct Visualization of a Mechanochemically Induced Molecular Rearrangement. *Angew. Chem. Int. Ed.* **2020**, *59*, 13458–13462.

(439) Germann, L.; Katsenis, A.; Huskić, I.; Julien, P.; Užarević, K.; Etter, M.; Farha, O.; Friščić, T.; Dinnebier, R. Real-Time in Situ Monitoring of Particle and Structure Evolution in the Mechanochemical Synthesis of UiO-66 Metal-Organic Frameworks. *Cryst. Growth Des.* **2020**, *20*, 49–54.

(440) Biliškov, N.; Borgschulte, A.; Užarević, K.; Halasz, I.; Lukin, S.; Milošević, S.; Milanović, I.; Novaković, J. In-Situ and Real-time Monitoring of Mechanochemical Preparation of Li2Mg(NH2BH3)4 and Na2Mg(NH2BH3)4 and Their Thermal Dehydrogenation. *Chem. Eur. J.* **2017**, *23*, 16274–16282.

(441) Rathmann, T.; Petersen, H.; Reichle, S.; Schmidt, W.; Amrute, A.; Etter, M.; Weidenthaler, C. In situ synchrotron X-ray diffraction studies monitoring mechanochemical reactions of hard materials: Challenges and limitations. *Rev. Sci. Instr.* **2021**, *92*, 114102.

View Article Online
DOI: 10.1039/D2CP01458K

Table 1: Materials transparent in the mid-IR region suitable for transmission and ATR measurements.

Material	**Transparency range** (cm^{-1})	**Refraction index** (20 °C)	**Use**	**Comments**
KBr	$40000 - 400$	1.5	windows, pellets	soluble in water and alcohols
NaCl	$33000 - 625$	1.55	windows, pellets	soluble in water, slightly soluble in alcohols
CsI	$33000 - 160$	1.74 ($1000\,cm^{-1}$)	windows, pellets	soluble in water and alcohols
CaF_2	$50000 - 1000$	1.4	windows	soluble in solutions of ammonium salts
Si	$6700 - 1000$	$3.5 - 3.4$	windows, ATR	hard
Ge	$5000 - 660$	$4.1 - 3.9$	ATR	soluble in HCl + HNO_3 mixture and H_2O_2
Diamond	$50000 - 500$	2.4	ATR	extremely hard and inert
ZnSe (Irtran-4)	$16700 - 660$	$2.5 - 2.3$	ATR	soluble in acids, slightly soluble in water
ZnS (Irtran-2)	$20000 - 550$	$2.3 - 2.0$	ATR	soluble in acids, slightly soluble in water
TlBr + TlI (KRS-5)	$33000 - 250$	2.4	ATR, windows	toxic, sensitive to organic solvents, slightly soluble in water
TlBr + TlCl (KRS-6)	$25000 - 250$	$2.3 - 2.2$	ATR	toxic, sensitive to organic solvents, slightly soluble in water
$Ge_{33}As_{12}Se_{55}$ (AMTIR-1)	$10000 - 714$	$2.5 - 2.6$	ATR	
Al_2O_3 (sapphire)	$50000 - 2222$	1.65 ($2500\,cm^{-1}$)	windows, fibers, ATR	very hard, highly resistant to acids and alkalies up to 1000 °C
As_2S_3	$12500 - 1000$	1.56	fibers	sensitive to water
Polyethylene	down to far-IR	1.5	windows	strong absoption around 3000, 1500 and ($720\,cm^{-1}$)
Paraffine (Nujol)	$50000 - 600$	1.46	mulls	strong absoption around 3000 and ($1500\,cm^{-1}$)
Fluorolube	$50000 - 500$	1.38	mulls	